THE EVOLUTION OF EAST CANDOR CHASMA, VALLES MARINERIS, MARS: PROPOSED STRUCTURAL COLLAPSE AND SEDIMENTATION

Amanda Burden, BSc. (Hons.)

MSc, Earth Science

Submitted in partial fulfillment

Of the requirements for the degree of

Master of Science

Faculty of Math and Science, Brock University

St. Catharines, Ontario

Abstract

Valles Marineris (VM), Mars has a long history of sedimentary deposition. East Candor Chasma is located on the eastern flank of Valles Marineris. Previous studies of the chasma suggests a complex geological history of collapse and basin infill. Interior Layer Deposits (ILDs) in East Candor Chasma span over 475 km long, 145 km wide and range in elevation from -5.5 km to 3.5 km at datum. The ILDs can be separated into six different unit varieties-massive, thick layer unit, thin layer unit, steeply inclined unit, deformed layer unit, and thin mesa unit. The massive unit contains no visible layering and a distinct erosional style. Thick layer units are found overlying the massive unit and tend to thin upwards within the mound. The thin layer unit overlies the thick layer unit and can be observed truncating thick layering. A steeply dipping unit is anomalous and found only in one mound within the chasma. A Deformed layer unit is commonly observed along the walls of the chasma indicating post erosional slumping. A thin mesa unit is thought to be a late ash cover which conformably drapes all pre-existing geology.

Unconformities are observed throughout the chasma, three occur at an elevation of ~1000 m within the thick layer unit. This indicates the chasma likely underwent multiple periods of erosion and deposition. Attitude measurements taken within the layered units of the central mounds reveal a possible secondary collapse along the north wall of the chasma. The lower stratigraphic section along the north face of the central mounds reveals dips of ~20˚, indicating that the massive unit was likely eroded prior to thick layer unit deposition.

These observations can be used to interpret the geological history of East Candor Chasma. We suggest that a secondary collapse occurred along the north wall of the chasma after the massive unit was emplaced. Sedimentation and erosion continued after chasma collapse allowing for the emplacement of layer and thin mesa units. Two models for the history of East Candor Chasma are presented.

Acknowledgements

I would like to thank Frank Fueten for the opportunity to complete a thesis. Thank you for steering me in the right direction whenever I had a question about my research. Thank you to Bob Stesky and Rick Cheel, for their participation in reviewing my work. Their input during the writing process proved to be invaluable. Thank you to my other committee member, Mariek Schmidt, and Jessica Flahaut for reviewing my work. I would also like to acknowledge Jon Walmsley for his participation making digital elevation models available for me and assisting me with troubleshooting computer problems throughout this process.

Thank you.

Table of Contents

List of Figures

Chapter 1

Chapter 2

Chapter 3

Chapter 4

List of Tables

Chapter 2

List of Abbreviations

CRISM	Compact Reconnaissance Imaging Spectrometer for Mars
CTX	Context Imager
HiRISE	High Resolution Imaging Science Experiment
HRSC	High Resolution Stereo Camera
ILD	Interior Layer Deposit
MOLA	Mars Orbiter Laser Altimeter
VM	Valles Marineris

1.0 Chapter 1: Introduction

1.1 A brief Overview of the History of Mars

The similarities in Mars' geologic processes and its proximity to Earth make it a valuable research subject for planetary sciences and terrestrial-based fields of science. The discovery of water-ice and fluvial channels (Lucchitta, 1982) has further increased our curiosity of Mars and the possibility that life may have inhabited the planet at one time.

Mars accreted and differentiated over a few tens of millions of years during the formation of our solar system; separating into mantle, core and crust (Carr & Head III, 2010). The geologic history of Mars is divided by into three periods: the Noachian (4.5-3.7 GA), Hesperian (3.6-3.1 GA) and Amazonian (3.0 GA – present) (fig. 1). The Noachian was characterized by high rates of cratering, erosion and valley formation. The surface conditions of Mars were warm and wet allowing for widespread production of hydrous weathering products, such as phyllosilicates (Carr & Head III, 2010). It was during this time that erosion rates were at their highest. By the end of the Noachian erosion, rate and magnitude of impacts, weathering and valley formation fell dramatically. However, volcanism remained at a high average rate through the Hesperian, with at least 30% of the planet being resurfaced by volcanic processes (Carr & Head III, 2010). As Mars entered the Hesperian, episodic seas, outflow channels and canyons began to form. This was followed by sulfate production late in the era. Large-scaled floods occurred episodically, leaving bodies of water on the surface temporarily and eroding canyons (Carr & Head III, 2010). By the end of the Hesperian water activity at the planet's surface nearly ceased as the planet became cold and dry; any water at the planet's surface lost by evaporation to Mars' thin atmosphere. It was at this point in the planet's history the cryosphere formed as an ice-rich layer just below the surface of Mars. The

Amazonian is Mars' longest geologic period and characterized by the presence, accumulation and movement of ice. It is suggested that glacial processes are partially responsible for carving valleys and canyons, perhaps as part of ice-rich debris (Carr & Head III, 2010).

Dating events on Mars is primarily accomplished by counting craters the planets surface (Hartmann & Neukum, 2001; Michael & Neukum, 2010). This method has been calibrated by impact samples taken from the moon. Dating the surface of Mars is also accomplished by general observations and applying the principles of superposition and cross-cutting relationships. Most recent dating methods are obtained from analysis of lander missions and orbital spectrometers.

1.2 Obliquity and Climate Change

Mars' climate has changed greatly over time (Carr & Head III, 2010). This is largely due to obliquity, which are changes in the axial tilt of the planet. On Earth this, accompanied by precession and eccentricity, causes variation in a planet's climate. The effect is similar on Mars. Swings in obliquity of up to 60˚ resulted in significant changes in regional environment which may have led to many of the geologic features observed at the equator and mid-latitudes such as outwash channels, the layering of strata and sediment deposition (Touma & Wisdom, 1993; Mischna, et al., 2003). As Mars' temperature warmed by seasonal variations, water was freed from the icy poles, moving towards the equator and increasing the sediment load available for deposition. Great shifts in obliquity can cause catastrophic weather events resulting in a variety of fluvial and aeolian related landforms. Studying layered strata found on Mars can yield valuable information on the geologic history of Mars (Ward, et al., 1979; Jakosky, et al., 1995; Head, et al., 2003).

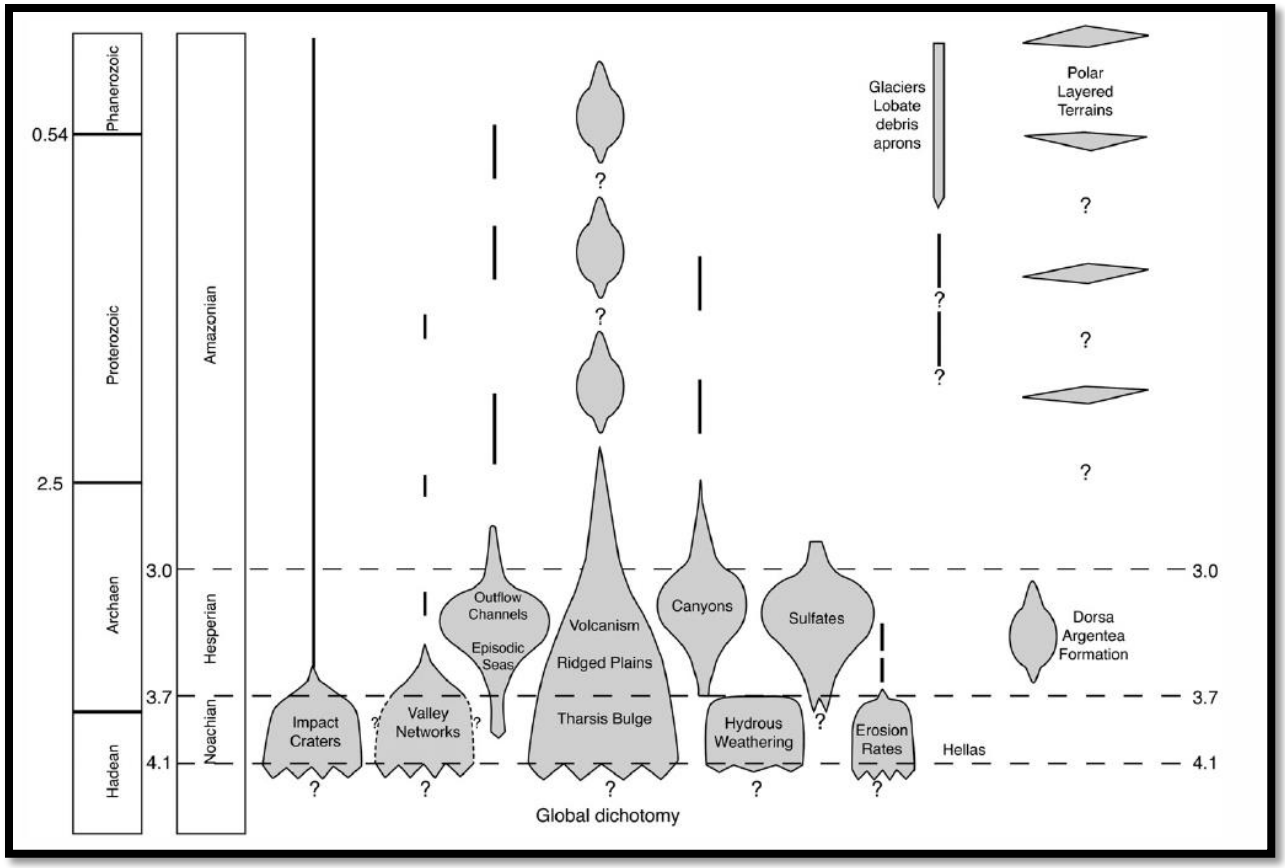

Figure 1-1: Illustration of Geologic activity as a function of time after Carr and Head (2009)

1.3 Valles Marineris

Valles Marineris (VM) (fig. 2) is the largest canyon system in our solar system. Spanning 4,000 km long and up to 11 km deep, it runs approximately 1/5 the circumference of Mars (Andrews-Hanna, 2012a). For comparison VM is almost as long as North America is wide, dwarfing any canyon system found on Earth. The region has been the focus of a variety of studies on volcanism, sedimentation, geochemical analysis, structural geology, fluvial processes and geomorphology (Tanaka, 1986; Luccitta, et al., 1992; Mege, 2001). VM is located just south of the equator on the western flank of the Tharsis region. The Tharsis region is a broad volcanic topographic high approximately 8,000 km across (Andrews-Hanna, et al., 2007). The region formed as the result of intrusive and extrusive volcanism during the Noachian

epoch. The formation of VM is widely debated (Tanaka & Golombek, 1989; Luccitta, et al., 1992; Mege & Masson, 1996; Andrews-Hanna, 2012a), however it is thought that Tharsis region played a key role in the formation of Valles Marineris.

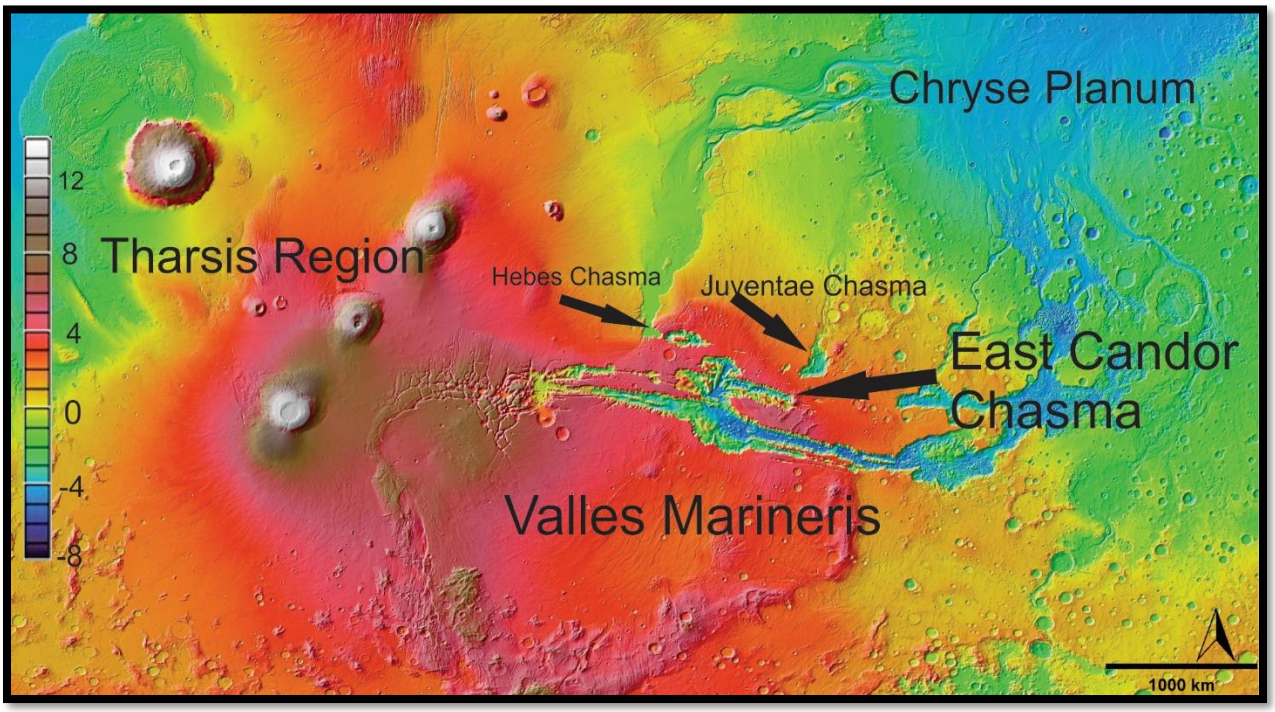

Figure 1-2 MOLA elevation map of Tharsis Region on Mars with Valles Marineris located in the center of the image. Image is MOLA colourized elevation with THEMIS day IR.

1.4 Valles Marineris Geologic History

Several interpretations have been proposed for the formation of VM. A widely accepted interpretation for the regions geologic history involves a two-stage process of basin formation followed by linking of the basins (Carr & Head III, 2010; Lucchitta, 1994; Schultz, 1998; Head, et al., 2001; Quantin, et al., 2004; Tanaka, 1986). Various models have been proposed for the collapse of the initial basin; tension fractures occurring deep in the planet crust (Tanaka & Golombek, 1989), magmatic activity produced by nearby

Syria Planum (Wilson & Head, 2002; Okubo, 2010), the release of large volumes of crustal ice or carbonates (Sharp, 1973; McKenzie & Nimmo, 1999; Spencer & Fanale, 1990).

A widely accepted interpretation for the geologic history of the Valles Marineris region (e.g., (Nedell & Squyres, 1987; Tanaka & Golombek, 1989; Luccitta, et al., 1992; Peulvast & Masson, 1993; Lucchitta, 1994; Mege & Masson, 1996; Head, et al., 2001; Wilson & Head, 2002; Quantin, et al., 2004; Mege, 2006; Golombek & Phillips, 2010; Andrews-Hanna, 2012a; Andrews-Hanna, 2012b) and references therein) is as follows:

During the Late Noachian to Early Hesperian, growth of Syria Planum drove radial emplacement of dikes, and related graben and pit craters, in the future area of VM (Wilson & Head, 2002). The intrusive activity caused weakening of the lithosphere in the area allowing subsidence to occur.

By the Early Hesperian, irregularly-shaped ancestral basins formed through subsidence that was superimposed on the earlier Sub-radial dikes, graben and pit craters (Metz, et al., 2010). This subsidence may have been related to the melting of ice held below the planets surface (Lucchitta, 1982). Sedimentary deposits subsequently accumulated in the ancestral basins under depositional conditions that may have been sub-aerial, sub-aqueous or a combination of both.

During the Amazonian, a series regional rift systems cut some of the ancestral basins and the sedimentary deposits (Tanaka & Golombek, 1989). Rifting on Mars is a different process from that which occur on Earth (Andrews-Hanna, 2012a; Andrews-Hanna, 2012b). Plate tectonics are responsible for rifting observed on Earth, while rifting on Mars is dominated by collapse to form subsurface basins. Rifting cut through the Candor ancestral basin, resulting in the formation of a composite graben through

parts of present-day Ophir and Candor Chasmata. Rift-related normal faults also cut through Melas ancestral basin contributing to the formation of Coprates-Melas-Ius Chasmata system (Okubo, 2010). Formation of these rift systems could have been driven by Tharsis-related stresses and may have been structurally influenced by the presence of the Syria-radial dike system and the ancestral basins. This episode of rifting may have also provided an outlet and drainage for any existing bodies of water that accumulated within the ancestral basins (Andrews-Hanna, 2012a).

The formation of VM is believed to have involved minor extension accompanied by vertical collapse (Fueten, et al., 2017). Mege and Masson (1996) estimate the amount of crustal stretching to be 2-10% as a result of passive rifting. The collapse of VM is thought to be contained by basin-parallel normal faults, where crustal stretching is the cause of these bounding faults. Andrews-Hanna (2012a, 2012b) provided a model which suggest faulting along VM is likely near-vertical to compensate for such minimal extension. Andrews-Hanna (2012a, 2012b) model is compliant with the observed depths of VM and is consistent with geological/geophysical observations.

1.5 Composition of Martian Crust Near Valles Marineris

Impact craters located around VM have indicated two distinct lithologies below the Martian crust: light-toned massive rocks and intact layers. The massive rocks are thought to represent Noachian crust because CRISM analysis has revealed that they are composed of low calcium pyroxene, olivine, smectites and putative serpentine (Quantin, et al., 2004). While the intact layers are thought to be a Noachian volcanic accumulation due to its enrichment in high calcium pyroxenes. The Noachian volcanic accumulation is thought to be up to 18 km thick and is the result of Tharsis activity (Quantin, et al., 2004). HiRISE and CRISM data have revealed the lower portion of the walls on eastern flank of VM are composed of well-preserved Noachian crust that contains no visible layering that can be detected with

current technology (Flahaut, et al., 2012). The western flank of VM is thought to be cut into material consistent with lavas or volcanic sediments based on observations from impact crater central peaks (Flahaut, et al., 2012).

1.6 Interior Layered Deposits

VM displays a complex history of sedimentary deposition by water and aeolian processes (Burr, et al., 2009; Carr & Head III, 2010). Mound forming sedimentary deposits within VM are referred to as interior layered deposits (ILD) and are an important part of analysis when considering the formation of the chasma and its associated geologic history (Fig. 3). Lucchitta et al. 1994 concluded that ILDs in VM make up 17% of the total area and 60% of deposits found within. ILDs occur in most chasma of VM and peripheral chasmata like Hebes, Juventae and Ganges (Okubo, et al., 2008). Layering within ILD mounds typically lie inclined or near-horizontal, they are largely-continuous layers of consolidated material. Occurring mainly within elliptical chasmata, they typically overlie chasma floors, walls and sometimes show onlap of chaotic terrain (Komatsu, et al., 2004). Layer thickness varies from a few meters to tens of meters in thickness (Nedell & Squyres, 1987). ILD sequences of hundreds to thousands of meters have also been observed, although less frequently (Komatsu, et al., 2004). ILDs are generally located in the center of chasms approximately 1 to 4 km lower than the surrounding walls, can easily be distinguished by their light to intermediate albedo, unique erosional style and fine layering (Komatsu, et al., 2004).

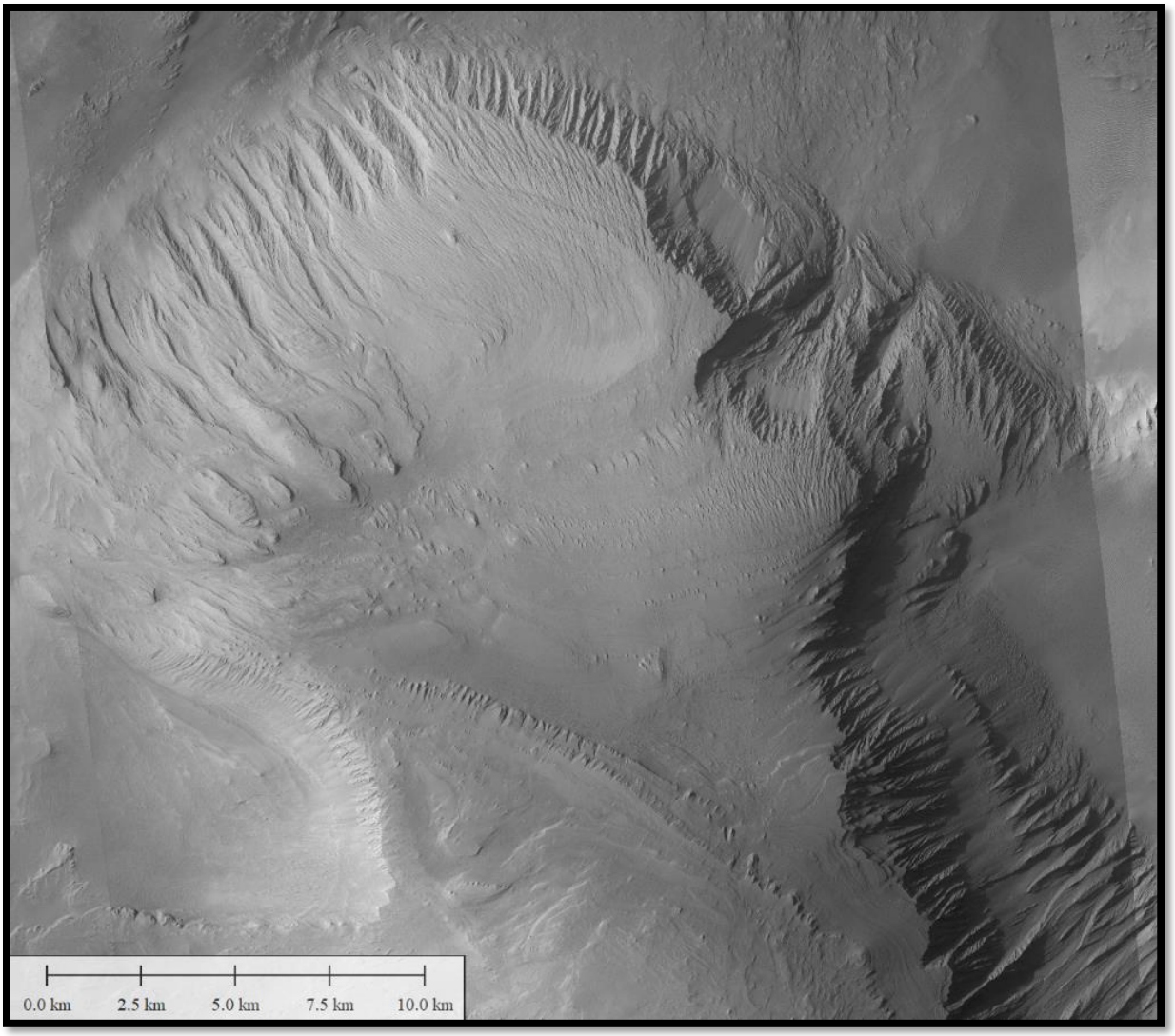

Figure 1-3: Interior layered deposits found in East Candor Chasma. North is top of page. Image is CTX 20 m/pixel.

1.7 Evidence of Glaciation in Valles Marineris

Lucchitta et al. (1981) was among the first to recognize glacial landforms on the surface of Mars by making a comparison to those found on Earth. Since then, the hypothesis that ice played at least a partial role in the creation of VM has gained support from additional work and better imagery (Lucchitta, 1982; Burr, et al., 2009). Gourronc et al. 2013 proposed that VM was entirely glaciated during the Late Noachian to Early Hesperian and still contains large volumes of fossil ice held below a low

ablation sediment surface. This hypothesis was made on the basis of glacially related geomorphology found within Ius Chasma, Central Candor Chasma and the junction between Corprates Chasma and Capri Chasma (Gourronc, et al., 2013). Gourronc et al (2013) outlines a boundary, known terrestrially as a glacial trimline, between the rough spur-and-gully morphology and smooth basal escarpment. They also identify associated glacial geomorphologic landforms such as: lateral benches, hanging valleys and truncated spurs along the walls, and hummocky terrains, lateral banks and layered benches for the floor morphology. The trimline in association with chasma floor morphology indicates an ancient glacial fill at various disintegration stages (Gourronc, et al., 2013). Using the trimline as a boundary for the extent of glaciation throughout VM, Gourronc et al. (2013) calculated the ice within the chasmata to be $0.3X10^6$ km^3 (Fig. 4).

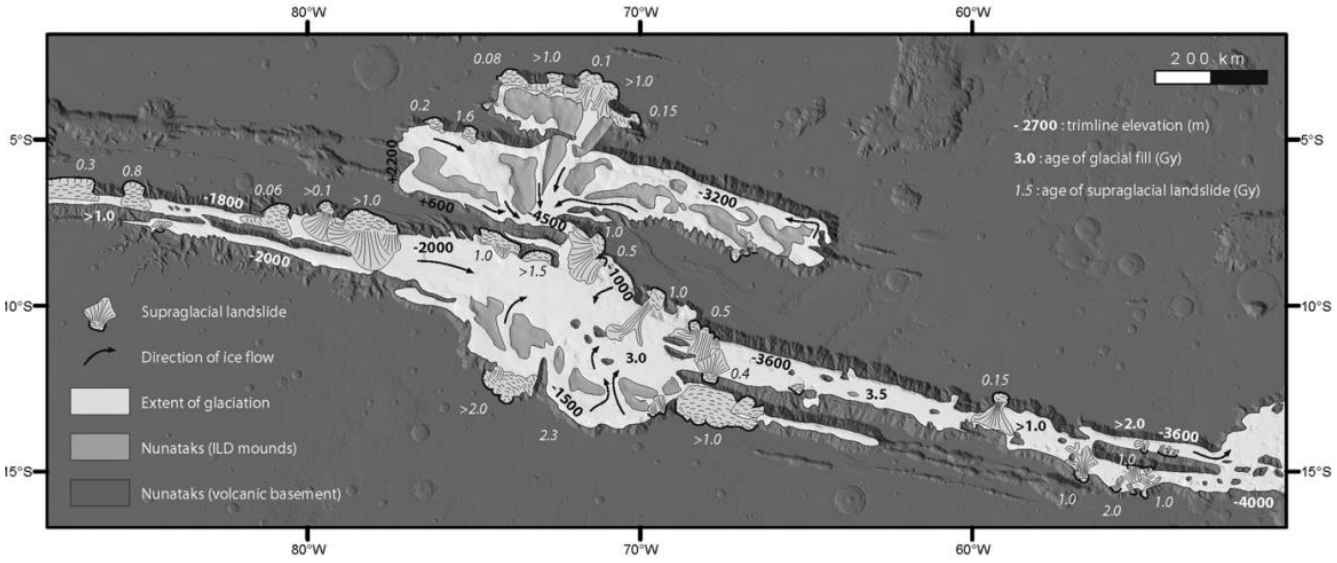

Figure 1-4: Proposed extent of glaciation and location of supraglacial landslides in Valles Marineris. After Gourronc et al. 2014.

1.8 Sulfates

Spectral analysis of ILDs within VM has revealed that hematite-bearing mineral as well as poly- and monohydrated sulfates are always associated with ILDs (Murchie, et al., 2009; Flahaut, et al., 2010). Sulfates are abundant in the VM region and have been detected in association with sedimentary deposits. It has been proposed that the sulfate occurrences are likely related to water and the climate history of Mars. The sulfates have been interpreted to represent a global climate change on Mars from the Noachian through the Hesperian (Flahaut, et al., 2010). This is marked by a change from monohydrated sulfates to polyhydrated sulfates (alkaline to acidic pH conditions) and a transition from a wetter to a drier environment (Bibring, et al., 2006). Conditions favouring the formation of hydrous minerals on Mars may have occurred for the majority of Mars' history, from the Noachian to the Amazonian (Quantin, et al., 2004). Fluvial activity was highest during the Middle Noachian into the Amazonian (Carr & Head III, 2010) allowing bodies of water to persist on the surface of Mars for extended periods of time. Evidence supports that monohydrated sulfates occur at lower elevations while polyhydrated sulfates occur at higher elevations (Flahaut, et al., 2010; Fueten, et al., 2014). Hydrated sulfates are known to form where water has been concentrated and exposed to prolonged periods of evaporation in a sulfur-rich environment (Roach, et al., 2009). A polyhydrated sulfate contains an extra water molecule and indicates material which is more porous or a higher degree of fluid pressure in the exposed area (Flahaut, et al., 2010). The study of sulfates in VM is important as it represent the largest sulfate reservoir known on Mars and contains vital information on the depositional history of ILDs in the area.

1.9 Interior Layered Deposit Formation Mechanisms

There is some debate on whether the ILD formed before or after formation of the chasma. Some propose that the sediments are Noachian in age, predating the formation of the chasma (Malin & Edgett, 2000; Catling, et al., 2006); providing evidence for support as layered materials in the spurs and ravines of the chasmata walls and other superposition relationships (Komatsu, et al., 2004). A model proposed by Andrews-Hanna (2012b) suggested that basin collapse and ILD deposition are linked, where sediments were deposited contemporaneously with basin collapse. The author proposed that extension at VM was controlled by intrusive activity. As the radial dikes were emplaced the lithosphere was weakened causing the blocks to subside until they reached an isostatic level. As sediments began to infill the additional load caused the basin to subside further. The total estimated subsidence is thought to be 8.6 $\pm$ 5.6 km (Andrews-Hanna, 2012b). Others suggest the sediments are Hesperian to Amazonian in age and accumulated during or after the formation of the chasma (Okubo, 2010). Evidence for the latter argument involves a more diverse means of analysis, with geomorphology, geologic mapping and structural analysis (Okubo, et al., 2008) and is therefore seen as the stronger argument.

Mars' surface shows a complex history of sedimentary deposition by water and aeolian processes. Strata outcropping within basins are particularly important because they provide information on Martian paleoclimate. ILD formation can be explained by processes similar to those found on Earth. A variety of processes and depositional regimes, including sedimentary and volcanic settings, have been proposed to explain ILD formation: Subaerial transport (Malin and Edgett 2000, Fueten et al. 2011); Subaqueous transport (Malin & Edgett, 2000); Lacustrine (Komatsu et al. 2004, Fueten et al. 2006, Flahaut et al. 2010); volcanic (Komatsu 2004, Malin and Edgett 2000, Flahaut et al 2010); sub-ice (Komatsu et al. 2004, Flahaut et al. 2010); mass wasting (Komatsu et al. 2004, Flahaut et al. 2010); seasonal snowmelt (Kite et

al. 2013, Fueten et al. 2014) and groundwater springs (Rossi et al 2008, Mangold et al. 2008); ash fall (Lucchitta 1990, Chapman 2002, Komatsu et al. 2003, Fueten et al. 2014); and Katabatic winds (Kite et al. 2013). Several formation mechanisms have been proposed to explain the deposition of ILDs and are described below. It is possible that more than one formation mechanism is responsible for the deposition of ILDs.

1.10 Subaerial Formation Mechanisms

Subaerial and subaqueous transport encompasses a variety of processes. Subaerial transport is affected by the atmosphere and wind effects can include processes like: dust storms, dust mantles, volcanic ash fall and aeolian processes (Malin & Edgett, 2000). Fine debris is easily transported through the atmosphere and the extensive distribution of light toned material provide evidence to support this hypothesis. Dust storms would likely have persisted throughout the planet's history and occur often on Mars to this day. Kite et al. 2016 presents a simplified model where aeolian deposits are observed in ILD mounds draping over pre-existing geology. They suggest that wind played an important role in erosion and deposition of mound material. Evidence to support the hypothesis was: layering orientations dipping away from crest of mound, unconformity-bound packages thin upwards, internal unconformities containing a dome shape, average dip magnitudes cluster at the mound height-to-width ratio and layer orientations frequently conform to modern topographic slope (Kite, et al., 2016). While there is good evidence to suggest aeolian processes on the planet's surface it is likely not the only mechanism of sediments deposition. Support for subaqueous processes can be found in many locations on the surface of Mars.

1.10.1 Subaqueous Formation Mechanisms

Subaqueous transport involves alluvial, lacustrine or deltaic mechanisms. Of these proposed mechanisms, the lacustrine setting is the most favourable. Nedell et al. (1987) provided evidence to support the lacustrine hypothesis by stating that wall sediments would have been deposited in the deeper portions of the chasma floors by gravity flows as nearly horizontal layers. Lucchitta (2010) has long thought VM could hold lakes on the surface of Mars by comparing the surface of Mars to known formations and processes found on Earth. Lucchitta (2010) noted that the equatorial region of Mars, in particular near VM, displayed landslides, debris flows, ravines and gullies that appeared to be the result of fluvial processes. One of the most convincing pieces of evidence provided in support of a lacustrine formation mechanism is the presence of sulfates found within the ILDs. The presence of sulfates provides geochemical analysis that has been replicated in a lab using Geochemists Workbench software under the same conditions that would have been found on Mars during the time of chasma formation (Al-Samir, et al., 2017). AL-Samir (2017) provides geochemical analysis of sulfate deposits within the chasma. These deposits indicate precipitation as a result of evaporation processes related to chemical reactions of sulfate solutions with chasma rocks. The resulting sulfate precipitations indicate Juventae Chasma likely contained a paleolacustrine lake (Al-Samir, et al., 2017). The horizontal/near-horizontal nature of the ILD indicate that water associated mechanisms would have been low-energy in nature, such as settling in lacustrine conditions. The lacustrine hypothesis requires that the sediments were deposited while VM was a series of troughs, before further extension formed a series of basins (Lucchitta, 1994). Some of the drawbacks of the lacustrine setting is that Mars would require a thick enough atmosphere to sustain large bodies of water for a prolonged period. These lakes would also have had to be as high as the chasma walls in the late stages of ILD deposition due to the height of mounds. This is possible if VM was a series of troughs, as suggested by Lucchitta (1994). A newer model provided by Andrews-Hanna (2012b) suggests that subsidence was driven by sediment infill and the two

remained in isostatic equilibrium. Fueten et al. (2014) agrees with Andrews-Hanna (2012) and hypothesize that water depth within some chasma was no more than a several hundred meters and the collapse occurred as multiple events. While the lacustrine method is well explained it lacks some important evidence, such as: the absence of overland streams, valleys and alluvial processes (Lucchitta 1994, Malin and Edgett 2000), the lack of confining barriers, the separation of ILD from walls by moats and no clear identifiable shorelines (Komatsu, et al., 2004). Theses inconsistencies can be explained by erosion, slope processes and depositional history of the area (Komatsu, et al., 2004).

1.10.2 Volcanic Formation Mechanisms

Deposits in the form of volcanic ash have been proposed and would explain the observed draping of sediments over pre-existing geology (Komatsu, et al., 2004). Evidence supporting volcanic origin of ILD formation are: variable lithologies of different ages and heights, massive, free-standing mounds, composition of ILD material, volcanic/tectonic setting and low albedo, high competence and weathering of layers (Chapman & Smellie, 2007). Evidence lacking in the volcanic origin of ILD is the large size emplacement when compared to terrestrial analogues (Komatsu, et al., 2004). The lower atmospheric pressure of Mars would cause higher eruption velocities, which would produce large deposits, but not to the scale measured within VM. Another problem with this hypothesis is the lack of vents observed within or near the area. Usually, volcanic materials would be localized near the source, but with no visible ruminants of volcanic vents within VM the layered deposits appear too remote to create such large deposits (Malin & Edgett, 2000). Furthermore, the absence of volcanic material on the plateau argues against volcanic origin. It is possible that the any plateau deposits were eroded by strong wind while those in the chasms were protected by the walls (Komatsu, et al., 2004).

It is possible that more than one formation mechanism is responsible for the formation of ILD within VM. All are possible forms of deposition under the appropriate conditions.

1.11 Erosional Features of ILDs

It is widely believed that Martian climate has changed dramatically over time, particularly in the Hesperian (Carr & Head III, 2010). This implies changes in erosional methods of ILDs throughout history (Head et al 2001). ILDs display a wide range of erosional features, this makes narrowing down the dominant erosive process difficult. It is likely that more than one erosional process has impacted ILDs in the past causing the variety of erosional features observed today (Armstrong and Leovy 2005). It is widely accepted that wind is the major erosional process predominantly influencing ILDs today. Large and small-scale dunes are the most common aeolian feature observed on the Martian surface. However, evidence supports more than just aeolian erosional methods. Some erosional features provide evidence of glacial erosion (Lucchitta, 1982; Hauber, et al., 2008; Gourronc, et al., 2013). While many more indicate fluvial erosion, like outflow channels, streamlined islands and furrows (Burr, et al., 2009). It is thought that catastrophic outflow events are responsible for merging chasms and removing some of the ILDs during the process (Lucchitta, 1994).

1.12 Purpose of study

This study focuses on the geology of East Candor Chasma. The central mounds of East Candor Chasma comprise some of the largest ILD deposits within the Valles Marineris. Determining the layer attitudes, thickness and elevation in the attempt to correlate the mounds within the central part of the chasma will provide insight into the depositional history of ILDs within Valles Marineris. The work is organized

into three chapters that separate types of layers that are observed within East Candor Chasma, geology of the central mounds and morphology of ILDs along the south wall.

Chapter 2 provides an overview of East Candor Chasma and analyzes the different types of layers that are observed within East Candor Chasma. The ILD material in the mounds has been grouped into five distinct varieties of bedding based on their appearance in CTX imagery: massive, thin layering, thick layering, deformed layering and thin mesa.

Chapter 3 analyzes the attitude and structure of the central mounds within East Candor Chasma; including a major unconformity that separates a massive unit from the layered unit. An attempt is made to correlate mounds throughout the chasma using layer attitude and unit variety. A discussion of ILDs along the south wall and the role that the chasma wall plays in deposition finishes the chapter

Chapter 4 focuses on a summary of observations found in East Candor and relates them to known observations throughout VM. A model for the geological history of East Candor is presented.

References

Al-Samir, M. et al., 2017. The paleolacustrine evolution of Juventae Chasma and Maja Valles and its implications for the formation of interior layered deposits on Mars. *Icarus,* pp. 125-143.

Andrews-Hanna, J. C., 2012a. The formation of Valles Marineris: 1. Tectonic architecture and the relative roles of extension and subsidence. *Journal of Geophysical Research,* Issue 117.

Andrews-Hanna, J. C., 2012b. The formation of Valles Marineris: 3. Trough formation through super-isostasy, stress, sedimentaton and subsidence. *Journal of Geophysical Research,* Issue 115.

Andrews-Hanna, J., Phillips, R. J. & Zuber, M. T., 2007. Meridiiani Planum and the global hydrology of Mars. *Nature,* pp. 163-166.

Burr, D. M., Carling, P. A. & Baker, V. R., 2009. *Megaflooding on Earth and Mars.* New York: Cambridge University Press.

Carr, M. H. & Head III, J. W., 2010. Geologic History of Mars. *Earth and Planetary Sciences,* pp. 185-203.

Catling, D. C. et al., 2006. Light-toned layered deposits in Juventae Chasma, Mars. *Icarus,* pp. 26-51.

Chapman, M. G. & Smellie, J. L., 2007. *Mars interior layered deposits and terrestrial sub-ice volcanos compared: observations and interpretations of similar geomorphic characteristics.* Cambridge: Cambridge University Press.

Flahaut, J. et al., 2012. Pristine Noachian crust and key geologic transitions in the lower walls of Valles Marineris: Insights into early igneous processes on Mars. *Icarus,* 221(1), pp. 420-435.

Fueten, F. et al., 2014. Stratigraphy and mineralogy of Candor Mensa, West Candor Chasma, Mars: Insights into the geologic history of Valles Marineris. *Journal of Geophysical Research: Planets,* 119(2), pp. 331-354.

Fueten, F. et al., 2017. The Evolution of Juventae Chasma, Valles Marineris, Mars: Progressive Collapse and Sdeimentation. *Journal of Geophysical Research: Planets,* Volume 122.

Fueten, F. et al., 2006. Structural study of an interior layered deposit in southwestern Candor Chasma, Valles Marineris, Mars, using high resolution stereo camera data from Mars Express. *Geophysical Research Letters,* 33(7).

Golombek, M. P. & Phillips, R. J., 2010. Mars Tectonics. In: T. R. Watters & R. A. Schultz, eds. *Planetary Tectonics.* New York: Cambridge University Press, pp. 183-232.

Gourronc, M. et al., 2013. One million cubic kilometers of fossil ice in Valles Marineris: Relicts of a 3.5 Gy glacial landsystem along the Martian equator. *Geomorphology,* Volume 204, pp. 235-255.

Hartmann, W. K. & Neukum, G., 2001. Cratering Chronology and the Evolution of Mars. *Space News Reviews,* 96(1-4), pp. 165-194.

Head, J. W. et al., 2001. Geological processes and evolution. *Space Science Reviews,* pp. 263-292.

Head, J. W. et al., 2006. Extensive valley glacier deposits in the northern mid-lattitudes of Mars: Evidence for Late Amazonian obliquity-driven climate change. *Earth and Planetary Science Letters,* pp. 663-671.

Head, J. W. et al., 2003. Recent Ice Ages on Mars. *Nature,* pp. 797-802.

Jakosky, B. M., Henderson, B. G. & Mellon, M. T., 1995. Chaotic obliquity and the nature of Martian climate. *JGR: Planets,* pp. 1579-1584.

Kite, E. S. et al., 2016. Evolution of major sedimentary mounds on Mars: Buildup via anticompensational stacking modulated by climate change. *Journal of Geophysical Research: Planets,* Issue 121, pp. 2282-2318.

Komatsu, G., Ori, G., Ciarcelluti, P. & Litasov, Y., 2004. Interior Layered Deposits of Valles Marineeris, Mars: Analogus subice volcanism related to Baikal rifting, southern Siberia. *Planetary and Space Science,* pp. 167-187.

Lucchitta , B. K., 1990. Young volcanic deposits in the Valles Marineris, Mars?. *Icarus,* pp. 476-509.

Lucchitta , B. K., 2010. Lakes in Valles Marineris. In: N. A. Cabrol & A. G. Edmond, eds. *Lakes on Mars.* Oxford: Elsvier, pp. 111-152.

Lucchitta, B. K., 1982. Ice Sculpture in the Martian Outflow Channels. *Journal of Geophysical Research,* pp. 9951-9973.

Lucchitta, B. K., 1994. Topography of Valles Marineris: Implications for erosional and structural history. *Journal of Geophysical Research,* pp. 3783-3798.

Luccitta, B. K. et al., 1992. The canyon system on Mars. *Mars,* pp. 453-492.

Malin, M. C. & Edgett, K. S., 2000. Sedfimentary Rocks of Early Mars. *Science,* pp. 1927-1937.

Mege, D., 2001. Uniformitarian plume tectonics: The post-Archean Earth and Mars, in mantle plumes: Their identification through time. *Geological Society of America,* pp. 141-164.

Mege, D., 2006. Graben Morphology, Dike Emplacement, and Tension Fracturing in the Thrasis Igneous Province of Mars. *Journal of Geophysical Research,* pp. 4-6.

Mege, D. & Ernst, R. E., 2001. Contractional effects of mantle plumes on Earth, Mars and Venus in the mantle plumes: Their identification through time. *Geological Society of America,* pp. 103-140.

Mege, D. & Masson, P., 1996. A plume tectonics model for the Tharsis province, Mars. *Planetary and Space Science,* 22(12), pp. 1499-1546.

Metz, J., Grotzinger, J., Okubo, C. & Milliken, R., 2010. Thin-skinned deformation of sedimentary rocks in Valles Marineris, Mars. *Journal of Geophysical Research,* Volume 115, pp. 1-28.

Michael, G. G. & Neukum, G., 2010. Planetary surface dating from crater size-frequency distribution measurements: Partial resurfacing events and statistical age uncertainty. *Earth and Planetary Science Letters,* 294(3-4), pp. 223-229.

Mischna, M. A., Richardson, M. I., Wilson, R. J. & McCleese, D. J., 2003. On the orbital forcing of Martian water and CO2 cycles: A general circulation model study with simplified volatile schemes. *JGR: Planets,* pp. 1-25.

Murchie, S. et al., 2009. Evidence for the origin of layered deposits in Candor Chasma, Mars, from mineral composition and hydrologic modeling. *Journal of Geophysical Research,* Volume 114, pp. 1-15.

Nedell, S. S. & Squyres, S. W., 1987. *Formation of the layered deposits in the Valles Marineris, Mars.* Woodlands, United States, pp. 88-90.

Okubo, C. H., 2010. Structural Geology of Amazonian-aged layered sedimentary deposits in southwest Candor Chasma, Mars. *Icarus,* pp. 210-225.

Okubo, C. H., Lewis, K. W., McEwen, A. S. & Kirk, R. L., 2008. Relative age of interior layered deposits in southwest Candor Chasma based on high-resolution structural mapping. *Journal of Geophysical Research,* pp. 1-15.

Peulvast, J. P. & Masson, P. L., 1993. Erosion and tectonics in Central Valles Marineris (Mars): a new morpho-structural model. *Earth, Moon and Planets,* 61(3), pp. 191-217.

Quantin, C., Allemand, P., Mangold, N. & Delacourt, C., 2004. Ages of Calles Marrineris (Mars) landslides and implications for canyon history. *Icarus,* pp. 555-572.

Roach, L. H. et al., 2009. Testing evidence of recent hydration state change in sulfates on Mars. *JGR: Planets,* pp. 1-13.

Schmidt, G., 2015. *Geology of Hebes Chasma, Valles Marineris, Mars,* s.l.: s.n.

Schultz, R. A., 1998. Multiple-process origin of Valles Marineris basins and trough, Mars. *Planetary and Space Science,* 46(6-7), pp. 827-829.

Tanaka, K. L., 1986. The stratigraphy of Mars. *Journal of Geophysical Research.*

Tanaka, K. L. & Golombek, M. P., 1989. Martian tension fracture and the formation of grabens and collapse features at Valles Marineris. *Lunar and Planetary Science,* pp. 383-396.

Touma, J. & Wisdom, J., 1993. The chaotic obliquity of Mars. *Science,* pp. 1294-1296.

Ward, W. R., Burns, J. A. & Toon, O. B., 1979. Past Obliquity oscillations of Mars: The role of the Tharsis Uplift. *Journal of Geophysical Research,* pp. 243-259.

Wilson, L. & Head, J. W., 2002. Tharsis-radial graben systems as the surface manifestation of plume-related dike intrusion complexes: Models and implications. *JGR: Planets,* 107(E8), pp. 1-24.

2.0 Chapter 2: Unit Classification of ILDs in East Candor Chasma

2.1 Introduction

East Candor Chasma contains some of the largest continuous ILD mounds in VM. Malin and Edgett (2000) defined three classes of ILD units within VM as layered, massive and thin mesa (Figure 2-1). This classification was based on visual appearance, texture, thickness and layering style. Layered units are described as light to intermediate toned, are made up of units that can be described as thin or thick (a few meters to 2000 meters), and contain one to hundreds of thin, tabular sub-units or beds (Malin & Edgett, 2000). Bounding surfaces are visible between layering as a dark lineation that can be traced the length of the unit. Massive units are light to intermediate toned, hundreds of meters to a few kilometers thick, display no visible internal layering and in some instances, include forms that are transitional from layered to massive. There have been a few documented occurrences where well-bedded layered units appear below the massive units (Malin & Edgett, 2000). It is more common to see massive beds at the base of the chasms, overlain by layered units followed by thin mesa units (Malin & Edgett, 2000). Thin mesa units typically consist of dark or intermediate toned, thin, mesa-forming materials. These are found nearly everywhere layered or massive units occur and have surfaces that vary from smooth to pitted to ridged and grooved (Malin & Edgett, 2000). Thin mesa units lie unconformably over layered and massive units (Malin & Edgett, 2000). This relationship can be best observed on slopes where layered units exposed and thin mesa units drape across the underlying beds (Okubo, 2010). The relationship between the thin mesa, layered and massive beds has been used to conclude that the depositional history of ILD formation is multistage (Fueten, et al., 2014). Unconformities within East Candor Chasma appear to be angular unconformities or disconformities; providing evidence to support multi-stage deposition. In this chapter, the ILDs in East Candor are classified using more diverse variety of categories to interpret the depositional history of the ILDs found within the chasma.

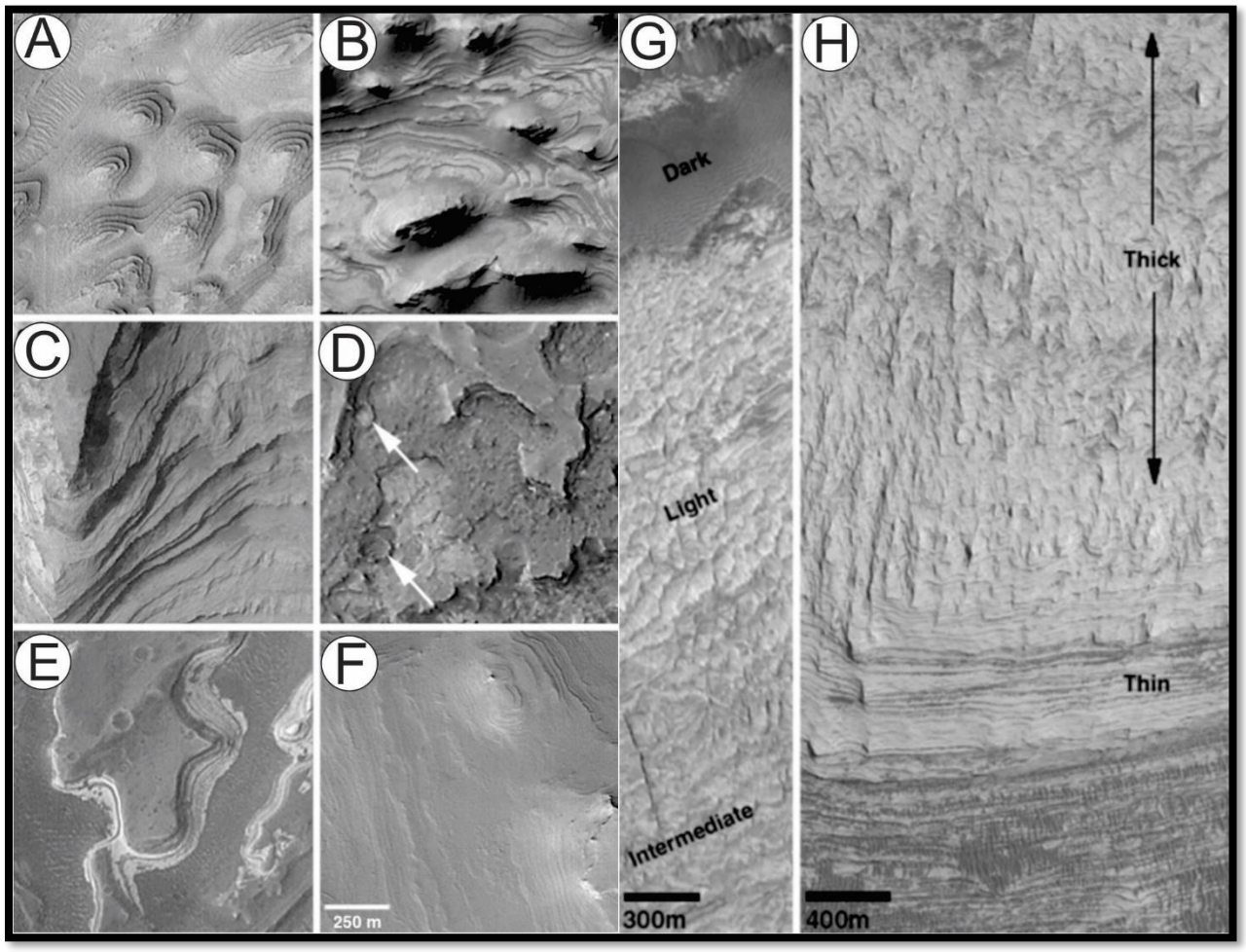

Figure 2-1: Layer unit styles detailed after Malin & Edgett (2000). Six images on left depict a variety of ILD found around and in VM-A: Stair-stepped hills in Arabia Terra; B: Cliff-bench terrain in Southwest Candor Chasma; C: Irregular cliff-bench on slope in Terby Crater; D: Cliff-bench terrain with layers displaying different tone and interbedded craters in Terra Meridiani; E: Alternating light- and dark-toned, banded outcrop in Holden Crater; F: Dust-mantled (uniform tone) cliff-bench outcrop in Henry Crater. Images on the right depict albedo of layering (light, intermediate and dark) (G) as well as styles of layering (thin and thick) (H).

2.2 ILDs in East Candor Chasma

East Candor Chasma is located on the northeastern portion of VM and contains multiple ILD mounds. The chasma is 475 km long, 145 km wide and ranges in elevation from -5.5 km on the floor of the

chasma to 3.5 km at the highest point on the central ILD mounds (Fig 2-2). The chasma is contained on three sides by chasma walls, the fourth side opens into Central Candor Chasma. The chasma is long and relatively narrow in comparison to its length. In the central part of the chasma there are 4 major ILD mounds (A-D) with 4 smaller minor mounds (1-4) (Fig 2-2). These minor mounds are treated as four distinct deposits that will be discussed further in the chapter. Additional deposits along the chasma walls will also be described, as layering is observed draping the south wall of East Candor Chasma. The deepest part of the chasma is located along the base of the north wall. It is thought that this section of the chasma contains a major fault that likely runs the length of the wall (Lucchitta, 1994). Evidence has been presented in support of an ancient lake occupying the chasma with sediments being deposited over time (Lucchitta, 1994; Fueten, et al., 2017). Lucchitta (1994) proposed that the basins could have been filled by kilometer deep lakes before they were filled with sediments. Fueten, et al. (2017) suggested that ILD formation, elevation and erosion is subject to changes in lake levels within Juventae Chasma. It is possible that much of VM has been subjected to changes in lake levels over time including East Candor Chasma.

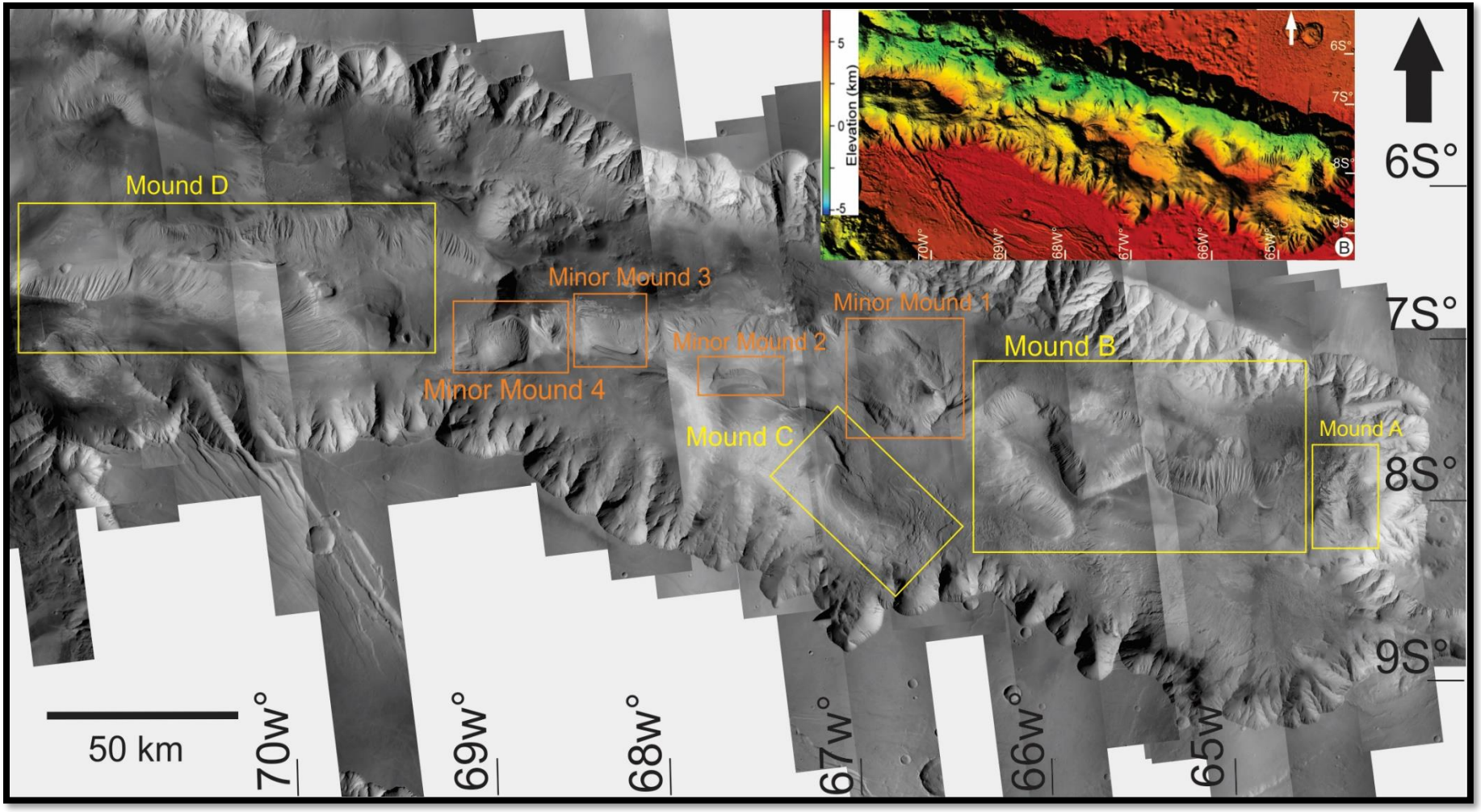

Figure 2-2: East Candor Chasma CTX mosaic 20 m/pixel. Inset B: HRSC Elevation map 50 m/pixel. CTX Mosaic 20m/pixel, mound out in yellow; minor mound outlines in orange.

2.3 Current Interpretation of East Candor Chasma's Geological History

High Resolution mapping suggests the geological history of East Candor Chasma is complex. Okubo (2017) is in the process of producing detailed geologic maps based on HiRISE images for an area in the chasma to the north of Nia Mensa (Fig 2-3). Nia Mensa is the official name given to Mound C. A section on the north end of the mesa encompasses the contact between massive sedimentary rocks that make up most of Nia Mensa and the stratified sedimentary and mass-wasting deposits exposed between Nia Mensa and the northern wall (Okubo, 2017). That work provides evidence that at least four geologic units were affected by soft sediment deformation in the form of subsurface sediment mobilization. A trough network identified in the northeastern portion of Okubo's (2017) HiRISE mapping area has been interpreted as the vent area for erupted mobilized sediments (mud flows). It is thought that the soft sediment deformation occurred after the ILDs were emplaced as the sediment flows cover pre-existing geology. These findings indicate that the local sediments were poorly indurated, and water saturated at the time of deformation (Okubo, 2017).

Le Deit (2008) produced a simplified map of East Candor detailing the major landforms in the chasma (Fig 2-4). Layered deposits, consolidated or remobilized, make up the largest portion of the chasma. Other landforms of the chasma include: the canyon floor, landslides, wall slopes and wall remnants. Spur and gully morphology has been reworked by mass wasting processes; landslides are visible along chasma walls and floor (Peulvast, et al., 2001). The most active sedimentary process currently observed is Aeolian, producing dunes and yardangs (Le Deit, et al., 2008). ILDs are located in the central part of the chasma and in contact with much of the southern wall. Material that comprises ILD in East Candor Chasma is similar to other ILDs within VM and the surrounding region (Gourronc, et al., 2013; Okubo, 2016).

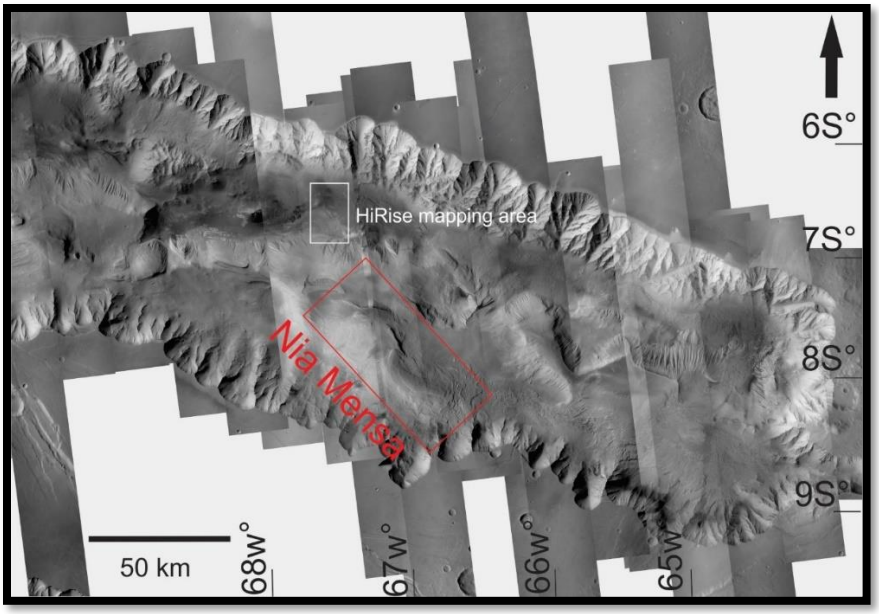

Figure 2-3: Nia Mensa outlined in red with northern Nia Mensa HiRISE geology mapping area outline in white.

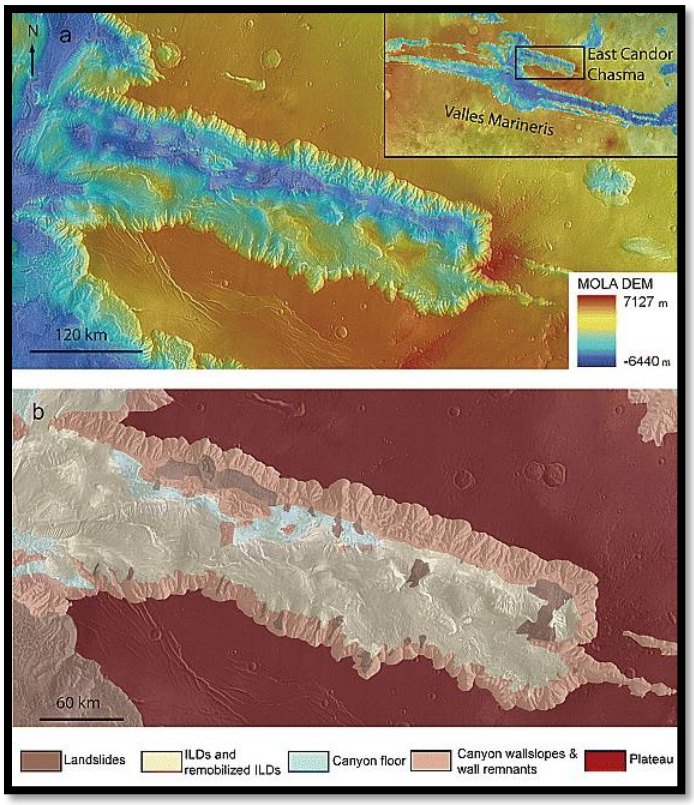

Figure 2-4: (a) location of East Candor Chasma on Mars. MOLA topographic map overlapping mosaic of THEMIS IR. (b) Simplified geologic map of East Candor Chasma Drawn from mosaic of MOC, THEMIS and HRSC (La Deit et al., 2008).

2.4 Sulfates

in East Candor Chasma

In East Candor a magnesium-rich variation of monohydrated sulfate, known as kieserite, and polyhydrated sulfates occur within the same deposit along the north wall of the chasma (Roach, et al., 2009). The area is comprised of a well-defined thick layer unit (Fig. 2-5). The deposit alternates between kieserite and the polyhydrated sulfate six times. A relationship was established between the alternating sulfates and their associated dips. The kieserite-dominated benches are found on cliff-forming units and polyhydrated sulfate-rich material is more common on flat units (Fig. 2-6). This is consistent with findings in other areas of VM (Flahaut, et al., 2010). Several hypotheses for these results have been proposed: (1) kieserite converting to a polyhydrated state once exposed to current surface conditions; (2) kieserite conversion requires a warmer and wetter environment in order to progress further; (3) changing brine chemistry allowed for a multisulfate evaporite assemblage (Roach, et al., 2009). There are complications with all three of the following hypotheses that need to be considered, such as the presence of other phases that are spectrally neutral upon analysis and unknown kinetics of sulfate phase change under Martian conditions (Roach, et al., 2009).

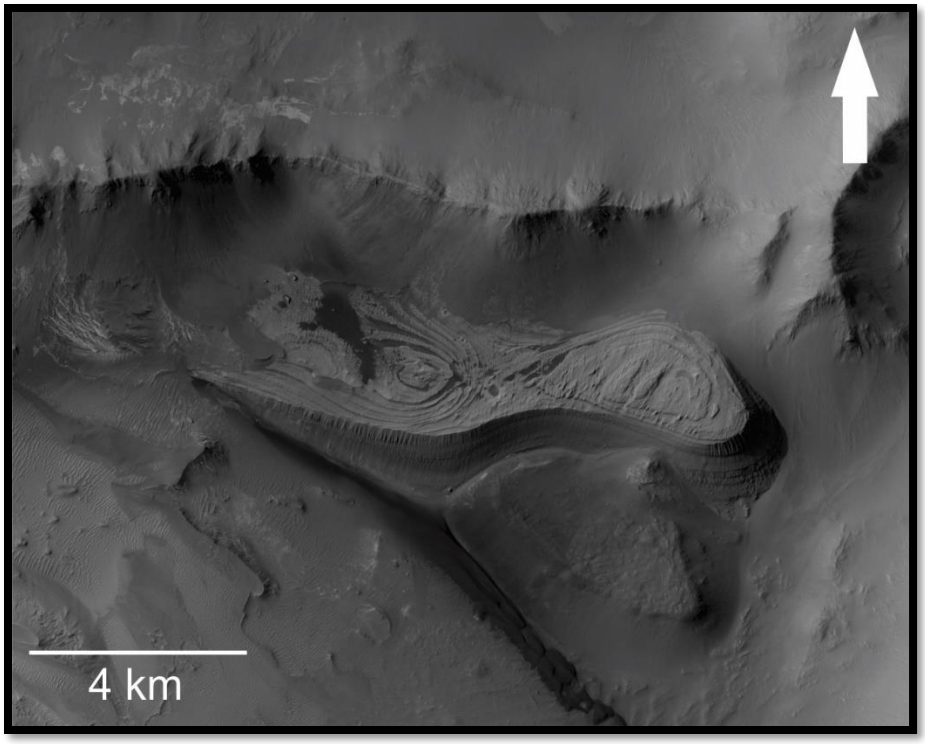

Figure 2-5: ILD with layering along the north wall of East Candor Chasma. CTX imagery 20 m/pixel.

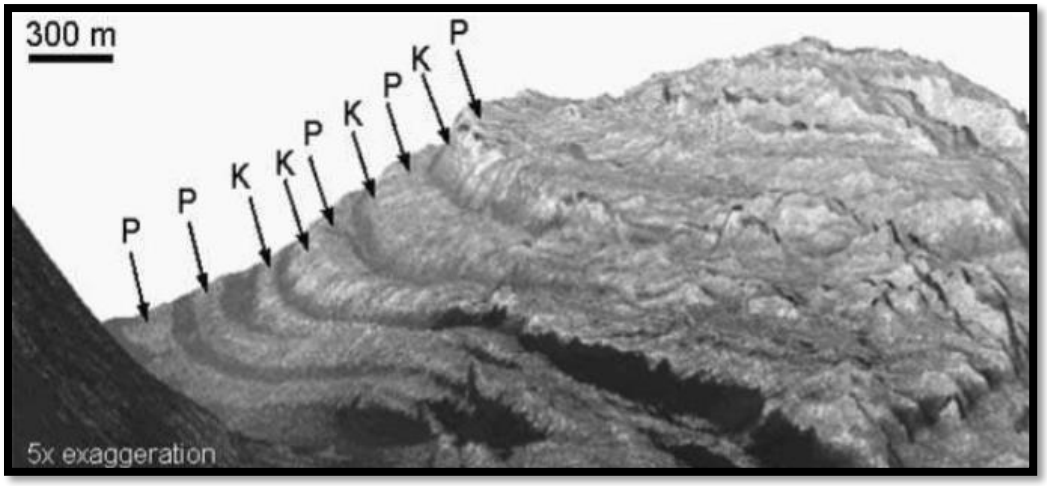

Figure 2-6: Alternating Kieserite-dominated units, labeled k, and polyhydrated sulfate-dominated units, labeled P. Kieserite units appear to have steeper slope than Polyhydrated sulfate units. Image facing east near north wall of chasma. Source: Roach et al., (2009).

2.5 Methodology for Layer classification

Data was acquired using multiple sources of satellite imagery, including: High Resolution Stereo Camera (HRSC), Context camera (CTX) and High-Resolution Imaging Science Experiment (HiRISE). CTX DTMs were calculated with NASA Ames Stereo Pipeline (Broxton & Edwards, 2008; Moratto, et al., 2010). HRSC, at a resolution of 50, 75, 100, and 175 m/pixel, served as the digital terrain model (DTM) base map for CTX and HiRISE imagery. A CTX mosaic, with resolution of 5m/pixel resolution, was registered to a HRSC composite DM. HiRISE, with a resolution of 0.5 m/pixel, imagery used to collect fine detailed analysis on layering style and visual data where relevant. In some instances, poor HiRISE and CTX imagery was substituted with HRSC imagery to ensure completeness of area mapping. A composite CTX map was made to depict 6 different layering styles within the ILDs of East Candor Chasma (Fig. 2-15) and is the focus of this chapter.

2.6 Layer Unit Classification

2.6.1 Layer Unit Varieties of East Candor Chasma

The sedimentary deposits in East Candor Chasma contain diverse layering styles that can be separated into different units -massive unit, thick layer unit (bench subunit), thin layer unit, thin mesa unit, deformed unit, steeply dipping unit-, discussed in more detail below. For the purpose of this study, a unit of a specific ILD is characterized by a combination of lithologic features that provide evidence of the unit's origin. This chapter focuses on categorizing the sedimentary layer varieties based on appearance, relative thickness and erosional features. Because erosive features can be indicative of competence, it is considered an indicator of determining ILD unit variety. The massive unit displays prominent ridge and gully texture when eroded. Although erosional style is not, on its own, a good indicator of a deposit's

composition, it can be distinct enough to identify a unit and is only used in conjunction with other indicators such as tone and thickness. Tone is used to describe the albedo (light, intermediate, dark) of ILD within the imagery. Tone cannot be quantified by a specific value as images are processed and enhanced before release. Throughout the chasma six distinct types of layering styles are recognized in this study: massive, thick layering, thin layering, deformed layering, steeply dipping layering and thin mesa.

2.6.2 Massive unit

The massive unit (Fig. 2-7) is light toned, has no visible layering and is eroded into a series of parallel linear downslope depressions when eroded. In East Candor this unit is located primarily stratigraphically below layered units. Mounds A, B and D are example locations. These mounds display a lower massive unit that is overlain by layered units (Fig. 2-8). There are a few locations where a layered unit appears stratigraphically lower than the massive unit (Fig. 2-9). Two sites occur along the northern wall where a suggested chasma-wide fault exists, north of minor-mound 2 near the northern wall of the chasma. In those areas the massive unit appears to be emplaced stratigraphically above a layered unit. It is rare to find this order of sequence; however, it has been described in other areas of VM by Malin and Edgett (2000). Layering within the massive unit cannot be ruled out, as layering might not be visible in the available image resolution.

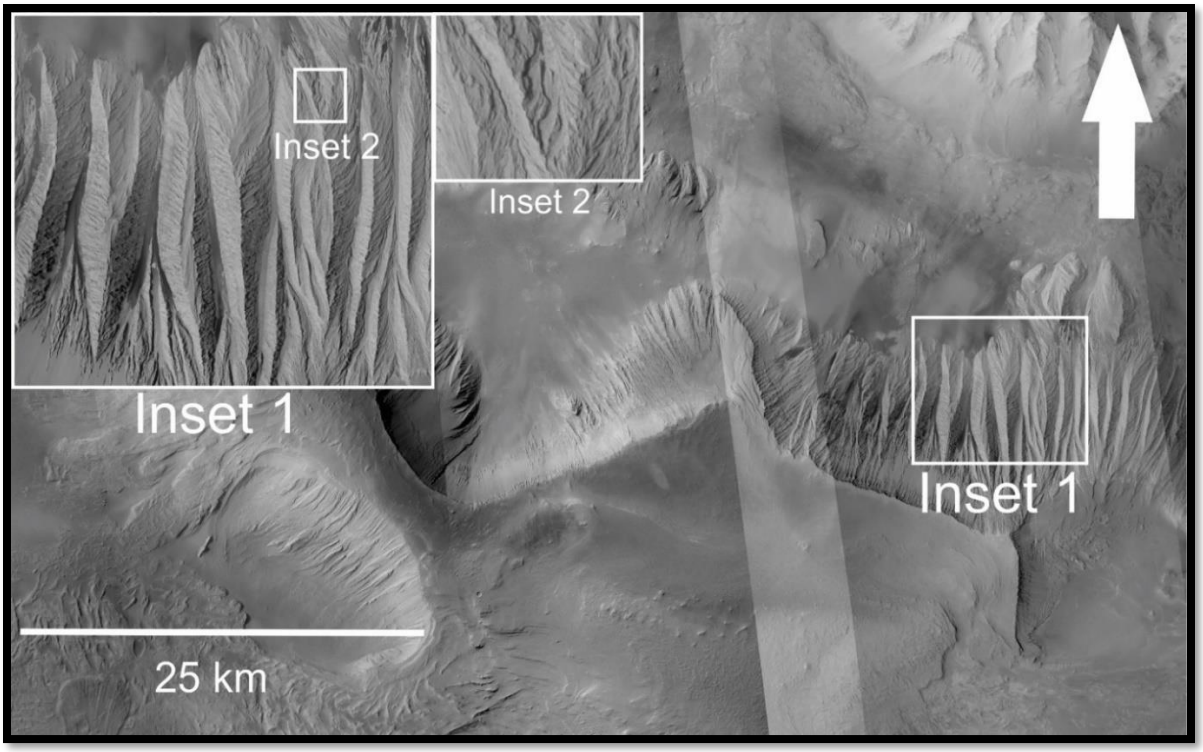

Figure 2-7: Example of massive unit found at base of ILD mound in East Candor. Insets 1 & 2 show close up of erosional texture massive unit displays.

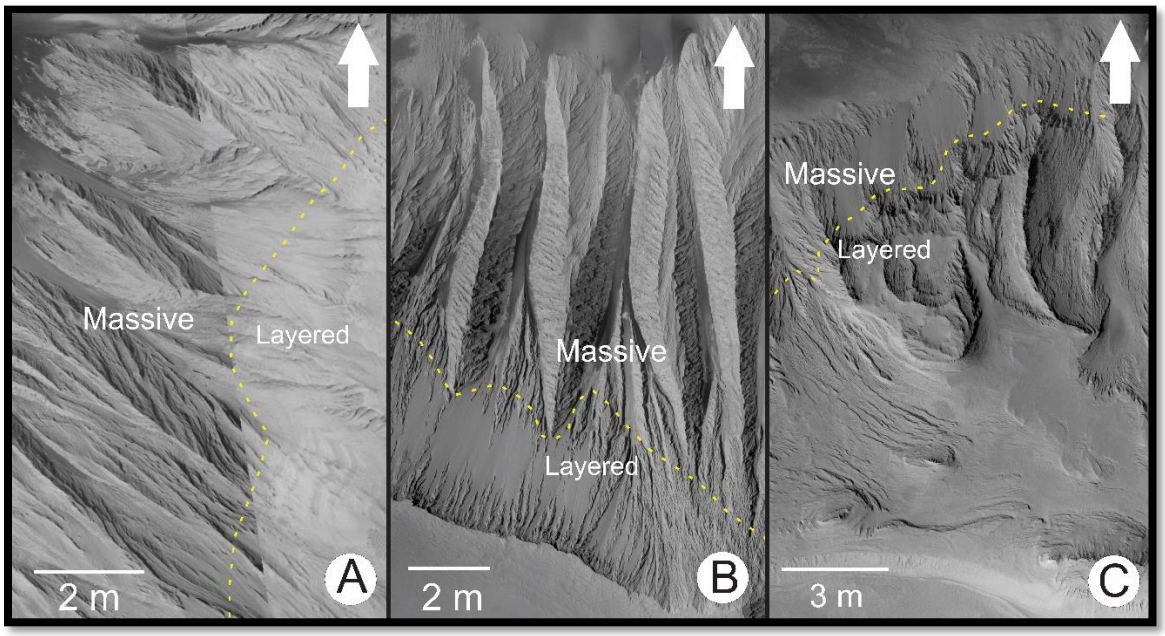

Figure 2-8: Mounds A, B and D from left to right. Images display massive unit stratigraphically lower than layered unit. Topographic high is at left in A and bottom in B & C.

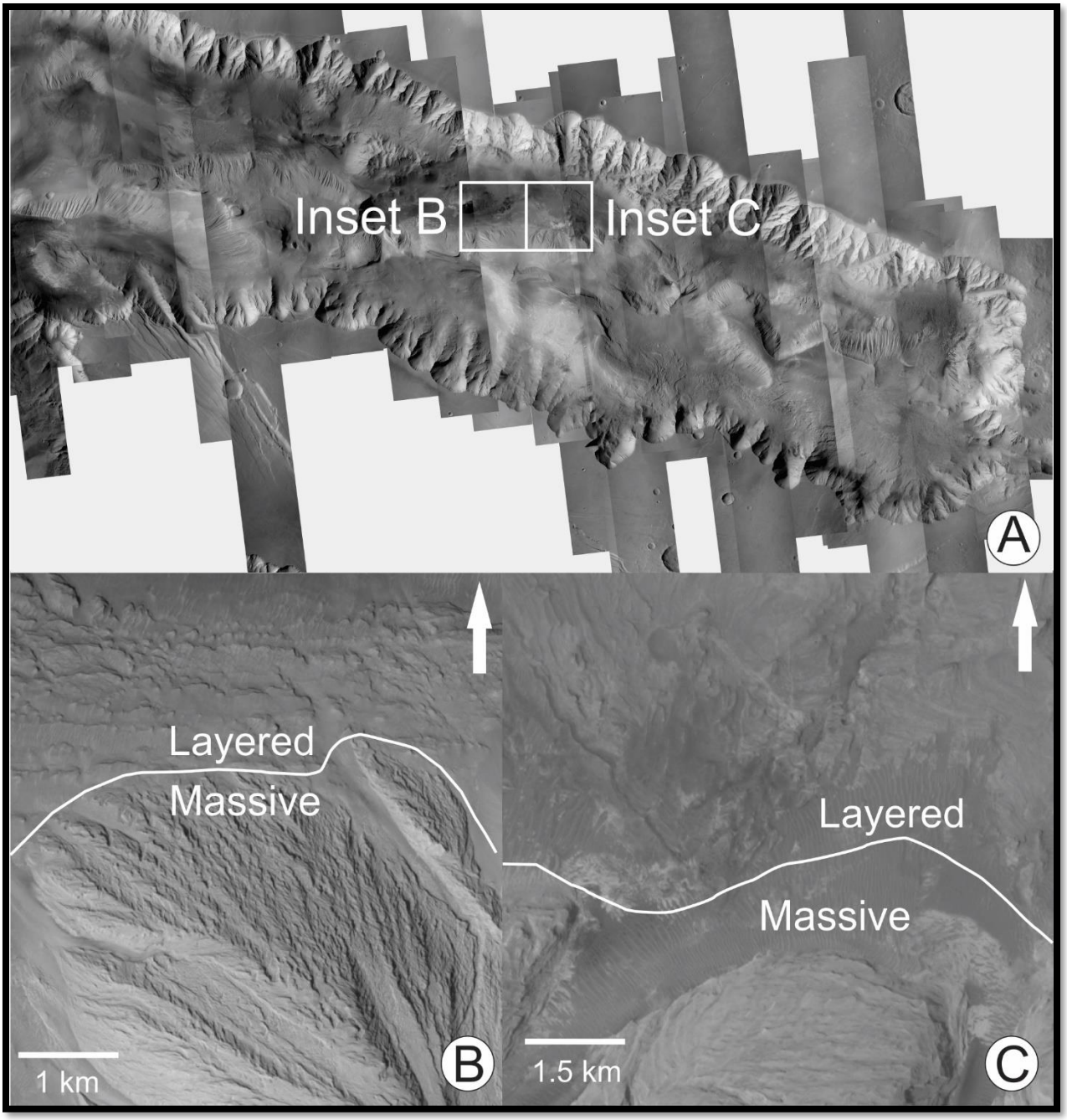

Figure 2-9 A: Inset boxes show area where massive unit is observed stratigraphically higher than layered unit in East Candor Chasma. B: Occurrence where massive unit appears to lie stratigraphically above layered unit located east of Minor Mound 3. C: Occurrence where massive unit appears to lie stratigraphically over layered unit, located northeast of Minor Mound 2. Layered unit can be observed best in upper left corner of image.

2.6.3 Thick layered Unit

The thick layered unit (Fig. 2-10) is light to intermediate toned, contains visible thick layering within the unit and is most often located in the mid-to-upper stratigraphic sections of ILD. Layer thickness within this unit ranges from ~2 km to ~25 m (see appendices). The thick layered unit displays a sub-unit, referred to as the bench subunit, which contain layers ~1-2 km in thickness. This sub-unit tends to be stratigraphically lower than other thick layers. It is uncertain whether the bench layering contains the same composition as the thick layering that is observed stratigraphically higher or whether it is the result of local erosion. Thick layer units occur in the central mounds, making up the largest portion of the chasma's ILDs outcropping at the surface. Layer thickness in the thick layered unit is variable within East Candor, forming cliffs and a variety of benches. In some of the largest ILD mounds containing thick layering, these units appear to thin upwards in stratigraphic sequence. At the base of the mounds thick layering appears as benches, where the tops of the mounds display thinner layering (Table 2-1). Variations in layer thickness are only discernible when there is a clear bounding surface to distinguish benches. Figure 2-10 shows well defined bounding surfaces separating benches from one another. The thick layered unit is the largest and most expansive unit within East Candor. This unit is almost exclusively found in the central mounds and along the south wall near the east end of the chasma.

Table 2-3: Layer thickness measurements taken from various locations on Mound B.

Average Thickness of Layer in Unit Measured (m)	**Elevation Range of unit measured (m)**	**Layer Unit Variety**
1685.0	635-2330	Thick Layering (Bench)
970.0	960-1850	Thick Layering (Bench)
924.0	1376-2300	Thick Layering (Bench)
64.0	1709-2157	Thick Layering
41.0	2519-3008	Thick Layering
5.0	3007-3069	Thin Layering

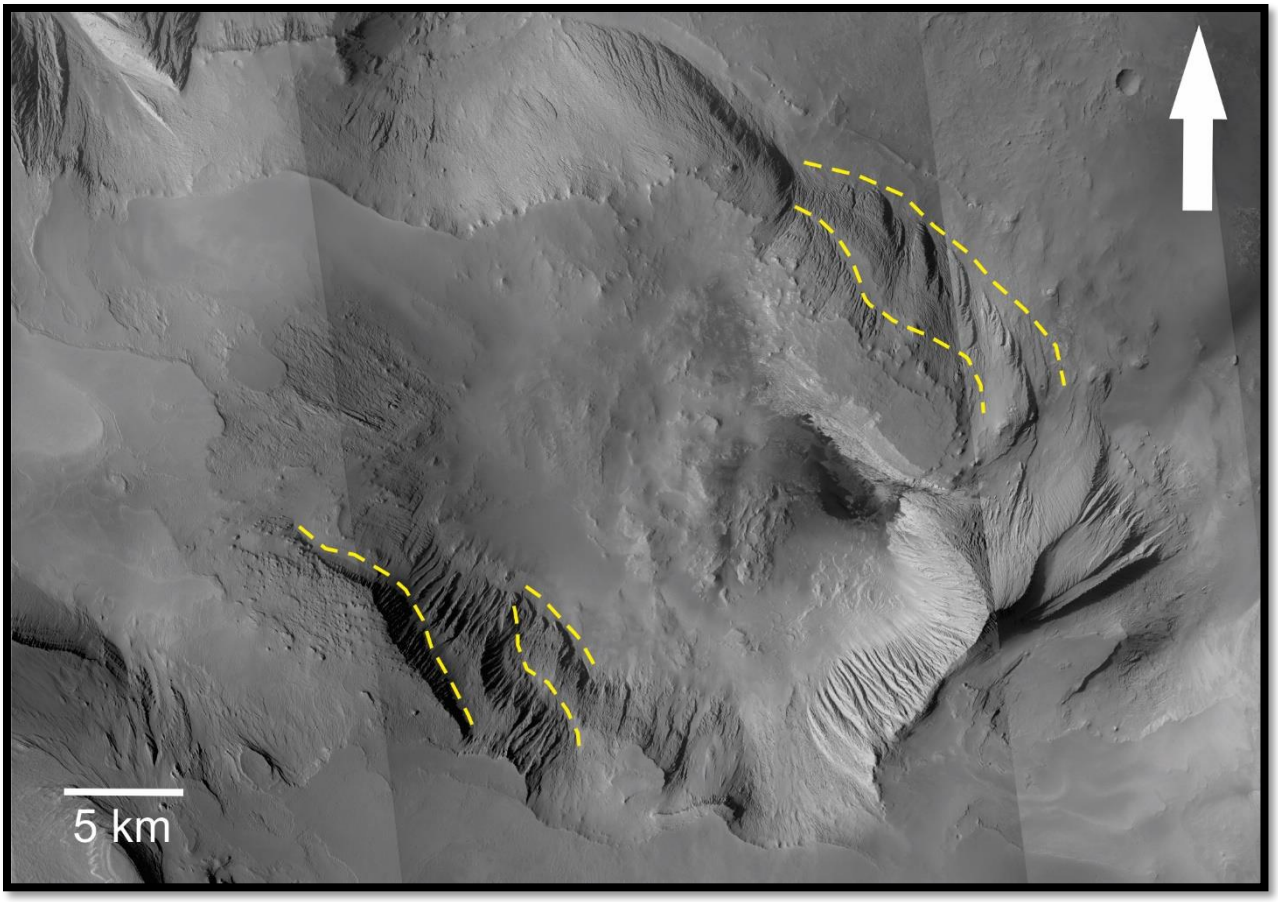

Figure 2-10: Example of Thick layered unit with well defined bounding surfaces found in East Candor Chasma. Topographic slope is to the north.

2.6.4 Thin layered unit

The thin layered unit (Fig. 2-11) is light to intermediate in tone, has visible layering and is often occurs on the uppermost stratigraphic sections of mounds and along the south wall of East Candor Chasma. Layer thickness ranges from <1 m up to ~25 m (see appendices). Within the upper-most sections of ILD mounds, thin layered material appears to be draping over the pre-existing geology conforming to the units below. This is interpreted from variations in dips observed in the upper sections of the mounds. Thin layered units contain one to hundreds of repeating beds often of approximately the same

thickness. These units appear to erode smoothly and contain mostly fine-grained materials (Malin & Edgett, 2000). The inset on the right of figure 2-11 shows the thin layering appearing to be either a later deposition on top of the thicker layered unit, or thinly layered material within the thick layered unit. At this point available imagery does not provide enough detail to determine which is true. The thin layered unit occurs in many locations within East Candor: along the southern wall, chasma floor, the tops of mounds and their sloping faces. The overall area covered by this unit is significantly smaller than the thick layered unit; however, patches of the thin layer unit occur throughout the chasma.

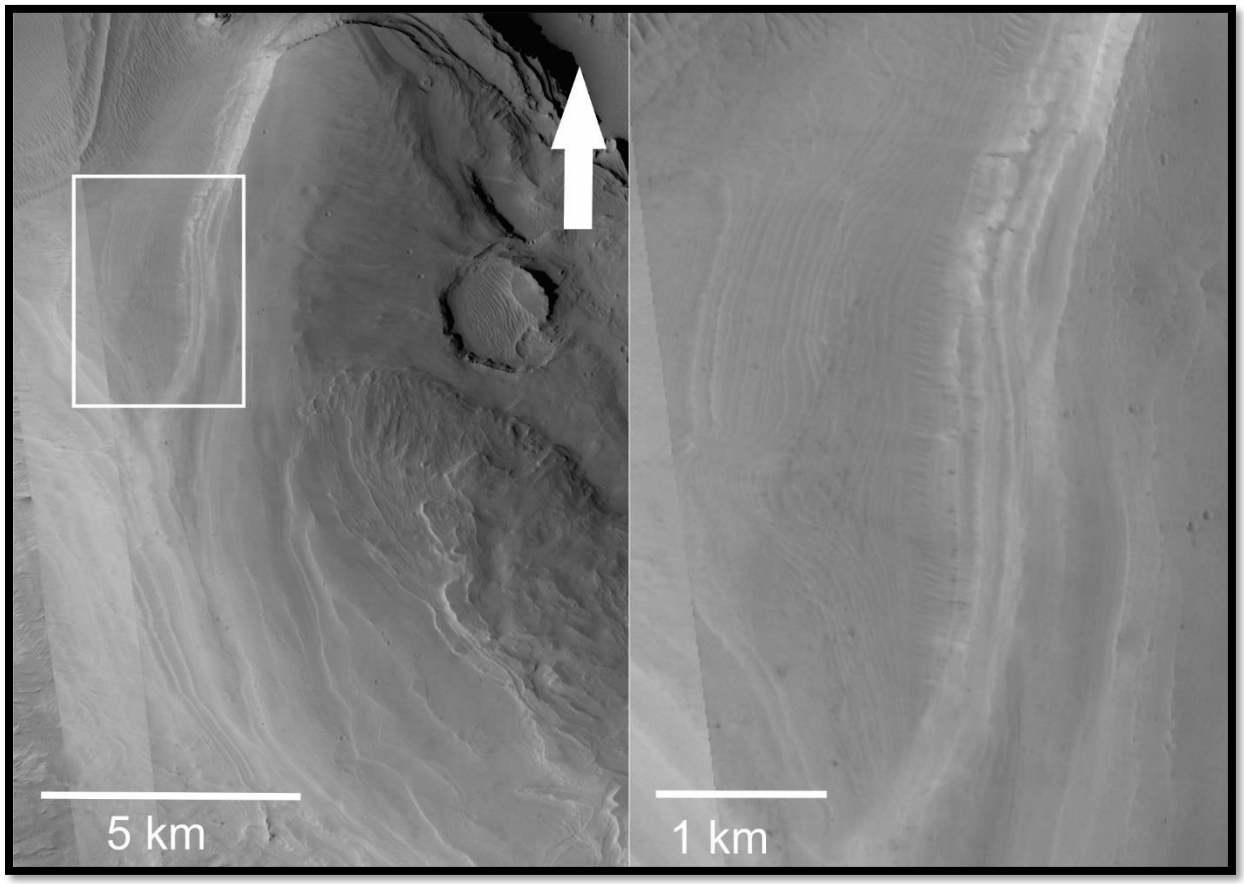

Figure 2-11: Example of Thin layering found in East Candor Chasma.

2.6.5 Steeply dipping thick unit

The steeply dipping thick unit (Fig 2-12) appears only along the east wall of the chasma in a roughly 46 km^2 area. This unit is composed of layering ~100 m thick with intermediate albedo. Characteristics that make this unit unique from the thick layer variety are its sharp erosional texture along the edges of the exposed layering and that it appears to be dipping steeply (~30˚) towards the southeast of the chasma (Fig. 2-12C). The dip is obvious prior to actual measurements and has subsequently been confirmed by measurements which will be presented in the next chapter. This unit is located at the base of Mound A on its east facing slope. To the north of this unit is a thick layered unit that dips to the northeast. Stratigraphically above both of these units is another thick layered unit that displays a much shallower dip to the northeast. The steep dip of this unit makes it an anomalous feature within East Candor.

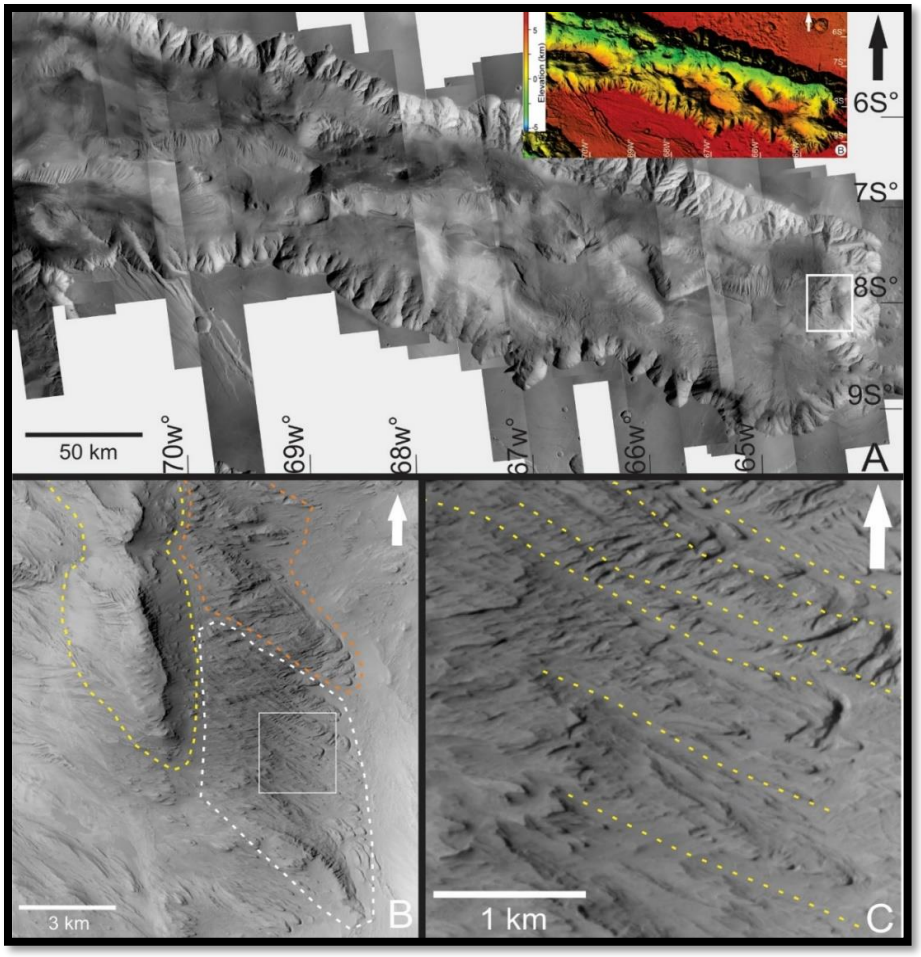

Figure 2-12 A: Steeply dipping unit location shown in inset on east side of chasma (Mound A). B: Steeply dipping unit outlined in white dashed line. Orange and yellow dashed lines display other thick layered units. C: Inset box in figure B with yellow dashed lines outlining layering.

2.6.6 Deformed layered unit

The deformed unit (Fig. 2-13) can be light or intermediate or dark toned. It may alternate between dark and light toned layering. The unit contains highly deformed layers that ranges form ~10 m to ~40 m in thickness. This unit is located near the north and south walls of the east end of the chasma displaying tight folds and faulting that outcrop at the chasm's surface. In some cases, thin mesa can be observed draping over this unit or lying in eroded pits and alcoves.

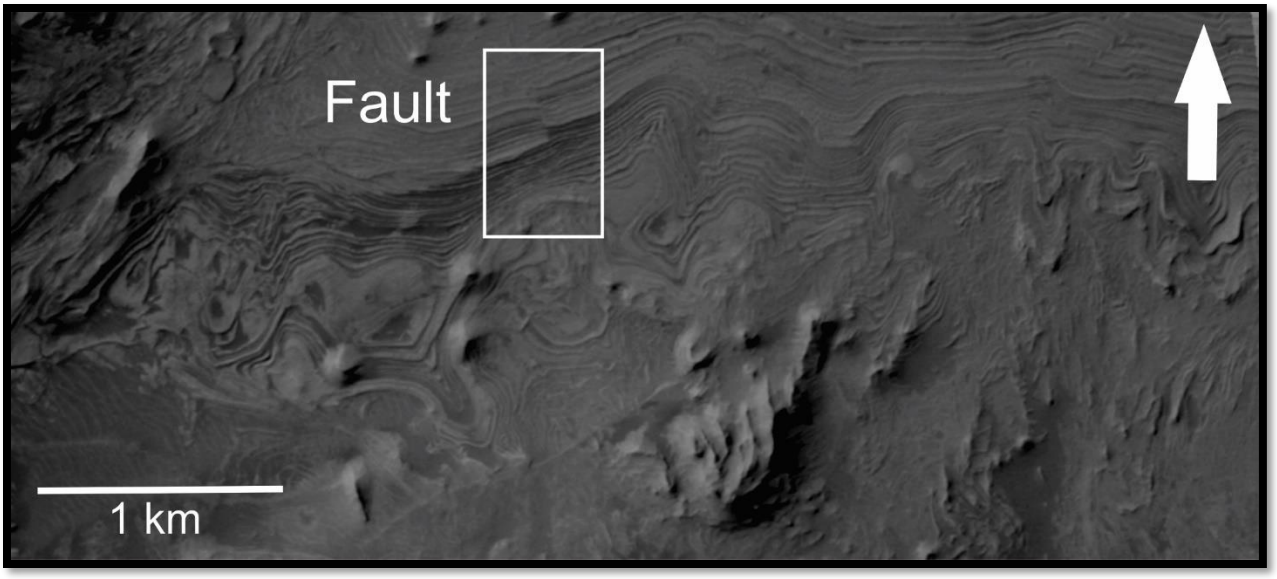

Figure 2-13: Example of deformed unit displaying tight folds and faulting within East Candor Chasma. Spurs from the south wall are to the south in the image; Mound B is to the north of the image. Topography is relatively flat in the image.

2.6.7 Thin mesa unit

The thin mesa unit (Fig. 2-14) is thought to be a late volcanic ash cover and is characterized by its intermediate to dark tone (Malin & Edgett, 2000). This unit lies unconformably over pre-existing geology and eroded material. The draping relationship is best observed at the tops of mounds and inclined layering. In East Candor Chasma, thin mesa is most commonly located in the central part of the chasma on the relatively flat areas of mounds and low angled slopes.

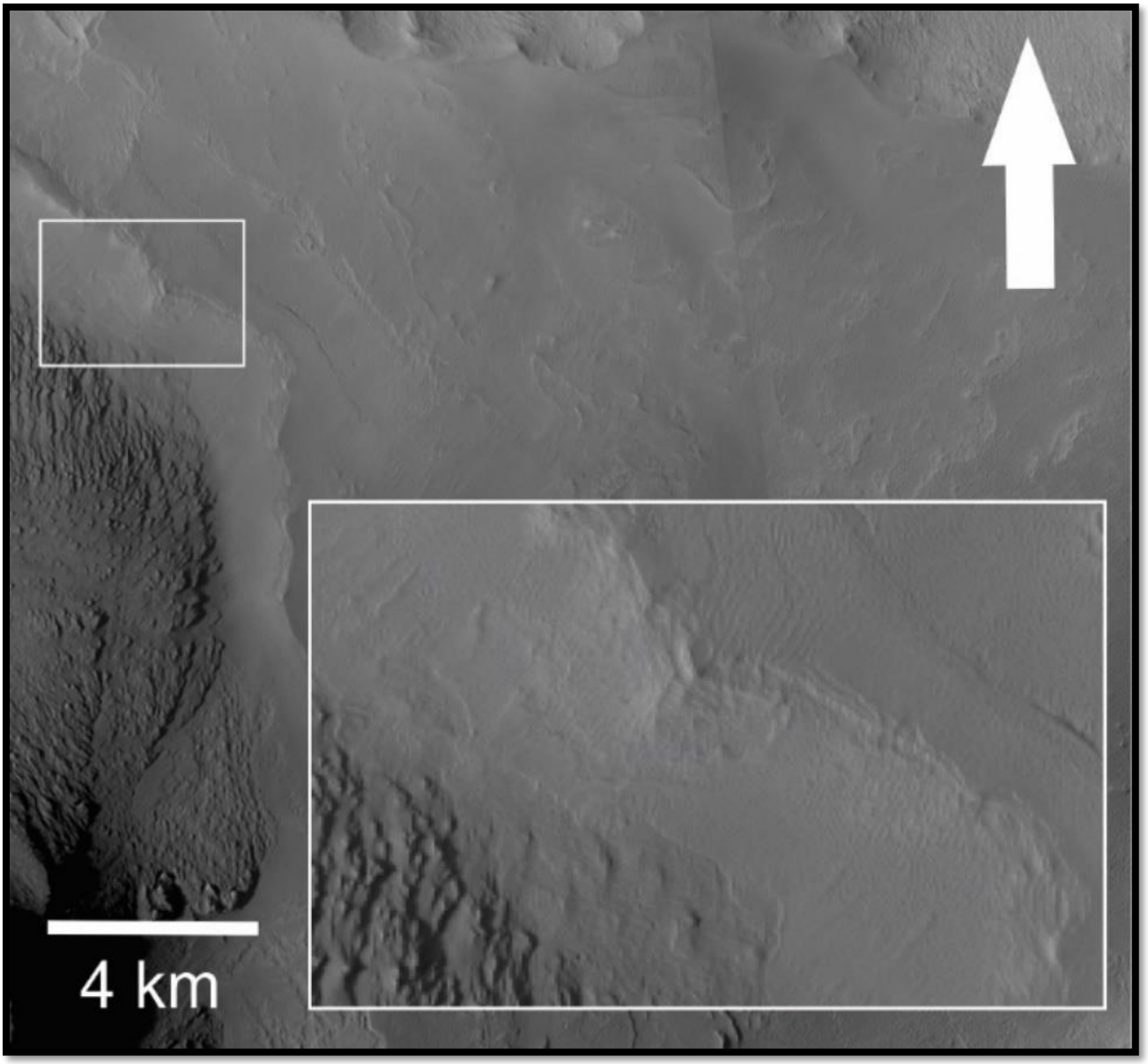

Figure 2-14: Example of thin mesa unit on the east flank of Mound D, likely comprised of a late volcanic ash fall.

2.7.1 Distribution of ILD Units throughout East Candor Chasma

A map was generated to display the distribution of the six layer unit varieties throughout the chasma (Fig. 2-15). A CTX mosaic was used as the base for this map; HiRISE was used where available to assure

accuracy. Each layer unit variety was assigned a different colour and polygons were used to define closed boundaries of each ILD unit. The imagery was visually inspected for features that identified each type of ILD, such as visual appearance, albedo, appearance of eroded material, presence of layers and their relative thickness (table 2-2). In instances where thin mesa covered another unit while the other unit was still clearly visible, the underlying unit is shown, not the thin mesa. This was done because the underlying unit provides more insight into the history of East Candor Chasma.

Table 2-4: Summary of ILD varieties found in East Candor Chasma

ILD Unit Variety	Albedo (tone)	Layer Thickness	Notable Features
Massive Unit	Light	Not visible	Elongated ridge and gully erosional feature
Thick Layered Unit	Light to intermediate	~2 km to ~25 m	Contains variably thick, well-defined layers
Thin Layered unit	Light to intermediate	~25 m up to <1 m	Contains thin layers which appear to erode smooth and easily
Steeply Dipping Unit	Intermediate	~100 m	Sharp erosional feature along exposed edge of layering
Deformed Unit	Light to intermediate to dark	~10 m to ~40 m	Displays tight folds and faults
Thin Mesa Unit	Intermediate to dark	None	Drapes pre-existing geology mimicking the underlying topography

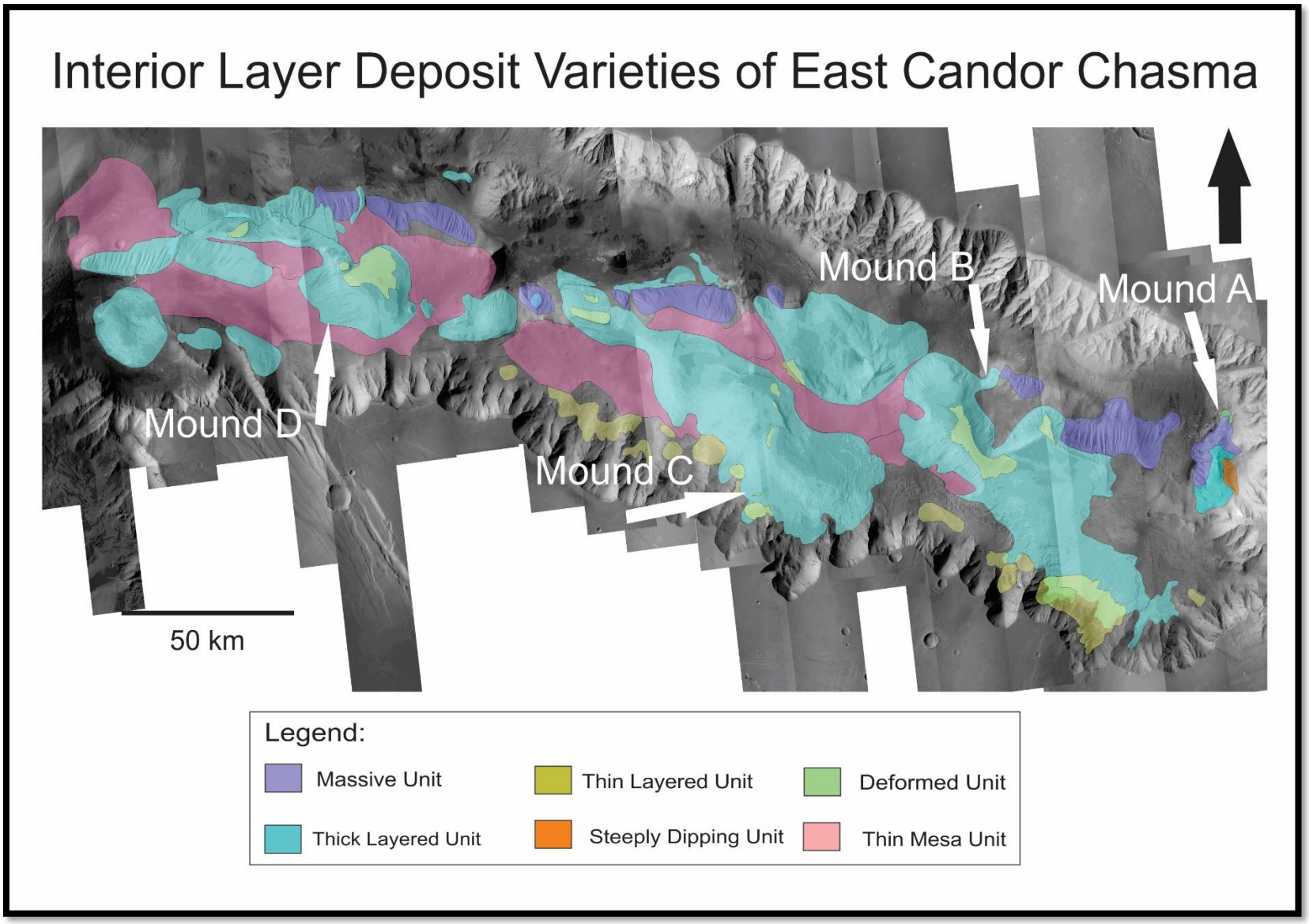

Figure 2-15: Map displaying the distribution of layer units in East Candor Chasma.

The six ILD unit varieties in East Candor can be observed through much of the chasma. The massive unit within East Candor discontinuously spans the length of the chasma, primarily outcropping on the north face of the central mounds. It is thought to be stratigraphically the lowest ILD unit present in the chasma based on observations along the north face of the central mounds. There are a few exceptions — located north of Mound A and Minor Mound 2 — where thick layered ILD material appears to be stratigraphically lower than the massive unit. A fan-shaped thick layered deposit with benches, located at the base of a massive unit just north of Minor Mound 2, is an example of this (Fig. 2-17). It is interpreted to have been deposited at the base of the massive unit. However, the geometry of the fan suggests that it was deposited at a lower elevation within the area of the proposed northern fault and is likely a later deposit positioned at a lower elevation than the massive unit. These locations can be explained using Okubo's (2010) interpretation of Layered Sedimentary Deposits (LSD), that were deposited after large-scaled chasma formation had ceased. These deposits are interpreted to be much younger than other layer deposits. It is therefore suggested that these layered deposits are not stratigraphically lower than the massive units, but rather were deposited at lower elevation near the base of the massive unit. One area that does not fit the criteria for Okubo's LSDs is located just to the west of the fan north of Minor Mound 3 (Fig. 2-18). The area depicts the unconformable boundary between a layered unit and overlying massive unit. This site is the only area observed in East Candor that appears to depict a massive unit deposit over a thick layered unit with a well-defined unconformity between the two. The layered unit is relatively thick and appears to be an older deposit. Okubo's LSDs often display deformation or disruption at the surface, which is thought to be the result of chasma reworking. Deformation is not observed in the layered outcrop as much of it is covered by the massive unit. There are multiple explanations for this geometry. One possible explanation for this is sediment remobilization. Perhaps the observed massive unit located in Figure 2-18 is the result of previously

eroded material that has been locally re-deposited after the layered unit was emplaced. It is possible that while a lake still existed on the surface of East Candor, mobilized sediments were emplaced, likely by aeolian processes, at Minor Mound 2. Another possibility is that a layered unit was deposited before the massive unit but does not outcrop at any other location of East Candor Chasma. The layered unit described in Figure 2-18 lies in some of the lowest topographic areas of East Candor. A third explanation will be offered in chapter 4, based on observations outlined in the next chapter.

Information obtained by separating ILDs into distinct units can be used to display the likely sequential relationship of units within the chasma. It is important to note that stratigraphy and elevation are not the same. Stratigraphy is the order in which sedimentary deposits are laid down. In geology, elevation is considered a measurement of height of a topographical surface with respect to a fixed datum. Folding and faulting is sometimes responsible for misrepresenting the stratigraphy of units, where a unit commonly found in the upper stratigraphy appears to be moved down in sequence due to faulting. In this work, elevation is only used to correlate units that appear to be of the same age and/or origin. There is no evidence of major faulting within the ILDs of East Candor. ILDs within the central mounds appear undisturbed with relatively continuous layers. However, nothing is known of the original floor, so a consistent base level cannot be defined. The thickness of the lowest-most units are therefore estimated.

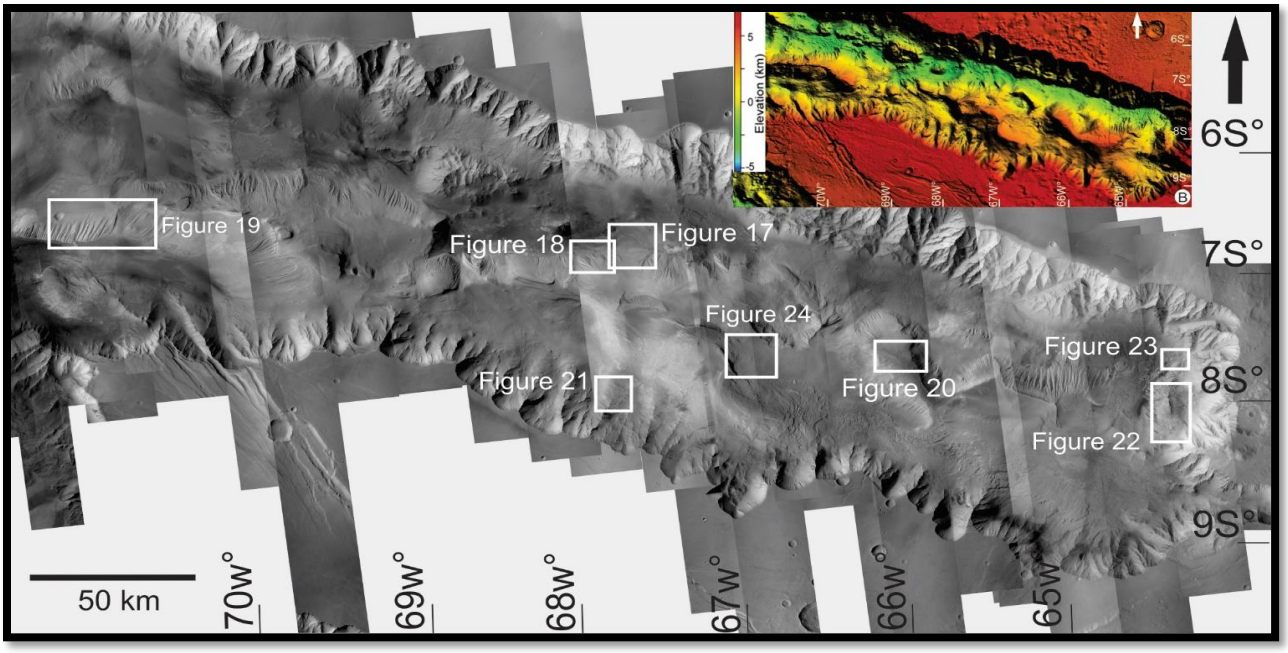

Figure 2-16: Location map displaying various figures outlined below.

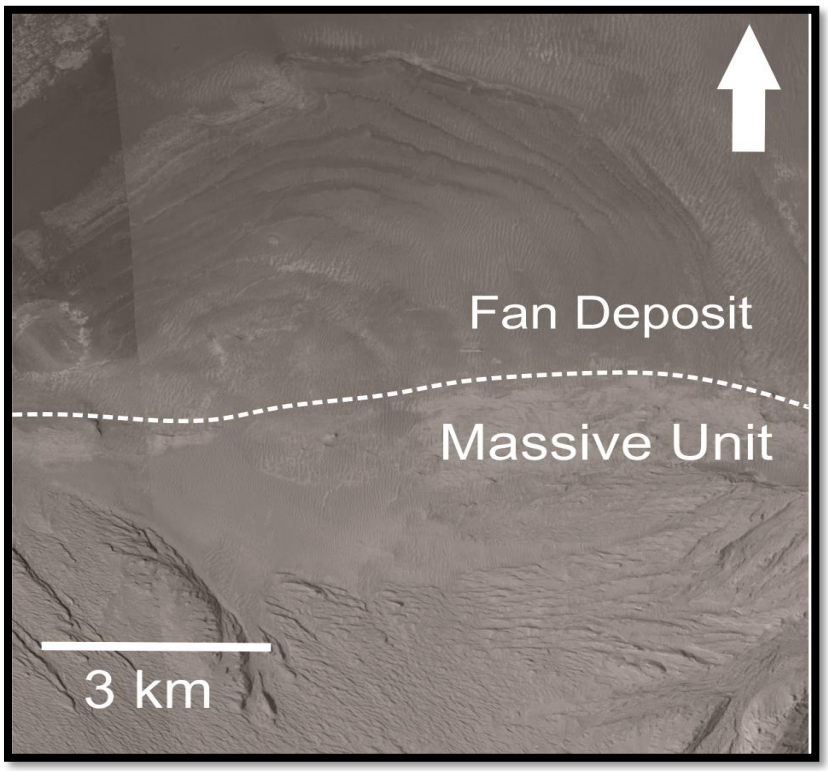

Figure 2-17: Layered fan located at the base of Minor Mound 2 displays bench-style layering. Lowest elevation of Massive unit at -3000 meters. Alluvial fan ranges in elevation from -3200 to -4200 meters. Dashed line indicates boundary between the two deposits. Topographic slope is to the north of image.

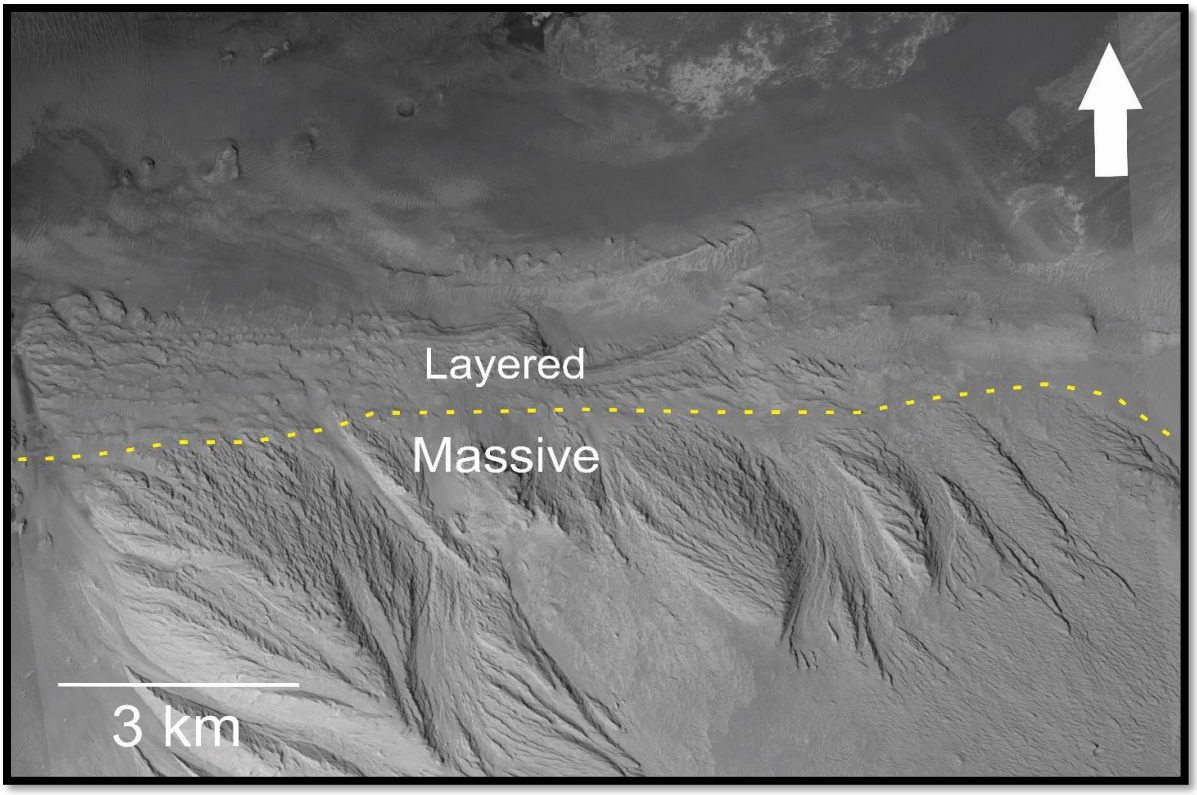

Figure 2-18: Area north of Minor Mound 2 that appears to have a massive unit stratigraphically higher than a layered unit. Topographic slope is towards the north of the image.

In the central mounds of East Candor there is evidence of two thick layered units where one unit is observed truncating the other. There is also evidence that there are at least 2 thick layered units that cannot be distinguished on the basis of morphology alone. The older unit displays evidence of erosion, which was followed by the deposition of a younger layered unit. This is best displayed in Mound D where cross-cutting relationships are visible on the south facing slope (Fig 2-19). Evidence of this has been found in other areas within VM, as indicated by Kite (2016).

East Candor displays changes in sedimentation style, often without a visible unconformable boundary separating the transition. Benches transition into a thick layering which then draped by thin layering (Fig. 2-20).

Figure 2-19: South face of Mound D displaying two layered units with opposing attitudes. Inset is close up of layered units. Image shows that erosion took place between two periods of deposition. Topographic slope is to the south of the image.

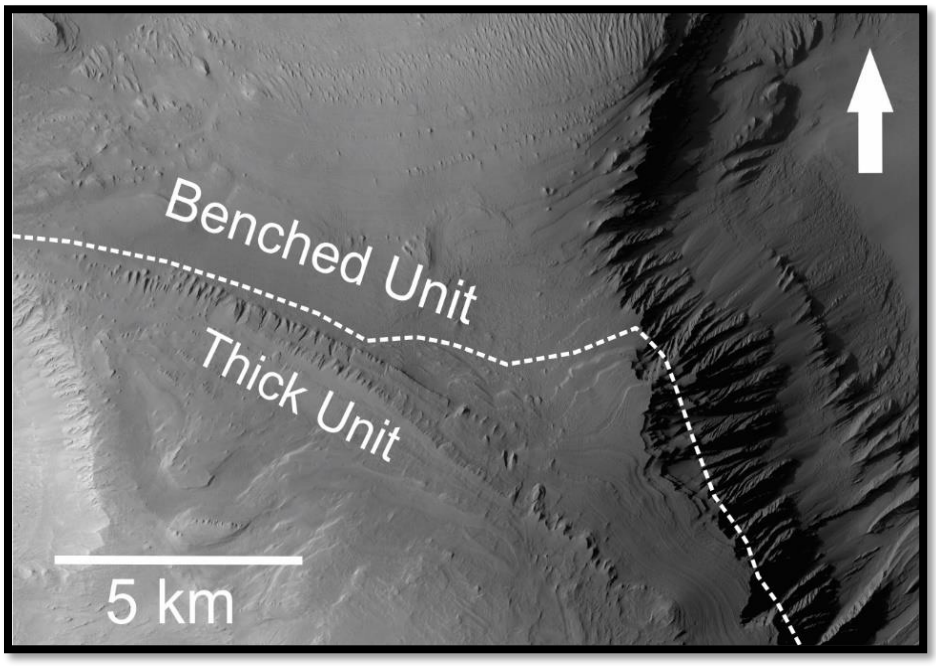

Figure 2-20: Western lobe of Mound B displaying where a bench unit is overlain by a thick layered unit. Topographic slope is to the northeast of the image.

The majority of locations of the thin layered unit are located along the south wall, draping the spurs and filling in the gullies (Fig. 2-21). Within the central mounds thin layering occurs on the upper-most parts of the mounds. In some cases, it is difficult to determine if the thin layering is part of the thick layering or a later covering that overlies the pre-existing geology.

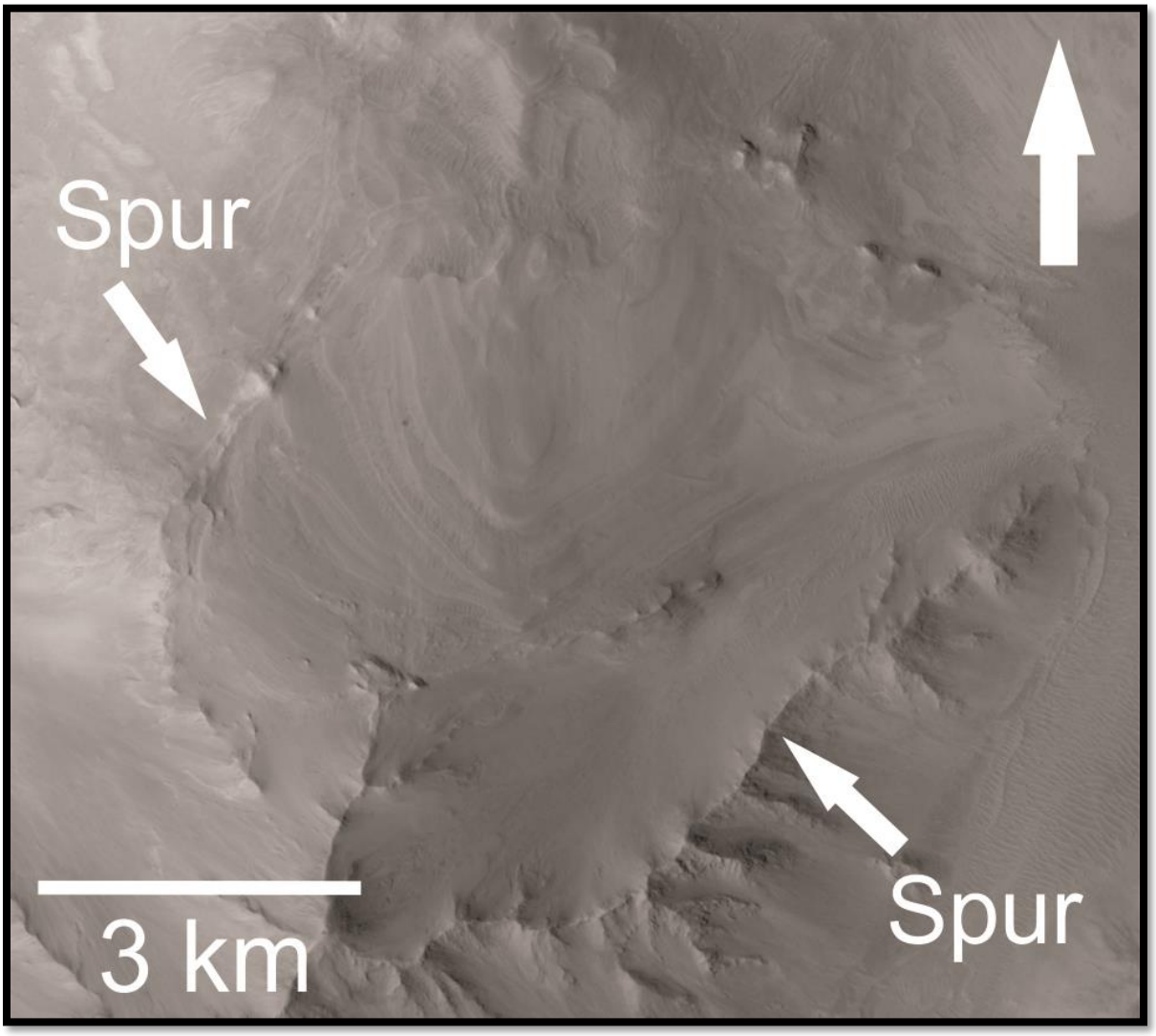

Figure 2-21: Thin layered unit bound by spurs along the south wall. Topographic slope is to the north of image.

The steeply dipping unit is located along the east wall of the chasma on the east flank of Mound A (Fig 2-22). The area displays a package of thick layering that dips at a much steeper angle and toward the opposite direction of other thick layered material, an occurrence which will be discussed further. It is thought that this particular variety of layered unit is unique in East Candor Chasma.

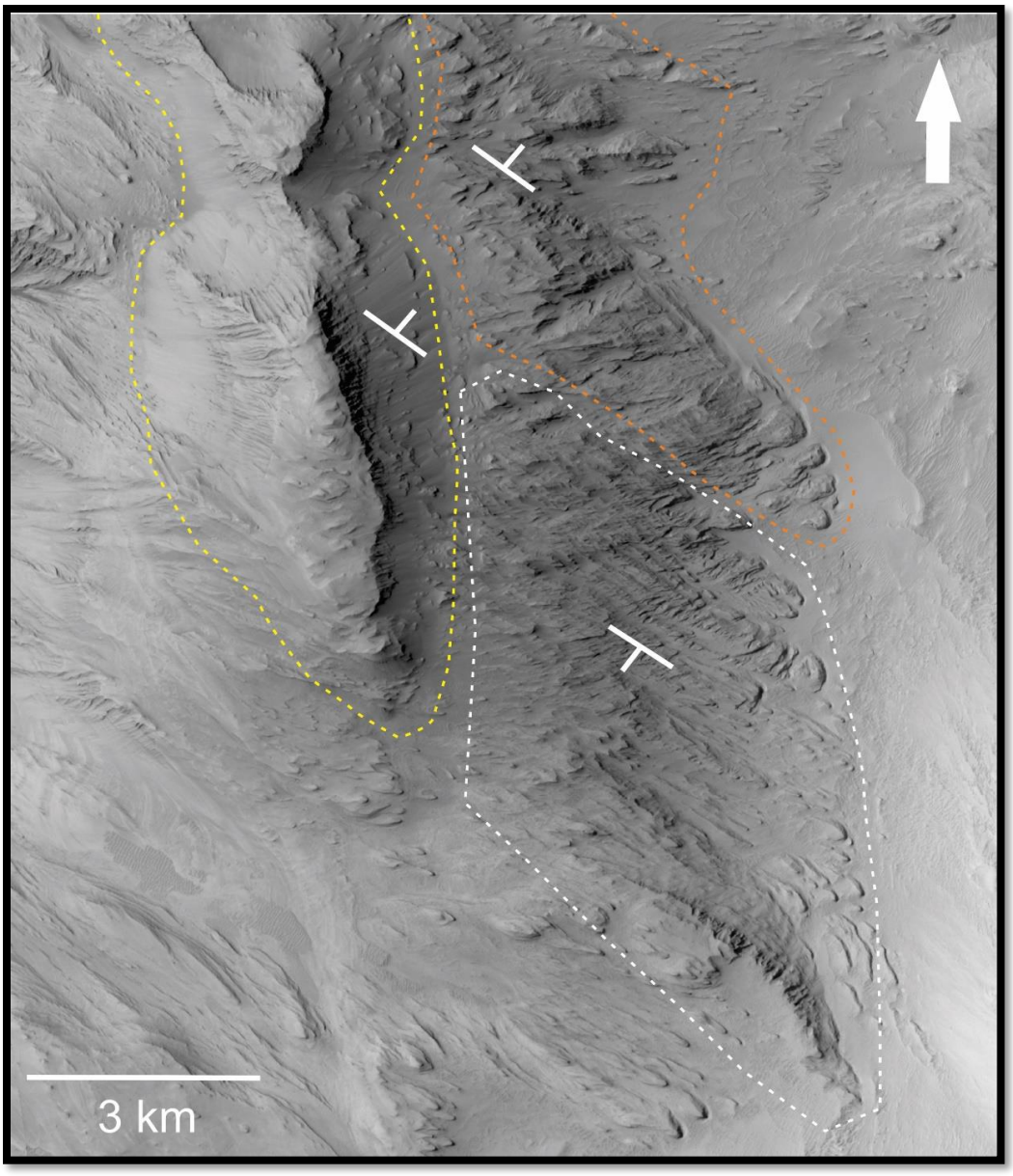

Figure 2-22: East flank of Mound A depicting a lower thick unit that steeply dips in the opposite direction of most other units in the chasma. To the north of this unit is another thick unit, both are overlain by shallow thick unit.

The deformed unit is composed of relatively thin layered materials, heavily folded and fractured. There are two areas where the deformed layered unit outcrops. Both occur near the chasma walls. The deformed unit occurring along the south wall appears to be composed of alternating high and low albedo layering. The deformed unit occurring along the northeast wall appears to be similar in appearance to Okubo's LSD and could have possibly been deformed by slumping (Fig. 2-23).

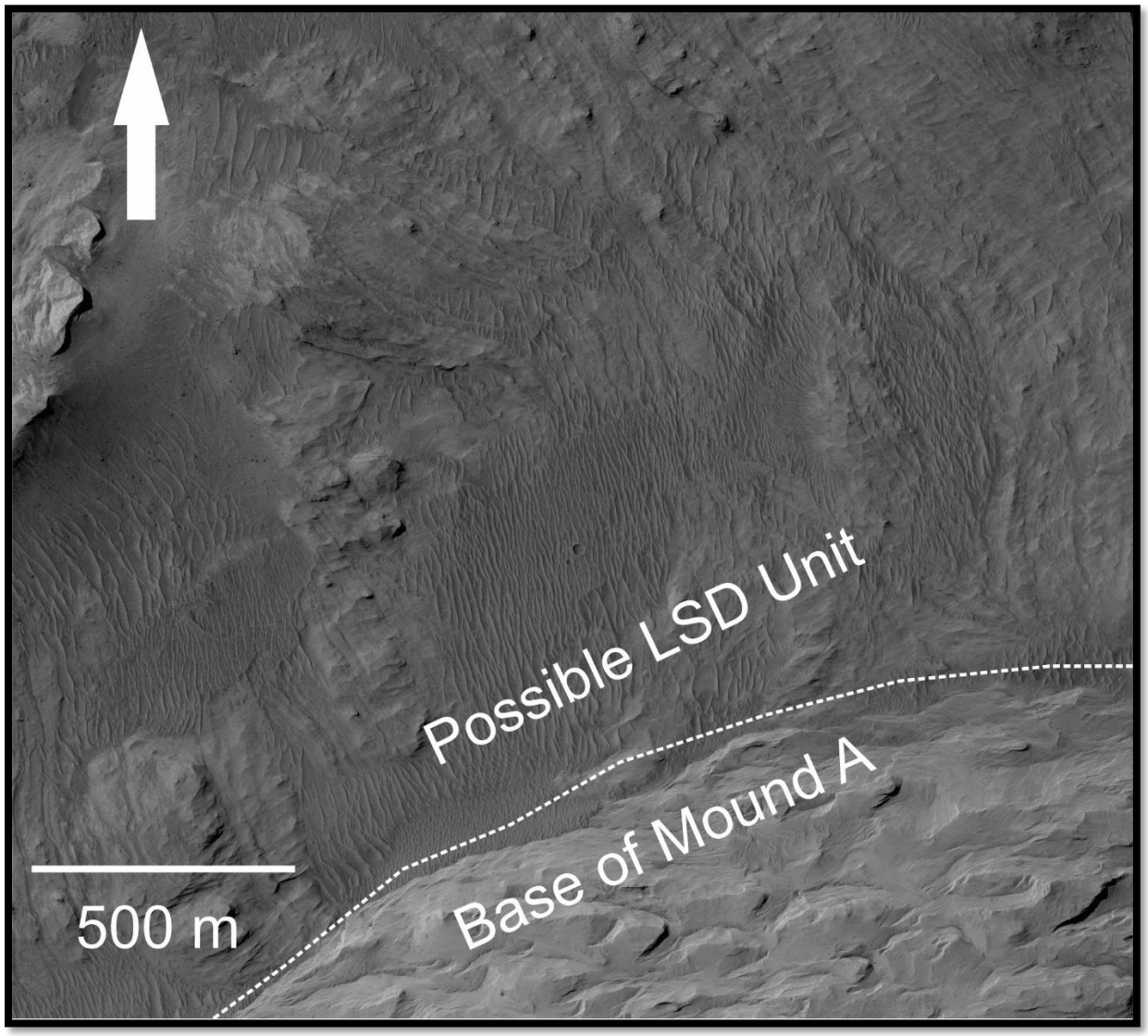

Figure 2-23: Deformed Layered Unit found north of Mound A. Topographic high is to the southeast of image.

The thin mesa unit is found throughout the chasma. This unit is thought to be a late deposit, possibly the result of ash fall. It lies unconformably over pre-existing geology displaying a smooth texture at the surface (Fig. 2-24). This unit is easily eroded so that it is only visible in pits or cracks that are shielded from the elements. Much of the thin mesa unit along the south wall is sufficiently thin to recognize the tops of underlying deposits. It can also be found on the tops of the mounds within East Candor providing a smooth texture to the upper surface. Areas where thin mesa is outlined on the map are unlikely to have undergone a high degree of erosion.

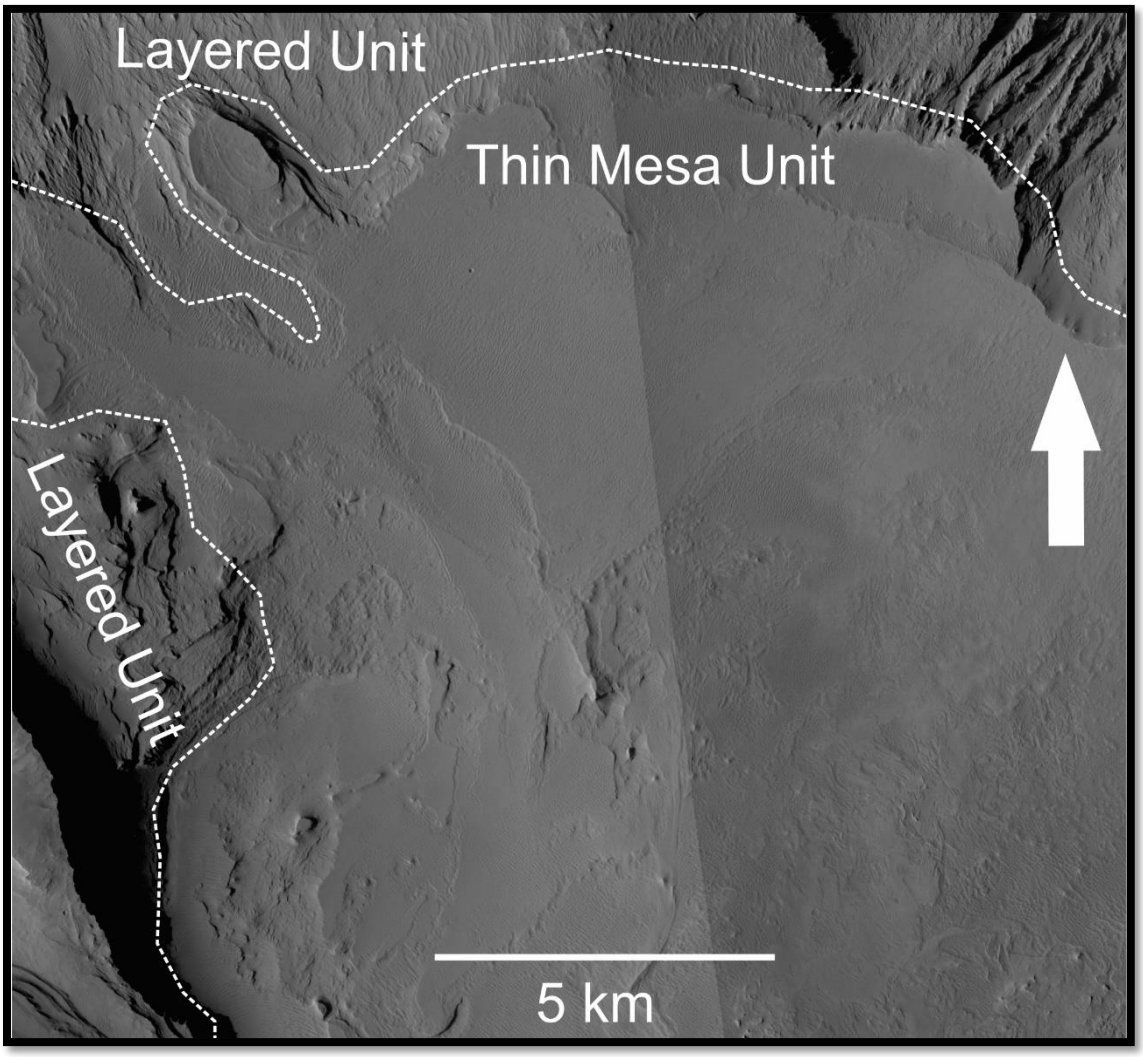

Figure 2-24: Thin Mesa Unit found east of Mound C (Nia Mensa), displaying draping over pre-existing geology.

In some instances, more than one layer unit variety was observed at the same location. This fact is reflected in the layer varieties map (Fig. 2-15) as one unit style overlapping another. Examples of this can be observed along the south wall and the tops of mounds where thin layering overlies a portion of thick layering. Areas left as undefined did not fit into one of the six categories. These areas may have displayed traces of a unit (less than 10% in a given area). It also included areas that were so heavily eroded or contained dunes or dust cover that determining ILD verity was not possible.

2.8 Discussion

East Candor Chasma contains highly complex geology, displaying a depositional history that include a diverse variety of ILD material that unconformities suggest has likely been deposited episodically over time. Topographically the chasma can be split into two areas: the lower lying north wall, that ranges from ~-2700 m to ~-5000 m, contains the lowest elevations in the chasma. The south wall sits higher than the north, ranging in elevation from ~1800 m to ~-2500m. These two regions are separated by the central mounds. The most common identifiable unit along the north face of the central mounds is the massive unit. It is thought that the massive unit is the lowest ILD in sequence stratigraphy.

The thick layered unit contains a diverse variety of layer thickness and appears to be stratigraphically above the massive unit. The layering in the thick layered unit tends to thin upwards and present evidence of unconformities separating packages (see appendices). Mound B is a good example of massive unit overlain by thick layered units, which in turn are overlain by thin layered units and finally thin mesa in East Candor (Figure 2-25). This could indicate a change in depositional environment over time, as well as a decrease in sediment availability. These two factors likely had an impact on a regional,

and possibly global, scale. The proposed stratigraphic sequence of units for the central mounds in East Candor Chasma is as follows: massive unit, thick layered unit (bench subunit), thin layered unit, thin mesa unit (Fig. 2-29). This succession is best observed in Mound B due to it's steep north-facing slope. It is also observed throughout the other mounds and minor mounds in East Candor Chasma.

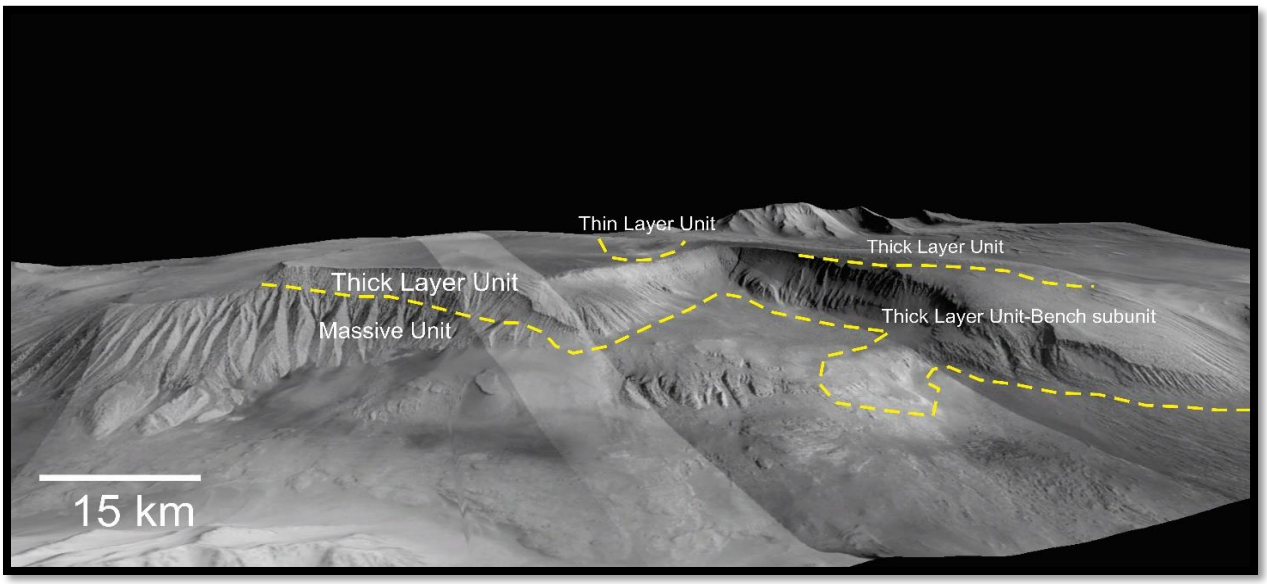

Figure 2-25: Stratigraphic succession found in Mound B of East Candor Chasma. Image facing south. V.E.=1X.

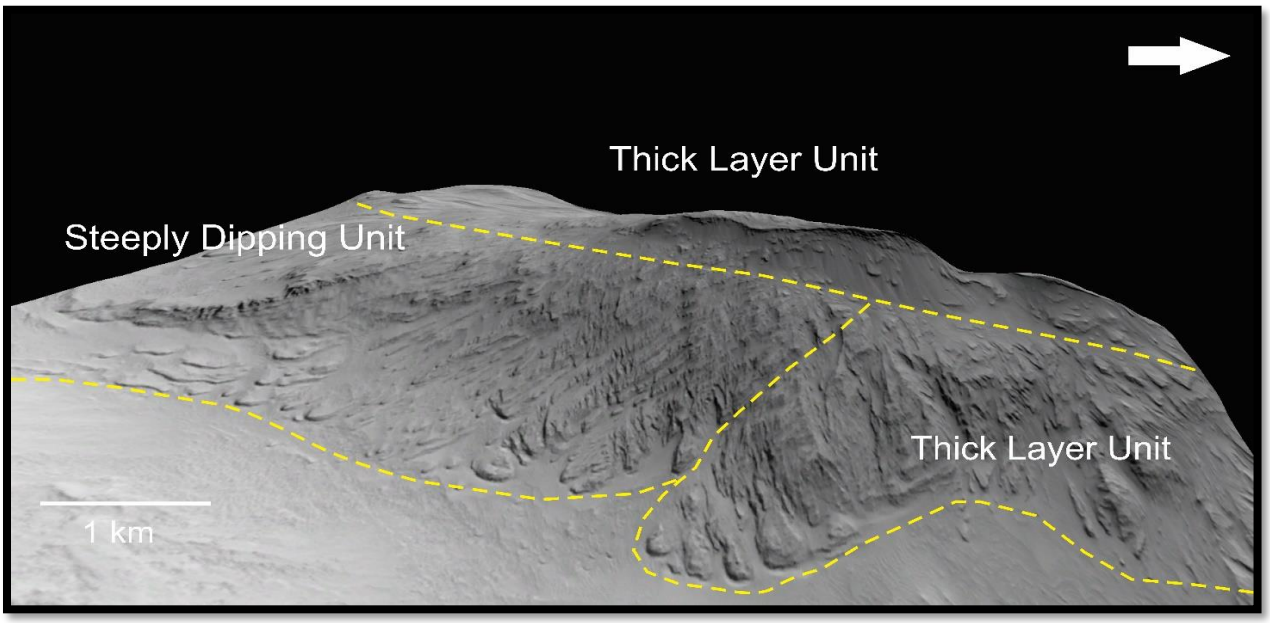

Figure 2-26: Stratigraphic sequence found in Mound A of East Candor Chasma. Image facing southwest. V.E.=1X.

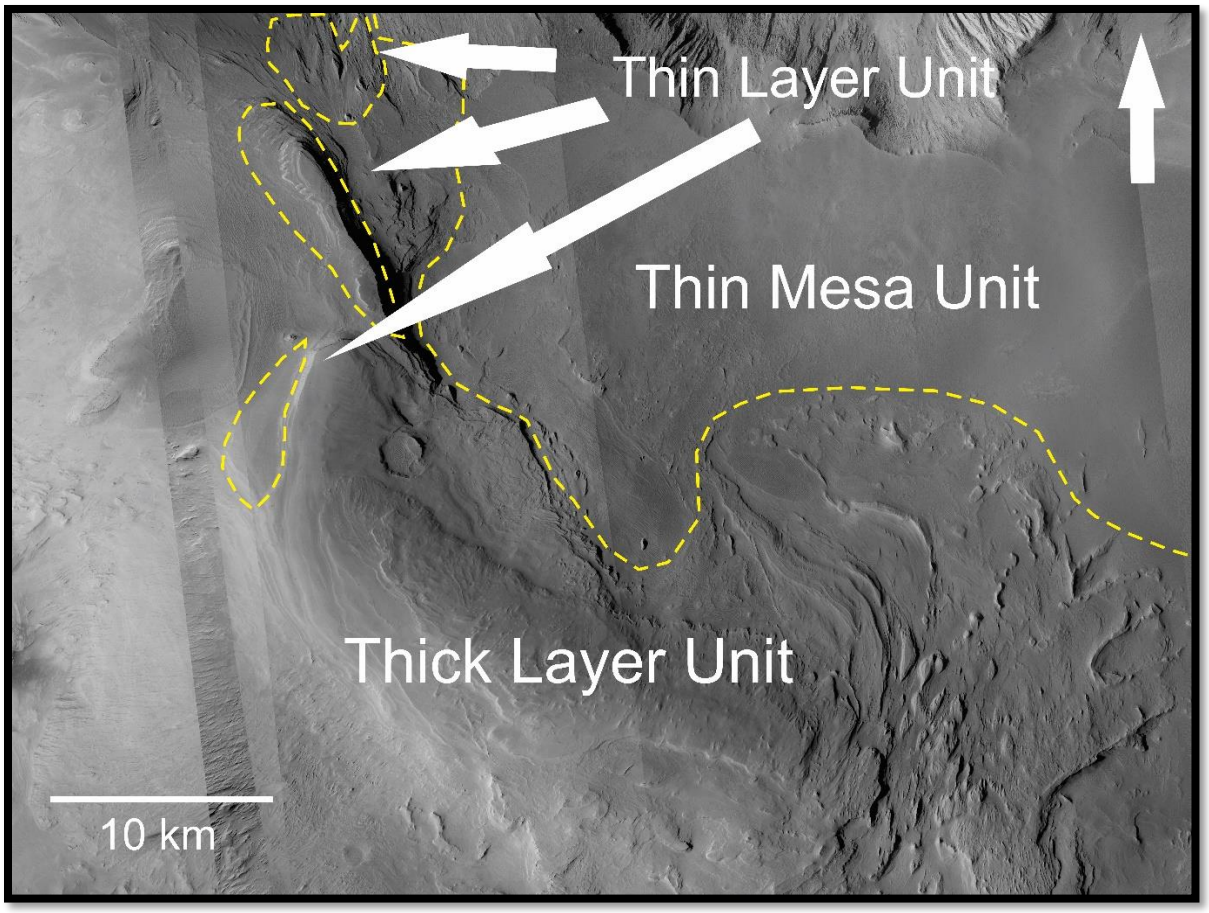

Figure 2-27a: Stratigraphic sequence found in Mound C of East Candor Chasma

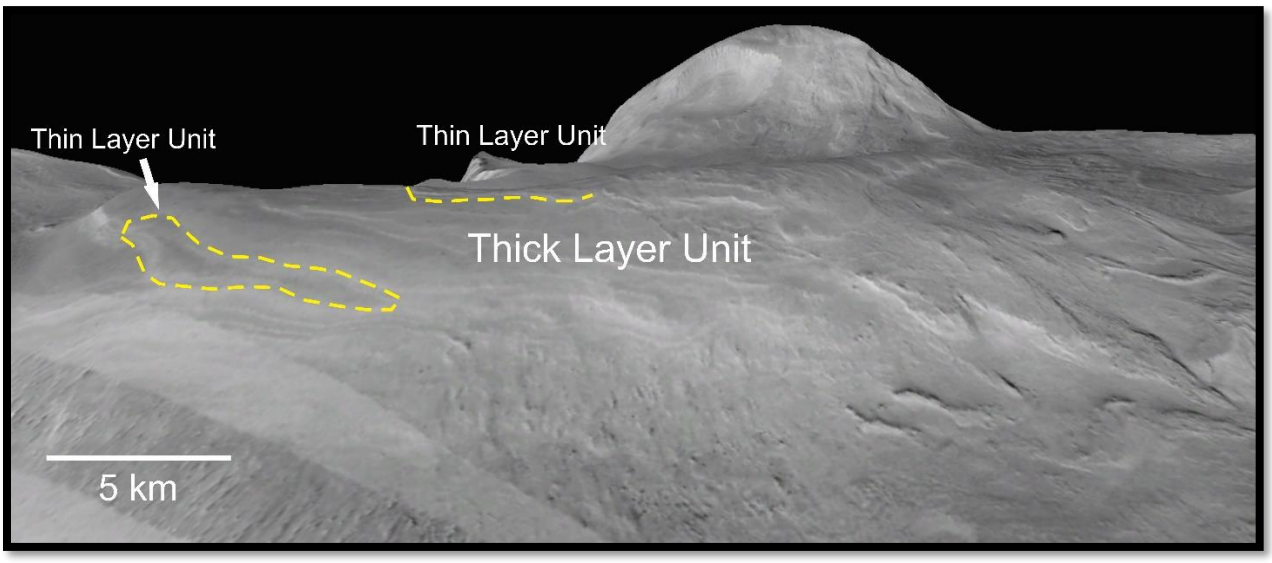

Figure 2-27b: Stratigraphic sequence found in Mound C of East Candor Chasma. Image facing southeast. V.E.=1X

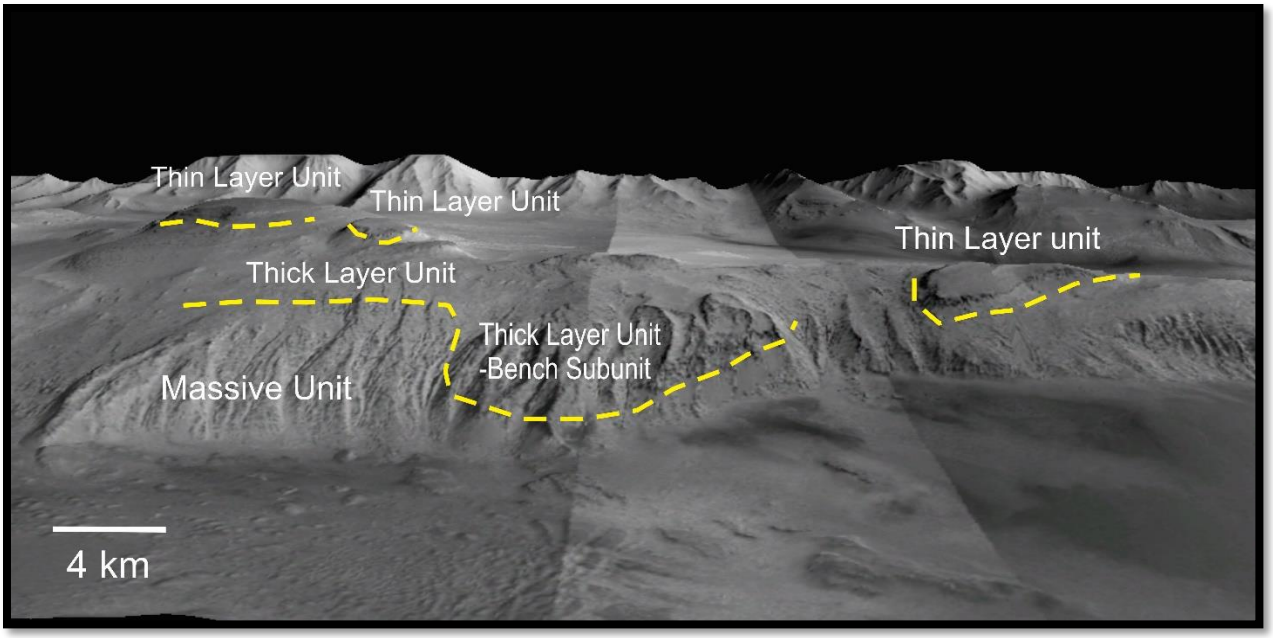

Figure 2-28: Stratigraphic sequence found in Mound D of East Candor Chasma. Image facing south. V.E=1X.

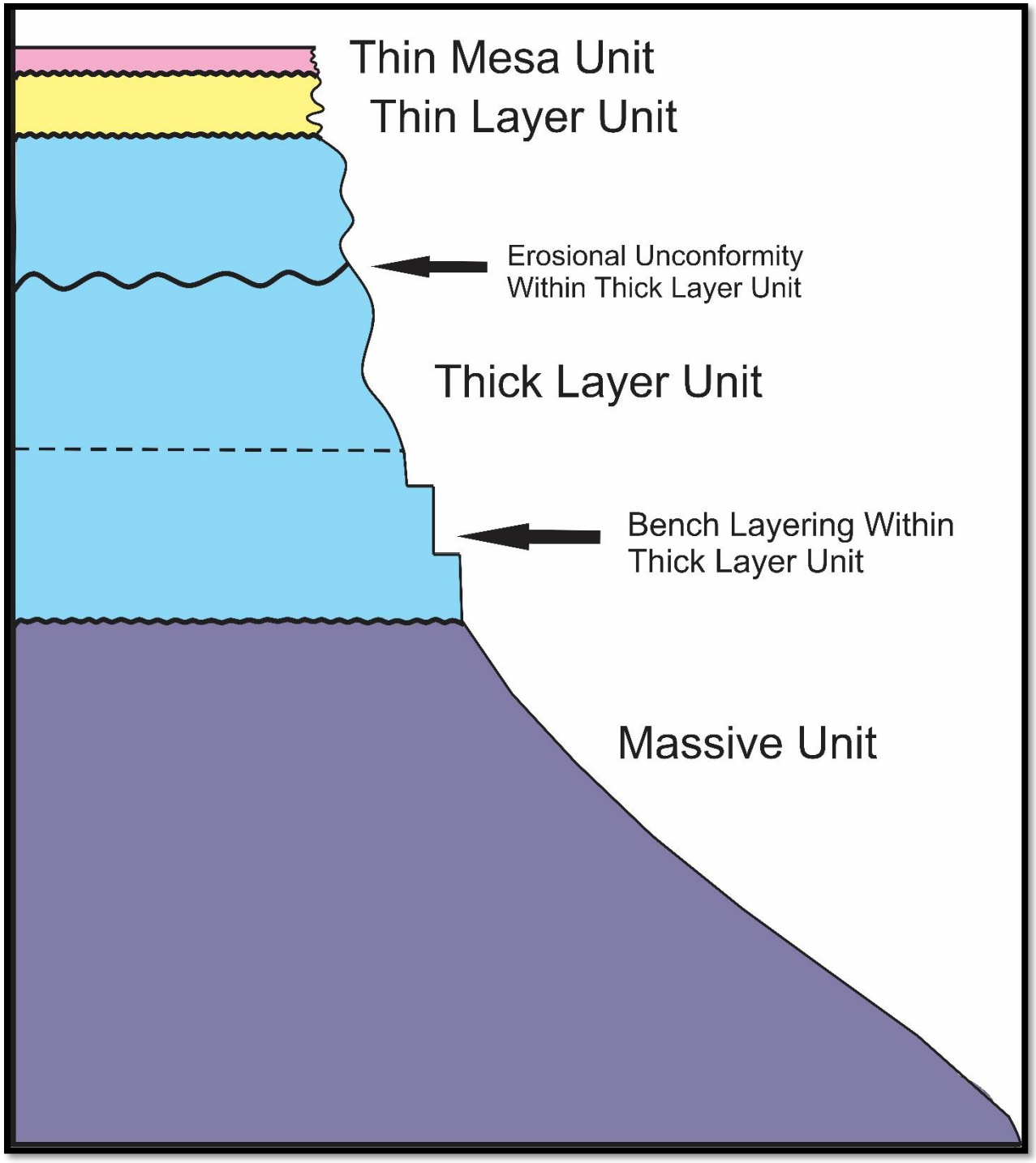

Figure 2-29: Proposed ideal stratigraphic succession within the central mounds of East Candor Chasma.

The thin layer unit appears to drape the south wall and the tops of central mounds. The thin layering on the west limb of Mound B could possibly be contained within the thicker layering below. However, the resolution of available imagery makes determining if there is indeed more thin layering within the thicker packages difficult. The thin layer unit is widely distributed throughout the chasma, even though its total area is smaller than for other units. This might indicate that the competency of the unit is low and easily erodible. The majority of the thin layered unit can be observed along the south wall. It is likely that the wall offers protection from erosive forces.

Similar to other ILD in VM (Fueten et al., 2017), the mounds in East Candor likely formed over an extended period of time, possibly with multiple episodes of deposition and erosion. Evidence for this is provided by multiple ILD varieties and unconformities separating various packages. Mound D provides the most convincing evidence of multiple episodes of deposition, as one thick layer unit is visibly truncating another. Evidence of erosion on the exposed lower thick layer unit is observed along the south face of the mound. This indicates that there was a period of time between episodes of deposition where erosion dominated the area.

The physical characteristics of all six ILD varieties within East Candor Chasma suggest they contain relatively fine-grained poorly indurated materials (Malin & Edgett, 2000). Evidence for this is unconsolidated debris throughout the chasma. There are no large boulders in any debris visible throughout the chasma. Although ILDs are compacted they comprise relatively weak materials highly susceptible to erosion (Hynek & Phillips, 2008). Evidence for this are rounded slopes, yardangs and few crater impact sites visible on ILD material.

East Candor Chasma displays a depositional history containing a diverse variety of ILD material that has likely been deposited episodically over time. Evidence supports multiple events of chasma-wide deposition and erosion. Unconformities outline transitions form one lithology to another. Deformation in ILDs along the chasma walls are likely the result of local stresses (e.g. slump or localized compression). Classifying various ILD material within the chasma will help better understand the areas depositional and geologic history. Chapter 3 discusses the attitude measurements of layered materials and will be used in conjunction with the classification system of ILD materials to form a connection to the different ILD mounds within East Candor Chasma.

References

Bibring, J. P. et al., 2006. Global Mineralogical and Aqueous Mars History Derived from OMEGA/Mars Express Data. *Science,* 312(5772), pp. 400-404.

Broxton, M. J. & Edwards, L. J., 2008. *The Ames Stereo Pipeline" Automated 3D Surface Reconstruction from Orbital Imagery.* s.l., s.n., p. Abstract 2419.

Flahaut, J., Quantin, C., Allemand, P. & Thomas, P., 2009. Morphology and geology of the ILD in Capri/Eos Chasma from visible and infrared data. *Science Direct,* pp. 175-185.

Flahaut, J. et al., 2010. Identification, Distribution and possible origins of sulfates in Capri Chasma (Mars), inferred from CRISM data. *Journal of Geophysical Research: Planets,* 115(E11).

Fueten, F. et al., 2014. Stratigraphy and mineralogy of Candor Mensa, West Candor Chasma, mars: Insight into the geologic history of Valles Marineris. *Journal of Geophysical Research,* pp. 1-24.

Fueten, F. et al., 2017. The Evolution of Juventae Chasma, vales Marineris, Mars: Progressive Collapse and Sedimentation. *Journal of Geophysical research: Planets,* Issue 122, pp. 1-27.

Fueten, F. et al., 2006. Structural study of an interior layered deposit in southwestern Candor Chasma, Valles Marineris, Mars, using high resolution stereo camera data from Mars Express. *Geophysical Research Letters,* 33(7).

Kite, E. et al., 2013. Growth and for of the mound in Gale Crater, Mars: Slope wind enhanced erosion and transport. *Geology,* Volume 41, pp. 543-546.

Komatsu, G., Ori, G., Ciarcelluti, P. & Litasov, Y., 2004. Interior Layered Deposits of Valles Marineeris, Mars: Analogus subice volcanism related to Baikal rifting, southern Siberia. *Planetary and Space Science,* pp. 167-187.

Le Deit, L. et al., 2008. Ferric oxides in East Candor Chasma, Valles Marineris (Mars) inferred from analysis of OMEGA/Mars Express data: Identification and geological interpretation. *Journal of Geophysical Research: Planets,* 113(E7).

Lucchitta , B. K., 1990. Young volcanic deposits in the Valles Marineris, Mars?. *Icarus,* pp. 476-509.

Lucchitta, B. K., 1982. Ice Sculpture in the Martian Outflow Channels. *Journal of Geophysical Research,* pp. 9951-9973.

Lucchitta, B. K., 1994. Topography of Valles Marineris: Implications for erosional and structural history. *Journal of Geophysical Research,* pp. 3783-3798.

Malin, M. C. & Edgett, K. S., 2000. Sedfimentary Rocks of Early Mars. *Science,* pp. 1927-1937.

Mege, D. & Masson, P., 1996. Amounts of Crustal Streatching in Valles Marineris, Mars. *Planetary and Space Science,* Volume 44, pp. 419-422.

Moratto, Z. M. et al., 2010. *Ames Stereo Pipeline, NASA's Open Source Automated Stereogrammetry Software,.* s.l., s.n., p. Abstract 2364.

Okubo, C. H., 2010. Structural Geology of Amazonian-aged layered sedimentary deposits in southwest Candor Chasma, Mars. *Icarus,* pp. 210-225.

Okubo, C. H., Lewis, K. W., McEwen, A. S. & Kirk, R. L., 2008. Relative age of interior layered deposits in southwest Candor Chasma based on high-resolution structural mapping. *Journal of Geophysical Research,* pp. 1-15.

Peulvast, J. -P. et al., 2001. Morphology, evolution and tectonics of Valles Marineris wallslopes (Mars). *Geomorphology,* Volume 37, pp. 329-352.

Quantin, C. et al., 2005. Sulfate deposits identified by OMEGA in Melas Chasma. *Lunar Planetary Science XXXVI,* Issue 1789.

Roach, L. H. et al., 2009. Testing evidence of recent hydration state change in sulfates on Mars. *JGR: Planets,* pp. 1-13.

3.0 Chapter 3: Layer Attitude Measurements of East Candor Chasma

3.1 Introduction

The ILDs within VM has been the subject of multiple studies in recent history (Lucchitta, 1994; Malin & Edgett, 2000; Lewis, et al., 2008; Carr & Head III, 2009; Andrews-Hanna, 2012a; Andrews-Hanna, 2012b; Okubo, 2010; Kite, et al., 2016; Fueten, et al., 2017; Al-Samir, et al., 2017), that provide an insight into how the chasma formed, the paleoclimate on Mars, obliquity variations and any structural reworking the basins that may have undergone following chasma formation. Candor Chasma is over 800 km long with an eastern and western basin. Kite et al. (2016), Okubo et al. (2008 & 2010) and Fueten et al. (2006, 2008, 2014) described studies on ILD structures within Candor Chasma. Their findings will be discussed further in this chapter as a comparison to the findings of this study.

Focusing on attitudes of layers, Kite et al. (2016) studied ILD in chasm's and craters within and surrounding VM. They suggest deposits made in the uppermost ~1 km of mounds formed by the accretion of draping strata in a mound-shape with attitudes dipping away from the crest. They inferred that shifts in obliquity may be responsible for mound erosion and deposition. Further, Kite et al. (2016) suggested that chaotic shifts in obliquity are the cause of major mound-spanning unconformities in VM. Kite et al. (2016) proposed that major mound-spanning unconformities are the result of low mean obliquity. Since chaotic shifts in mean obliquity are infrequent, large unconformities suggest a discontinuous span of liquid water over time (Kite, et al., 2016).

Fueten et al. (2014) observed layering of Candor Mensa in East Candor Chasma that is composed of two stratigraphically distinct units. A lower layered unit with parallel layers 4 to 14 m thick has nearly sub-horizontal attitudes. The upper unit of Candor Mensa is composed of thinner layering (< 3 m) with attitudes ranging from 3˚-9˚. Fueten et al. (2014) proposed that the two distinct packages were deposited in different environments.

Okubo (2008 & 2010) focussed on layering in Southwest Candor Chasma referred to as layered sedimentary deposits (LSD). His findings indicated layers which dip towards the north or the center of the chasma. The dip of these layers varies greatly (2˚ - ~30˚). The area is heavily faulted and deformed which Okubo suggests may have led to the steeply dipping beds. The majority of layer thicknesses throughout this study area are found to be 5 m thick with interspersed massive layers measuring up to 100 m thick. The steeply dipping beds found in the mapping area are consistent with sediments filling a pre-existing basin that were deposited after chasma formation.

This chapter focuses on attitude measurements obtained from three of the ILD varieties within East Candor Chasma. Measurements were taken on the central mounds and along the south wall and provide information on the deposition and potential insights into underlying geological structures. Since the chasma is nearly 500 km long and 150 km wide and contains a large volume of measurable ILD, it is possible to establish trends that occur throughout the chasma.

3.2.1 Methodology

3.2.2 Data Source

Data was acquired using multiple sources of satellite imagery, including HRSC, Context camera (CTX) and High Resolution (HiRISE). HRSC DTMs were downloaded and stitched together. CTX and HiRISE DTMs were calculated with NASA Ames Stereo Pipeline (Broxton & Edwards, 2008; Moratto, et al., 2010). HRSC, at resolutions of 50, 75, 100 and 175 m/pixel, served as the base map for CTX and HiRISE imagery. A CTX mosaic, with resolution of 5m/pixel, was registered to a HRSC composite DTM. HiRISE, with a resolution of 0.5 m/pixel, imagery used to collect attitude measurements and visual data where relevant. In some instances, poor HiRISE and CTX DTMs was substituted with HRSC attitude measurements. Attitude measurements were taken with HiRISE where relevant in order to ensure accurate results. A composite CTX map with attitude measurements from HRSC, CTX and HiRISE data was created to display collected data. This map will be discussed in detail later.

3.2.3 ILD Layer Attitude Measurements

To measure layer orientation, Orion software was used. Using 3D coordinates of manually selected points, Orion calculates a best-fit plane using a multi-linear regression (Fueten et al., 2006). The manually selected points are placed along the trace of the chosen layer, and strike and dip are calculated based on the points' positions. The points placed along the measured layer were manually moved along the initial transect until the calculated plane matched the observed trace of the layer. Dip measurements had an error between ±/-1˚ and +/-5˚. The error was kept at less than the value of the dip to ensure that the correct dip direction was identified. This was done by moving the manually placed points so that the standard deviation is kept low. The computed plane was visually verified by rendering a 3D image which projected the proposed plane over the existing topography (Fig 3-1). In an attempt to

ensure reliable results, multiple measurements were taken, using HRSC and CTX, in the same area with trace lengths as long as the layer visibly outcropped. A composite CTX map with attitude measurements from HRSC, CTX and HiRISE data was created. This map will be discussed in detail later.

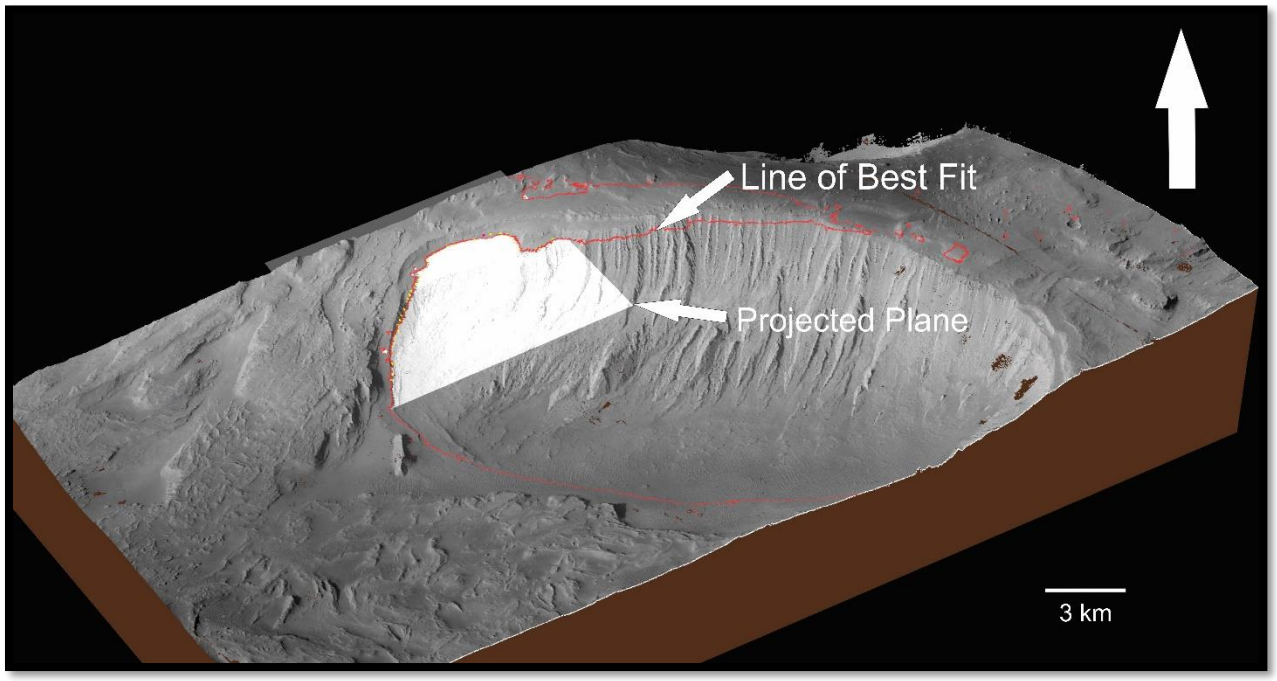

Figure 3-1: 3D rendering of measurement taken on mound B. The projected plane identifies the outline of the layered strata being measured.

Sets of layers, composed of groupings of contiguous parallel layers, were identified. The measurements conducted in layer sets generally had small variations in attitude between each layered outcrop. Attitude measurements were obtained from the mounds and ILD near the south wall. The terminology used in Chapter 2 to distinguish the mounds will be used here as well (Fig. 3-2).

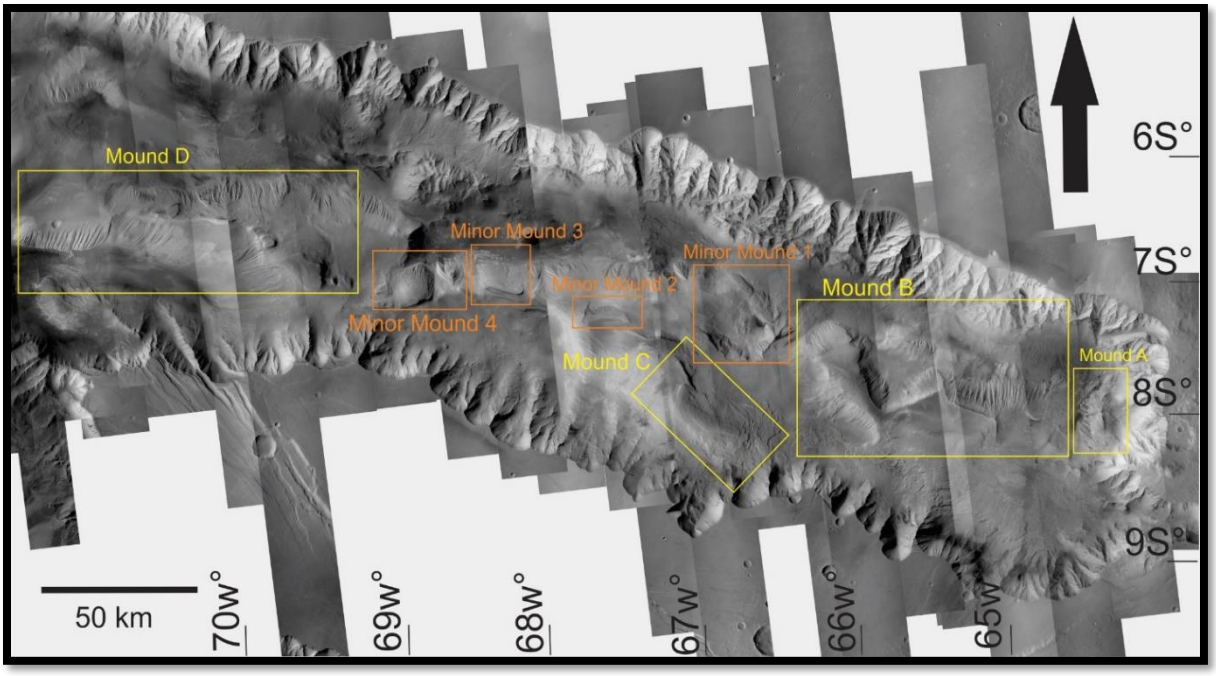

Figure 3-2: Identification of mounds and minor mounds of East Candor Chasma.

3.3.1 Attitude Measurements of East Candor Chasma

Chapter 2 presented six different ILD styles in East Candor Chasma. Three of these units (the thick layer, thin layer and steeply dipping units) display distinct layering, contain reasonably long trace lengths and are not disrupted by faults or folds. Layering within the central mounds and along the south wall provides enough exposure to make consistent measurements. Thick, thin and deformed layering is also clearly visible along the south wall in CTX imagery. Deformed layering yields little information on the original deposition of the material; thus, no attitude measurements were taken from this unit. The south wall contains well-layered ILD where almost 100 measurements were obtained. Over 200 attitude measurements were taken throughout East Candor Chasma.

3.3.2 Attitudes of Thick Layered Unit within the Central Mounds

Attitudes of the thick layer unit in the central Mounds of East Candor Chasma display a cluster of northward dips and strikes which parallel the chasma walls (Fig. 3-3). Thick layered units make up the largest area of layered units within East Candor Chasma, with several examples outlined below (Fig. 3-4). The thick layer unit layers tend to thin upward in stratigraphy, as has been documented in chapter 2. As the unit layers thin upward, the attitude of the ILD layering tends to decrease. In the upper stratigraphy of the central mounds, dips are near horizontal (3˚-6˚) (Fig. 3-5). Lower on the mounds and commonly on their north face, dips are much steeper, at 18˚-19˚ (Fig. 3-5). The dip thus appears to depend on the stratigraphic location of the layer in the mound, with stratigraphically lower layers having greater dips than those in the upper portions of the mounds. The strike associated with the dips at the upper portions of the mounds varies, while strikes associated with the dips lower in stratigraphy tend to be parallel to the length of the chasma, trending between 265° and 280°. To illustrate this tendency, Figures 3-5 and 3-6 depict mound B with several attitude measurements taken throughout the mound's elevation.

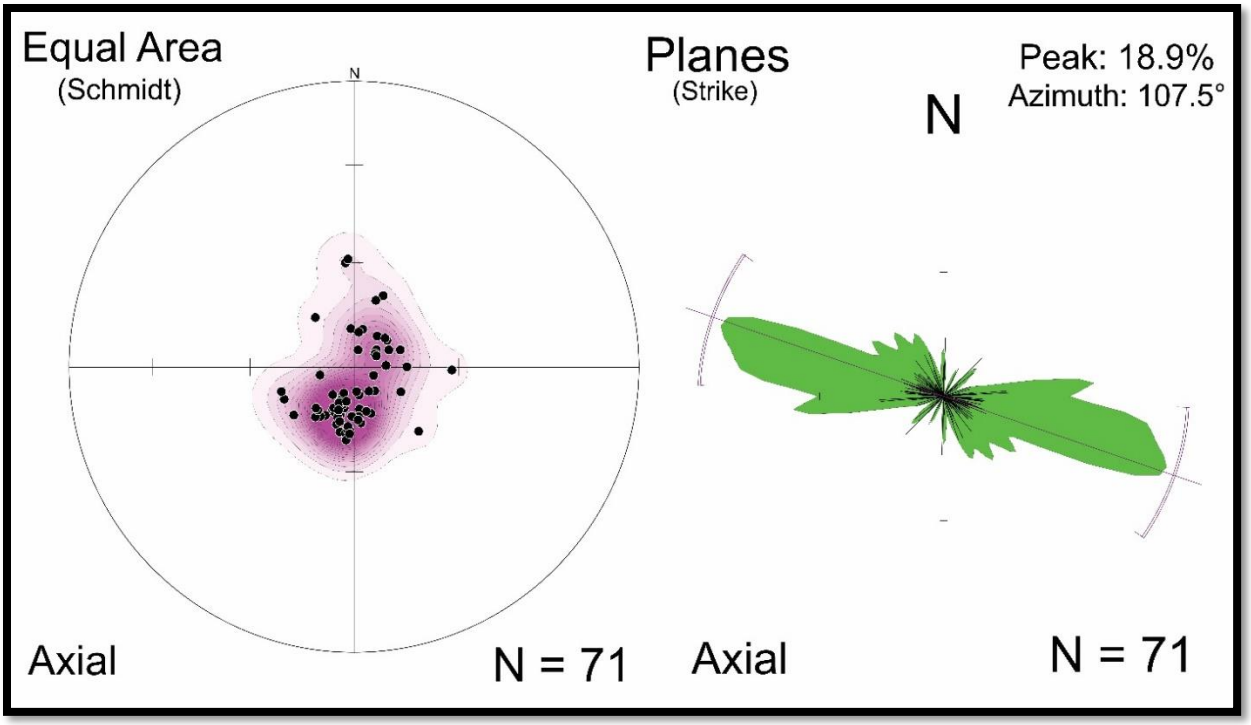

Figure 3-3: (Right) Schmidt net illustrating attitudes of thick layer unit found throughout the central mounds of East Candor Chasma. (Left) Histogram illustrating strike of thick layer unit found throughout the central mounds of East Candor Chasma.

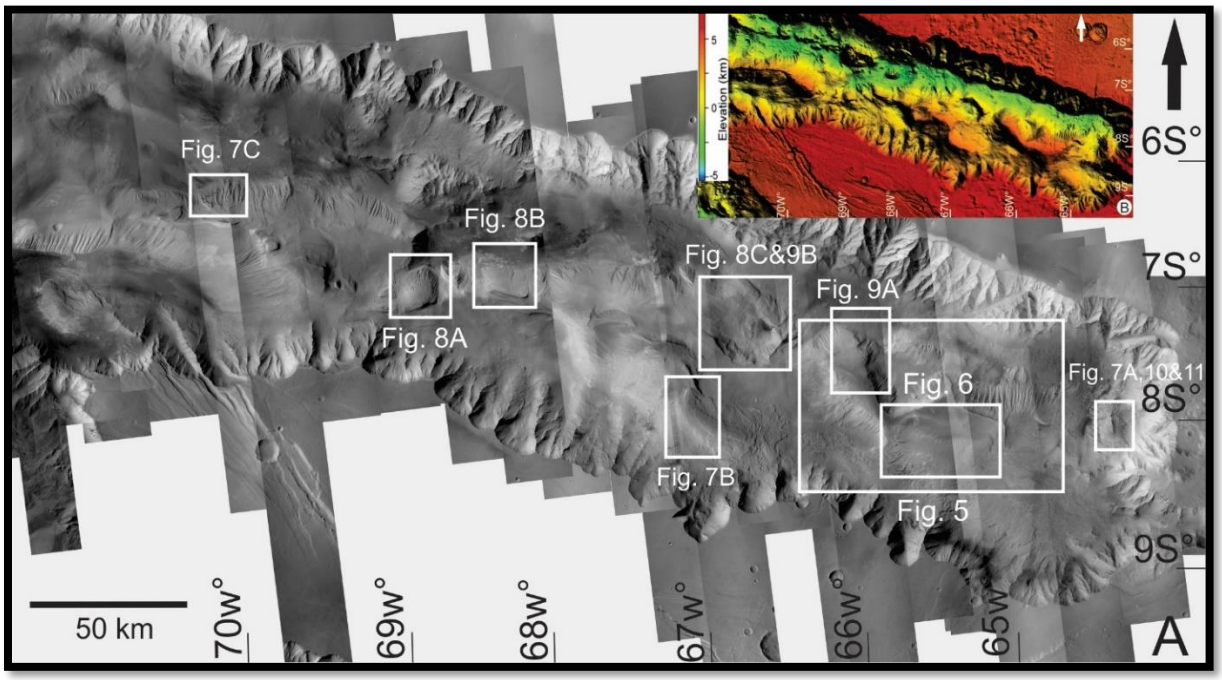

Figure 3-4: Locations of thick layer examples found in the central mounds of East Candor Chasma

Mound B is a is representative of a typical thick layer unit, as the majority of the mound is comprised of thick layered unit material. Benches are visible along the north and northwest face of the mound (Fig 3-5). Attitudes of layering display a wide range of dips. The lower, thick units on the north face dip 9˚-19˚ towards the north (Fig 3-5). While layering further up in sequence on the south face of the mound dip away from crest of mound at a shallower angle of 3˚-5˚, sometimes up to 11˚ along the edges of the mound (Fig 3-6).

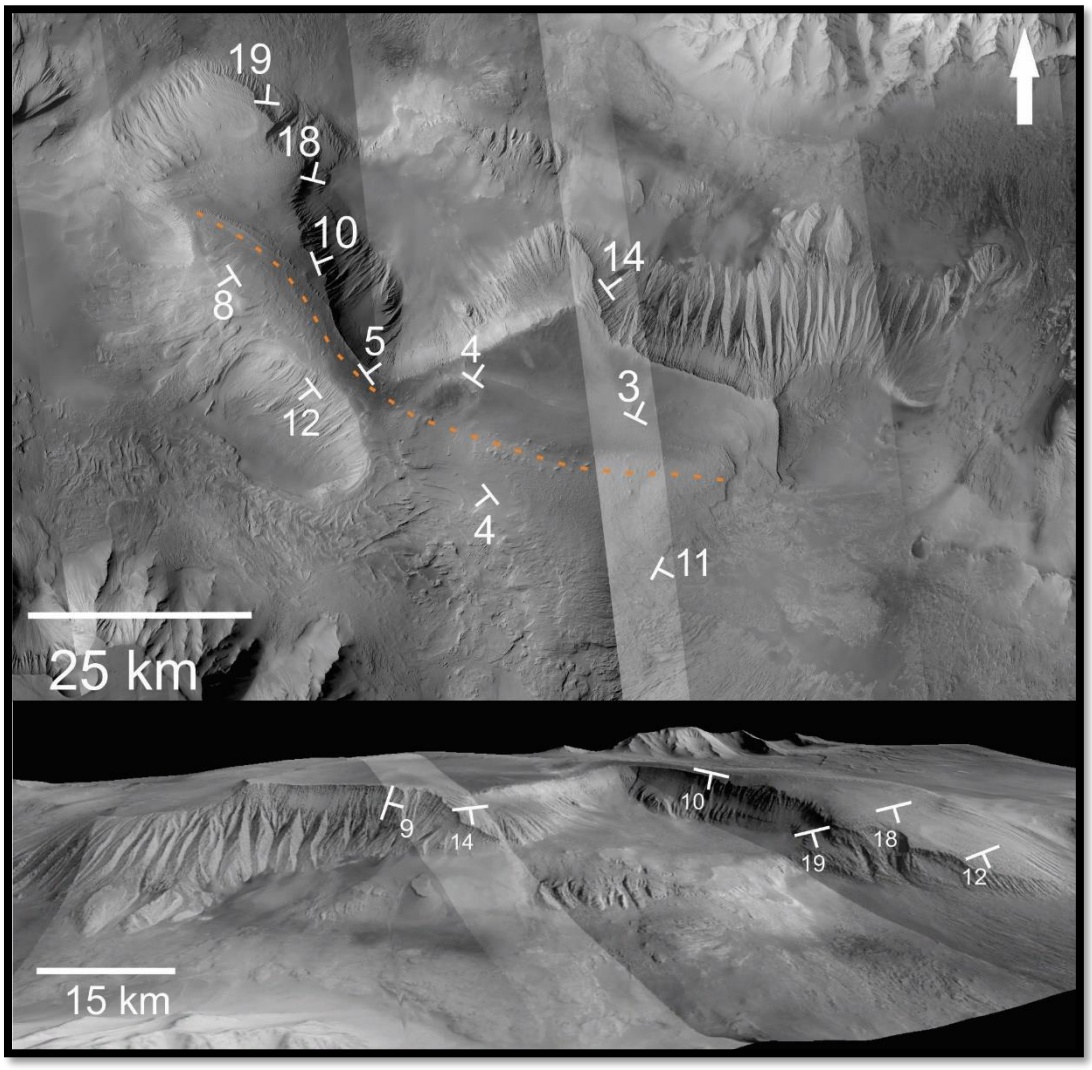

Figure 3-5 Upper: Mound B displaying dominant attitudes and crest of mound (dashed orange line). Lower: Mound B displaying exposed layering on north face with stratigraphically lower thick unit and respective dips. Image faces south.

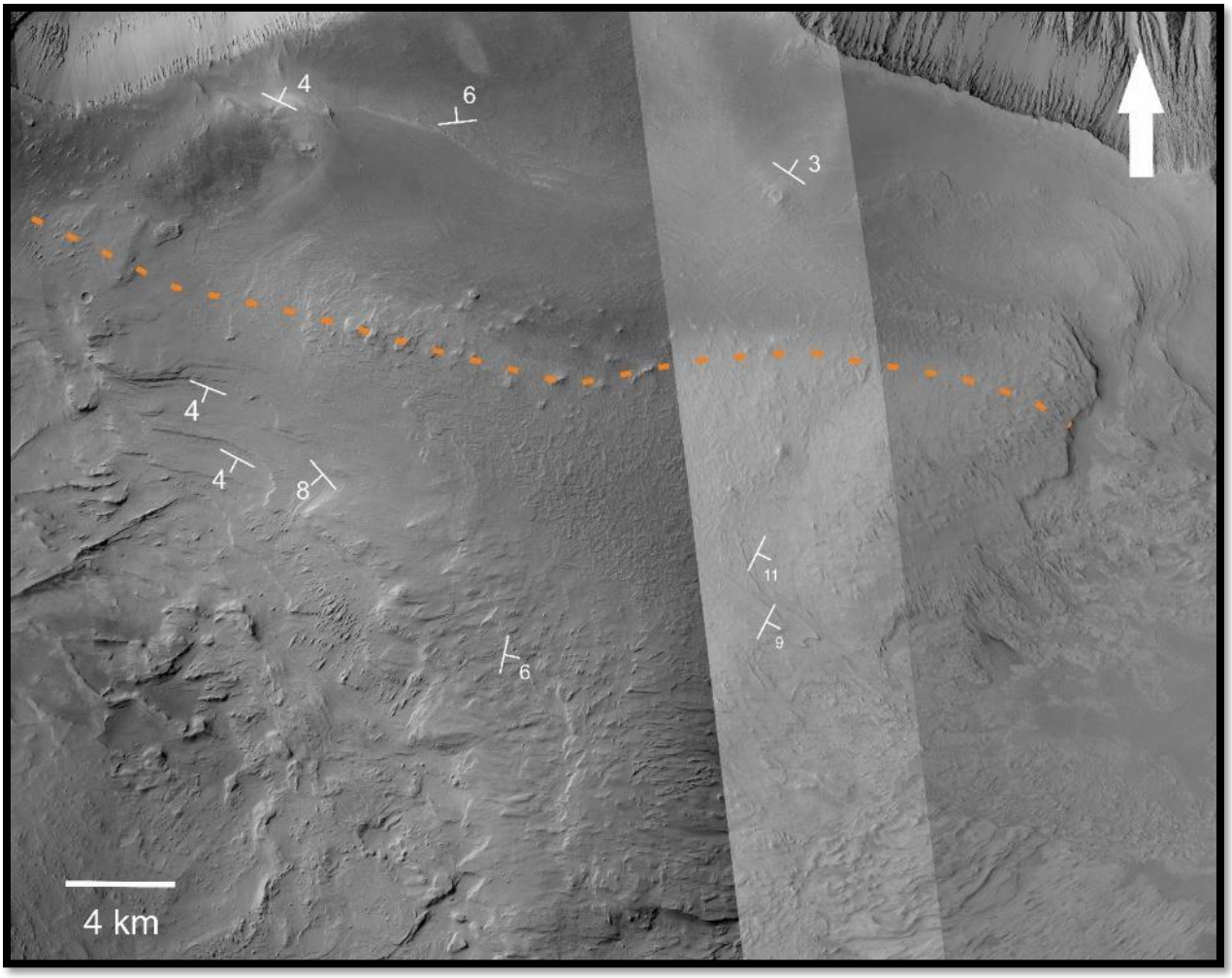

Figure 3-6: Mound B displaying exposed layering on south face with upper thick layer unit and respective dips. North is top of image.Orange dashedd line indicates the crest of the mound.

This attitude variation is not exclusive to Mound B. Shallow dips with varying strikes at the upper sections of mounds and steeply dipping thick layering with primarily chasma-parallel strikes can be observed in Mounds A, C, D (Fig. 3-7) and in Minor Mounds 1, 3, and 4 (Fig. 3-8).

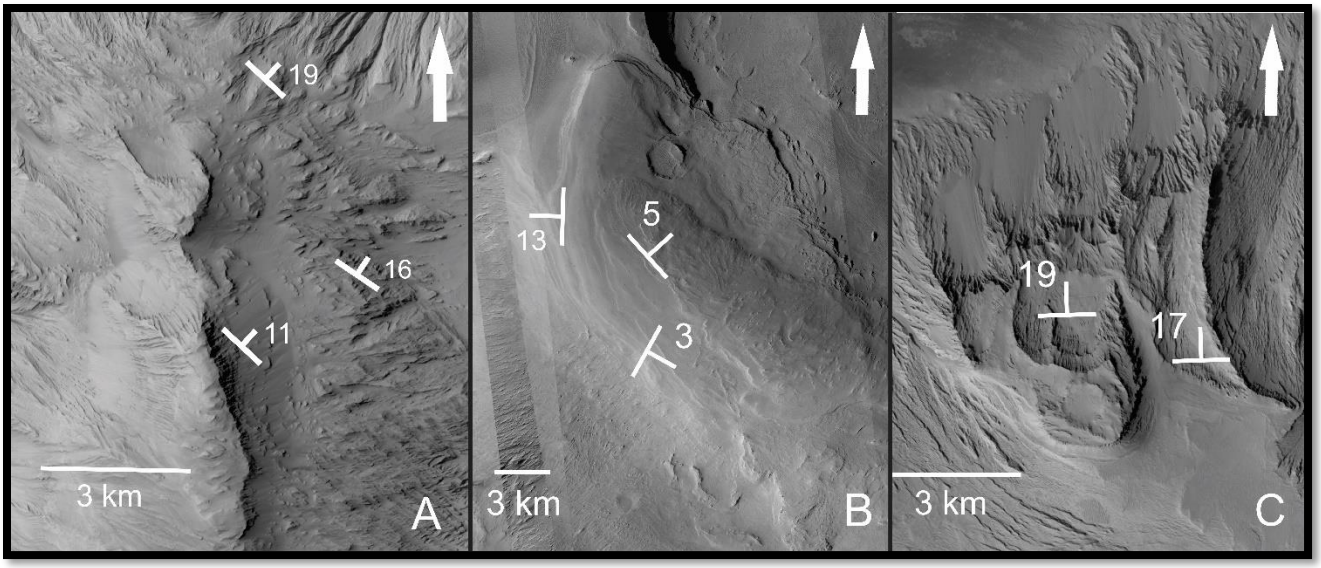

Figure 3-7: Attitudes of thick layering found throughout East Candor Chasma. (A) Attitudes of thick layering found in Mound A. Layers lower in stratigraphy display a steeper dip. (B) Attitudes observed in the upper secion of Mound C displaying dips with varying strike. (C) Attitudes of thick layering found in the lower stratigraphy of Mound D displaying steep dips in benches.

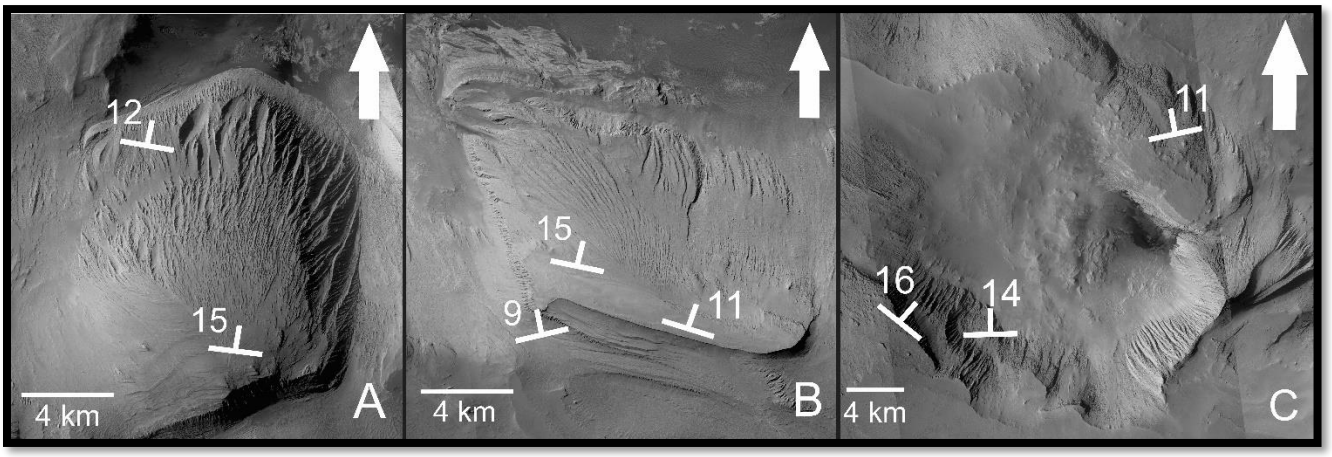

Figure 3-8: Attitudes of thick layering in minor mounds throughout East Candor Chasma. (A) Attitudes found in thick bench layering found in Minor Mound 1. (B) Attitudes of thick layering found in Minor Mound 3. (C) Attitudes of thick bench layering found in Minor Mound 4.

Benches are common throughout East Candor Chasma near the base of the thick layered unit. They are primarily observed in the central mounds, with only one visible outcrop occurring along the south wall. They commonly overlie the massive unit and are often overlain by thick or thin layering (Fig. 3-9). The benches dip primarily to the north between 12˚ and 19˚ but have been observed dipping as low as 8˚ and as high as 21˚. Individually measured layers between benches have the same attitudes as the benches, confirming that benches are exposed layers.

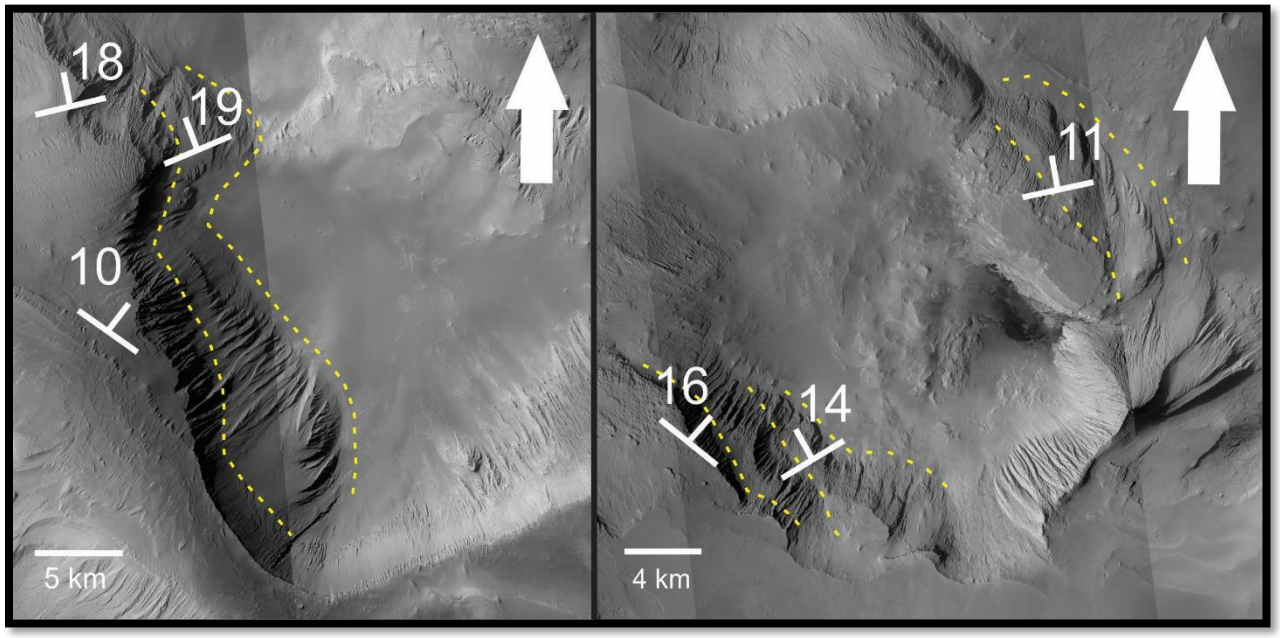

Figure 3-9: Example of benches found in East Candor. Image on left is part of Mound B. Image on Right is part of Minor Mound 1. Yellow dashes outline suspected bounding surfaces between respective bench layers.

3.3.3 Attitudes of Steeply Dipping Unit Within the Central Mounds

The unique steeply dipping lower unit of Mound A contains thick layering with dips in excess of 30˚ (Fig. 3-10 & 3-11). The average strike of the steeply dipping layering is 85˚, with an average dip of 30˚ (Fig 3-

11). The steeply dipping unit is surrounded by other layer units and chasma wall. To the north lies a thick layered unit with dips range from 16˚-19˚ to the northeast. Lying unconformably over both units is another thick layered unit whose layer attitude is measured at ~11˚ to the northeast.

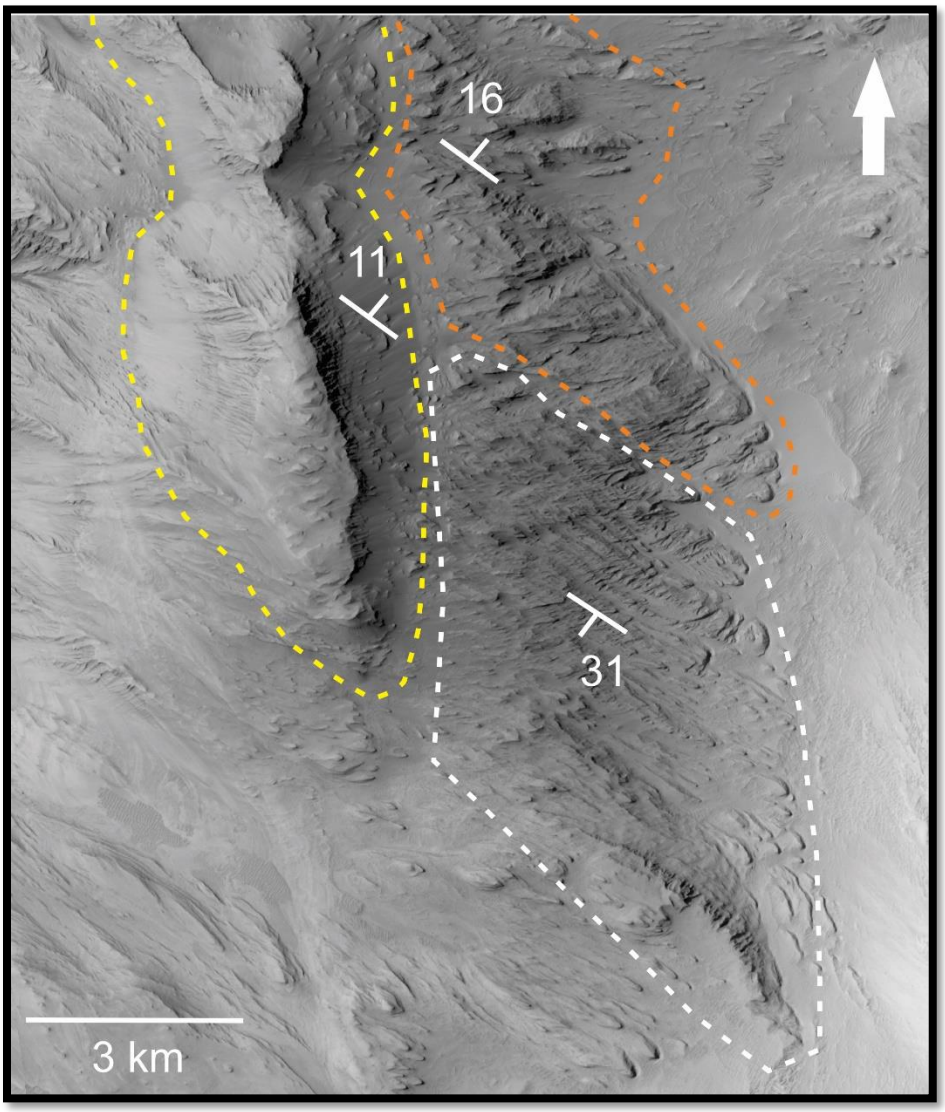

Figure 3-10: Mound A, steeply dipping unit outlined in white dashed area. Orange dashed area is a thick layer unit which lies to the north of the steeply layered unit. Yellow dashed area is a thick layer unit which lies unconformably over the two lower units.

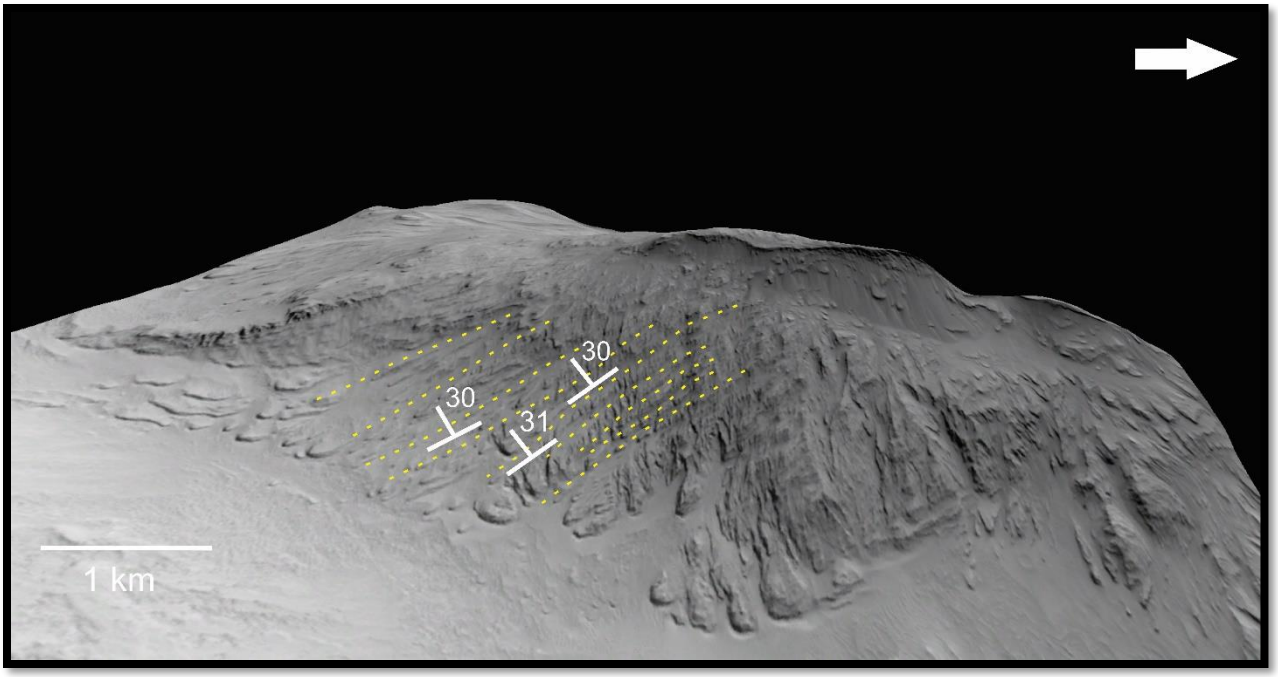

Figure 3-11: 3D image of Steeply dipping unit found on the lower east side of Mound A. Dashed yellow lines indicates layering with attitudes up to 31˚. VE: 1x's.

3.3.4 Attitudes of Thin Layer Unit within the Central Mounds

The attitudes of the thin layer unit display an even distribution with less variability in dip value compared to that of the thick unit (Fig. 3-12). The strike of the thin layers displays similar trends as in the thick layer unit, approximately parallel to the strike of the chasma walls (Fig. 3-12). The thin layering on the upper section of the mounds in East Candor drapes unconformably over the pre-existing geology (Figs. 3-13 & 3-14) and commonly display dips that are near-horizontal or moderately inclined (< 6˚). Because the thin layer unit drapes the pre-existing geology, deposits placed on topography that already has a steeper slope tend to have a greater dip. This feature is observed along the lower portion of Minor Mound 3 (Fig. 3-15). Obtaining accurate layer measurements on a sloping surface can be difficult due to downslope bias. The computed plane of the surface closely mimics the slope of the topography giving an

inaccurate attitude of the layered surface. Visually inspecting the projected plane on the sloped surface in 3D is required to ensure that actual layer measurements are obtained.

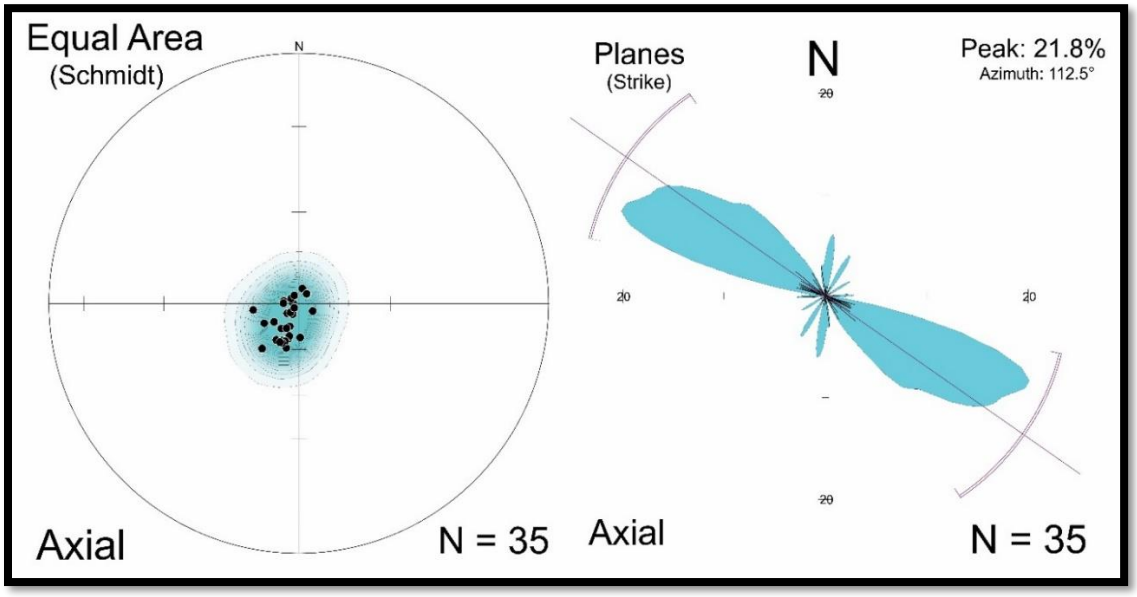

Figure 3-12: (Right) Schmidt net illustrating attitudes of thin layer unit throughout the central mounds of East Candor Chasma. (Left) Histogram illustrating strike of thin layer unit throughout the central mounds of East Candor Chasma.

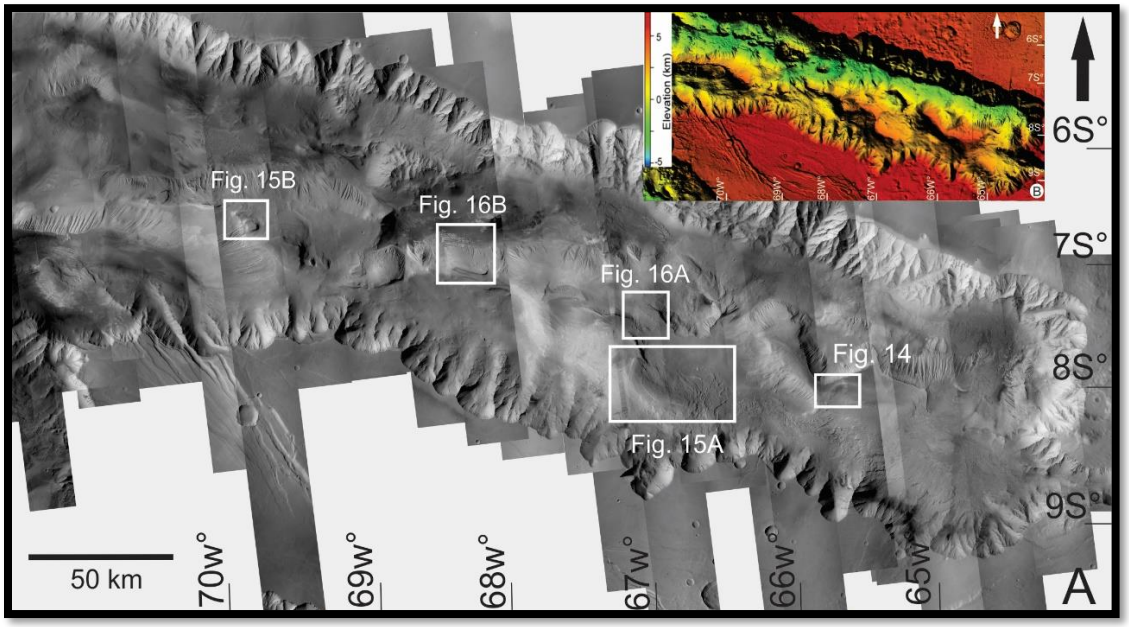

Figure 3-13: Locations of thin layer unit examples in the central mounds of East Candor Chasma

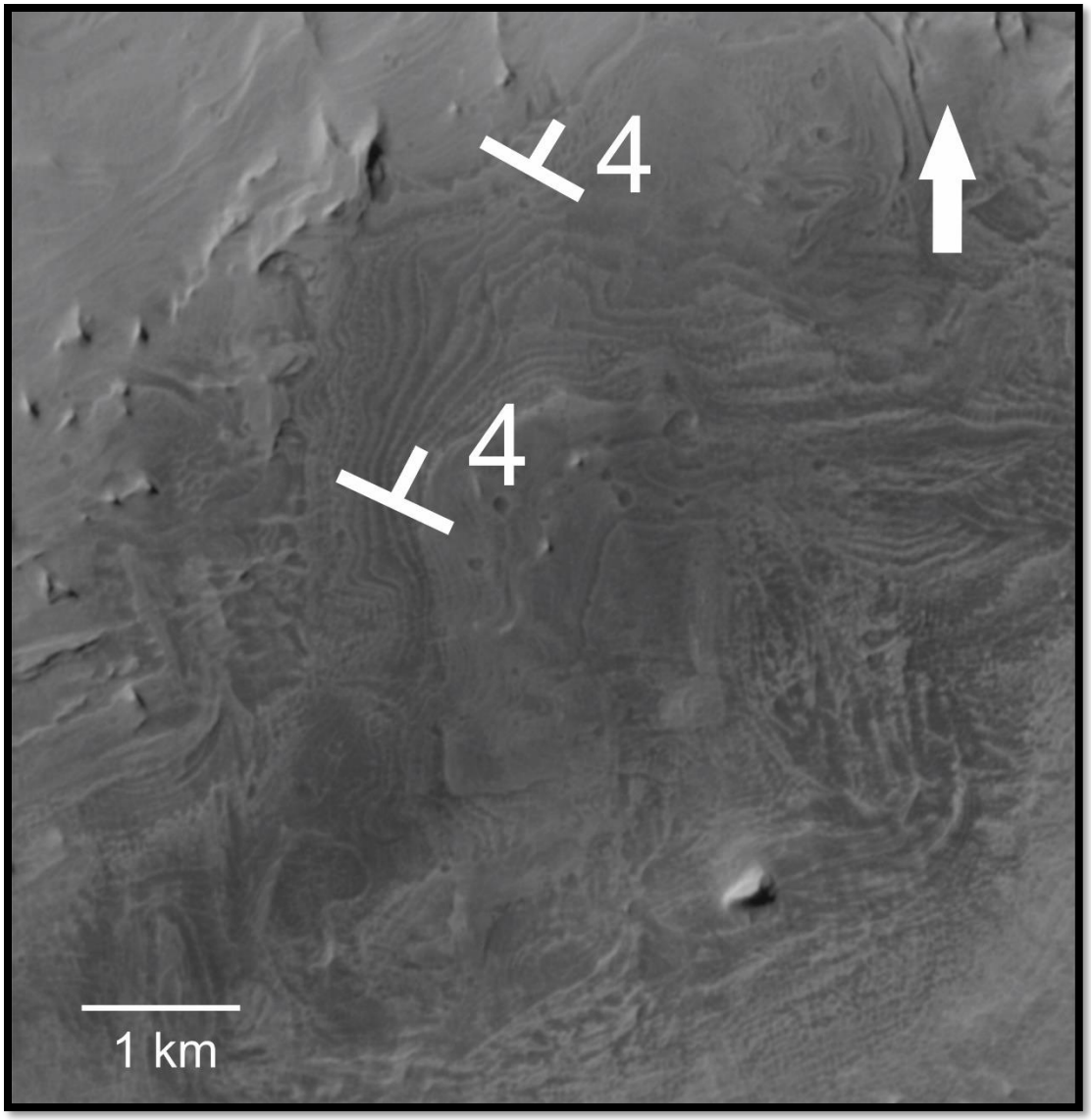

Figure 3-14: Fine layer unit on the top of Mound B. Topography slopes gently to the north of the image.

Thin layering can be observed on the tops of Mounds B, C and D; as well as Minor mounds 1 and 3 (Fig. 3-15 & 3-16). The strike of the thin layer unit varies throughout the central mounds but remains approximately NW-SE. This is consistent with the strikes observed in the thick layer unit.

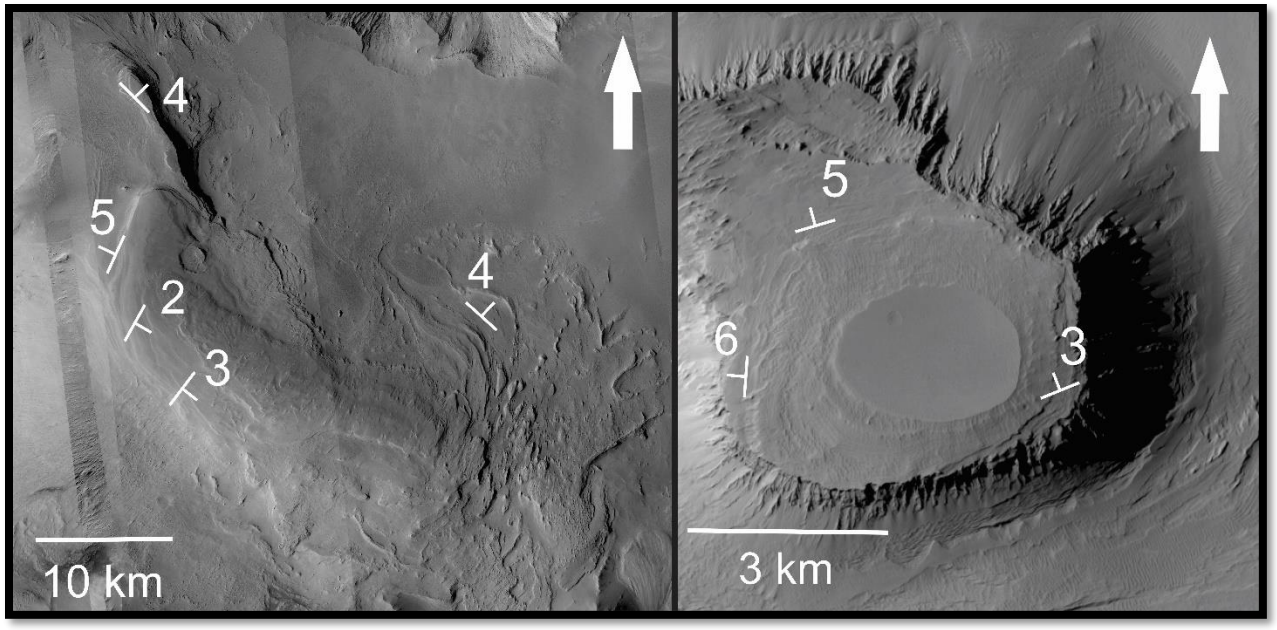

Figure 3-15: Thin unit observed on Mound C (Nia Mensa) (left) and Mound D (right) overlying the thick unit. Topography moves away from the crest of the mound.

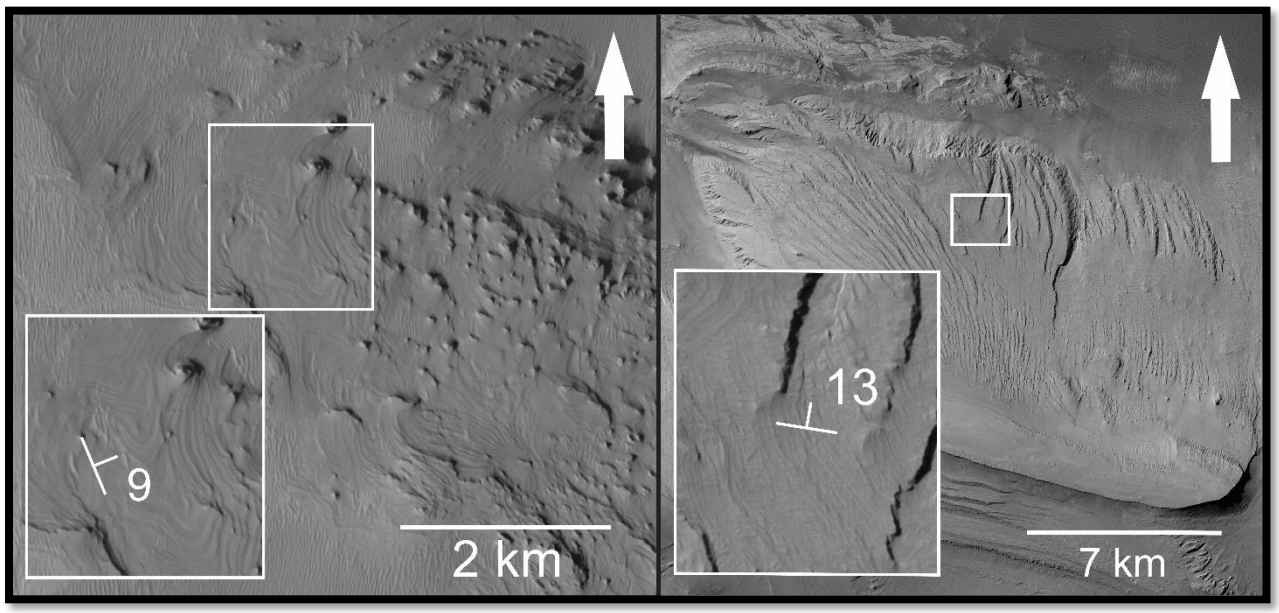

Figure 3-16: Fine layering observed in the southwest corner of Minor Mound 1 (left). Fine layering observed along the lower part of Minor Mound 3 (right). Topographic slope is towards the north of both images.

3.4.1 Thick Layer Unit along the South Wall

The south wall of East Candor Chasma contains an abundance of well defined ILDs (Fig. 3-17). Attitudes for the thick layered unit range depending on their position along the slope of the wall. Thick layering within the gullies can be near horizontal to 3˚-4˚ (Fig. 3-19), while dips along the spurs have a steeper angle, up to 12˚ (Fig. 3-19). Steeper attitudes of layering near the spurs of the south wall mimic the spur attitude further up the chasma wall. Overall attitudes of thick layer units along the south wall of East Candor Chasma have generally low dip values but significant variations in strikes (Fig. 3-18). Thick layer deposits drape the lower elevations of the spurs and fill in the gullies along the southeast wall of the chasma (Figs. 3-19 & 3-20).

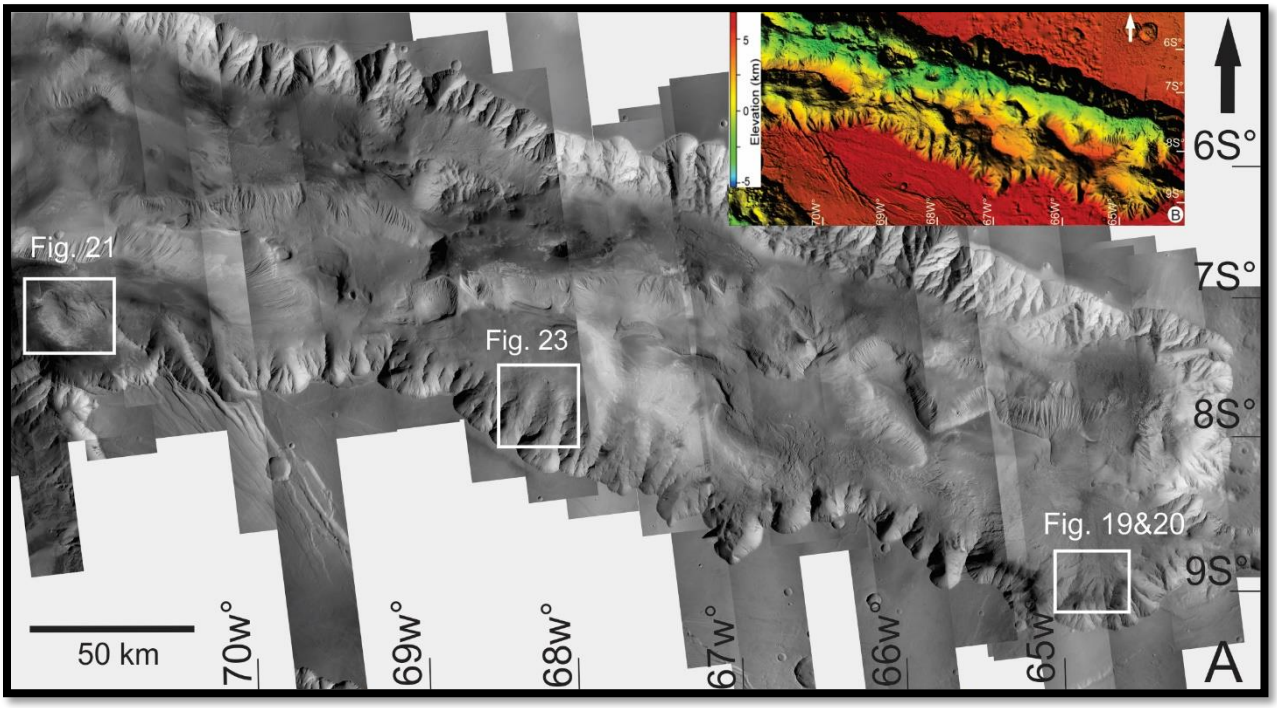

Figure 3-17: Locations of thick and thin layer unit examples in found along the south wall of East Candor Chasma

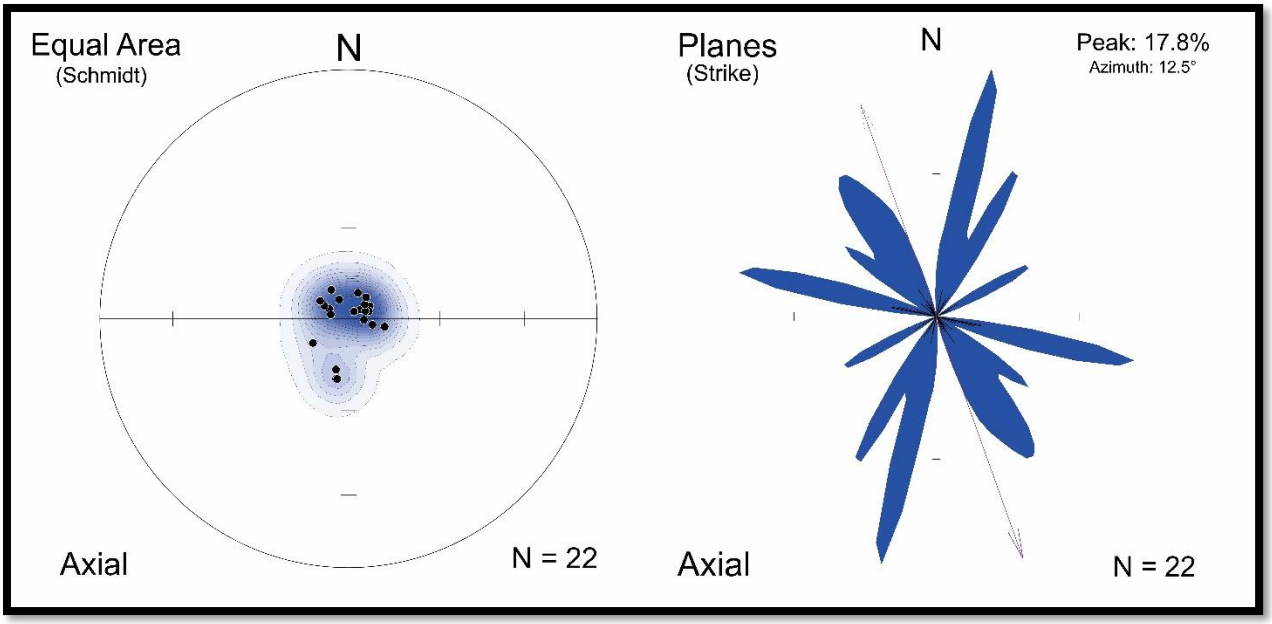

Figure 3-18: (Left) Schmidt net illustrating attitudes of thick layer unit found along the south wall of East Candor Chasma. (Right) Histogram illustrating strike of thick layer unit found along the south wall of East Candor Chasma.

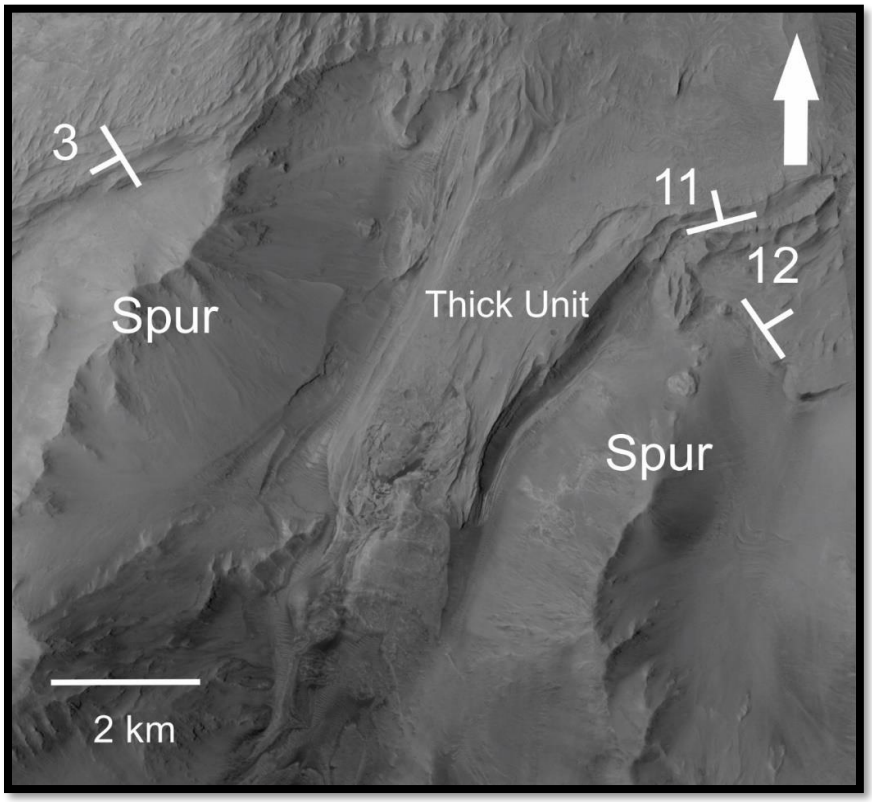

Figure 3-19: Thick unit filling in gully along the south wall of East Candor Chasma.

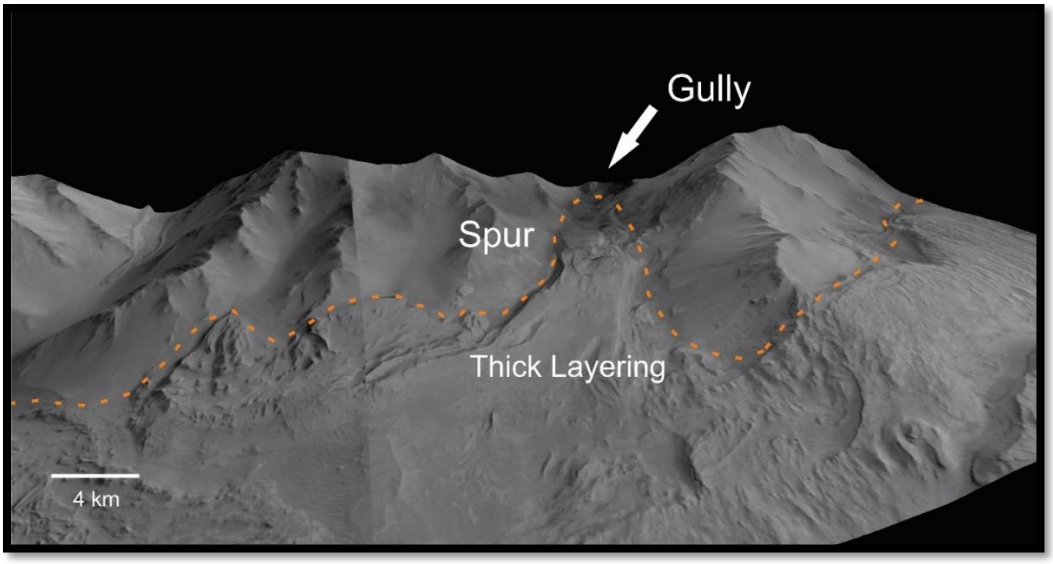

Figure 3-20: 3D view of thick layer unit filling in gully. Orange dashed line indicates boundary between spur and thick layering. View looking south.

As mentioned previously, along the south wall of East Candor Chasma is one bench unit (Fig. 3-21). The attitude of this deposit dips 17˚ towards the chasma floor. Lying unconformably above the bench is a well eroded thick layer unit which dips 10˚ towards the north. Inset B and C of Figure 3-21 display projected attitude planes that each thick layer unit could have extended to in the past shortly after deposition ceased.

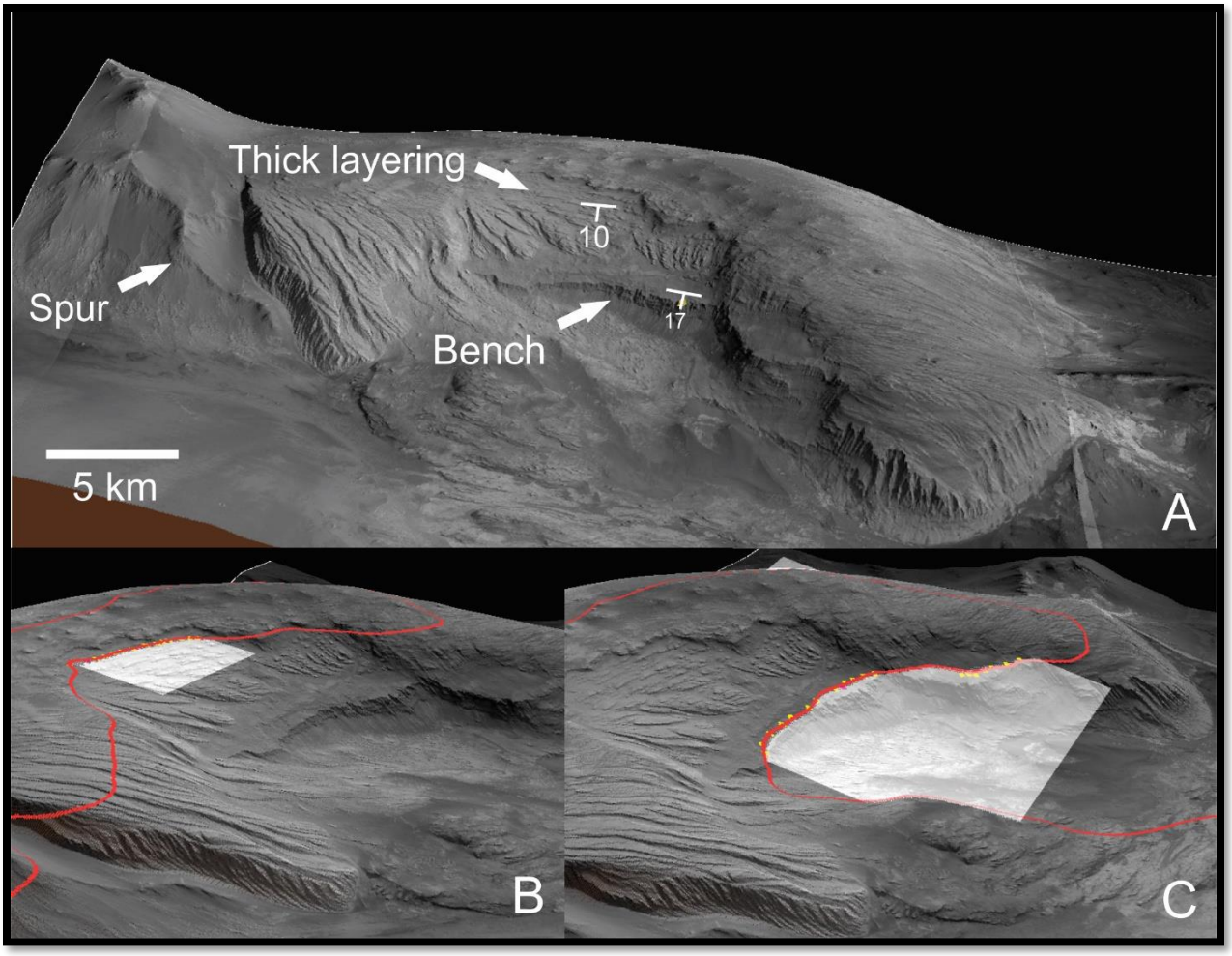

Figure 3-21: Steeply dipping unit within East Candor Chasma. Image A: faces south, outlines bounding spur, bench and thick layer; with respective dips. Image B: facing southwest, outlines plane of benched unit. Image C: faces southwest, outlines plane of thick unit.

3.4.2 Thin Layering along the south wall

Attitudes of thin layering along the south wall display a wide variation (Fig. 3-22). The thin layered unit is observed over a larger area and at a higher elevation along the spurs of the south wall. A high degree of variability is found in attitude measurements for this unit (Fig. 3-23). Some measurements are near horizontal at 2˚ and 3˚, while others are found as high as 20˚ to 26˚. The dip directions vary greatly depending on the layers position along the spurs and gullies. In some instances, thin layering can be

observed draping the base of an entire spur. The thin layering drapes the pre-existing geology of the spur and gullies and attitudes reflect the topography below.

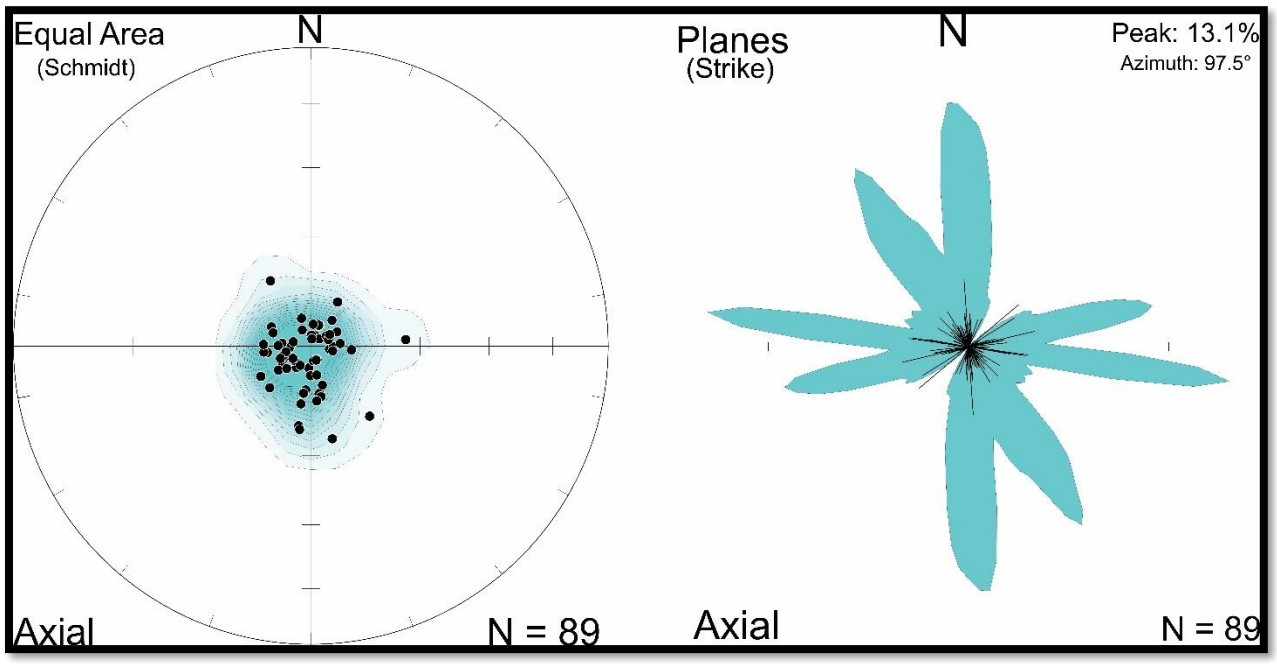

Figure 3-22: (Right) Schmidt net illustrating attitudes of thin layer unit along the south wall of East Candor Chasma. (Left) Histogram illustrating strike of thin layer unit along the south wall of East Candor Chasma.

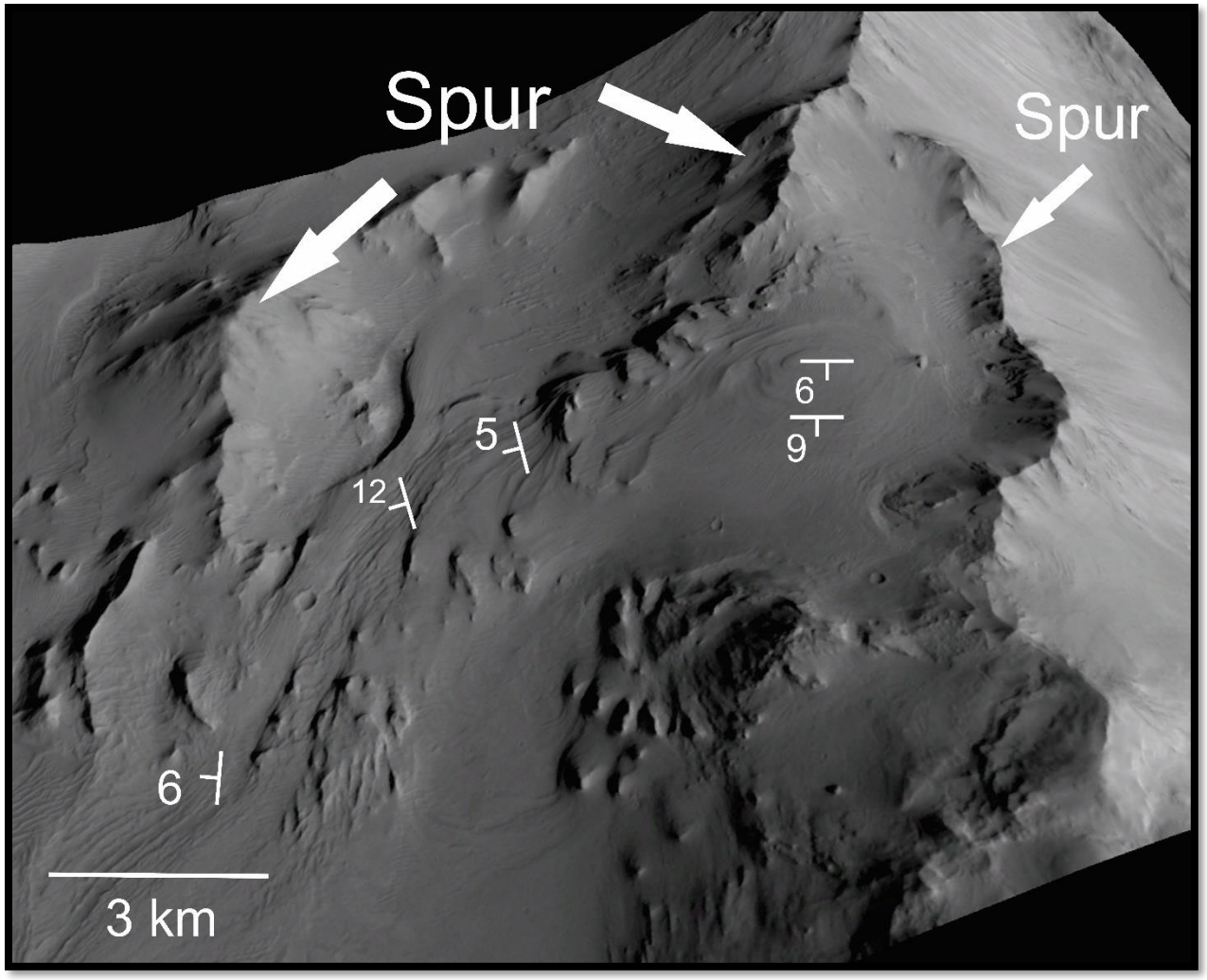

Figure 3-23: Thin layering along the south wall of East Candor Chasma. Dips are variable depending on their location to the spur.

3.5.1 Attitudes of unconformities in Thick Layer units

Unconformities have been observed throughout East Candor Chasma (Fig. 3-24). They are recognizable by appearance of layering and confirmed by attitude measurements. Where the layering is confirmed to be dissimilar in orientation by the attitude measurements the packages have an unconformity between them.

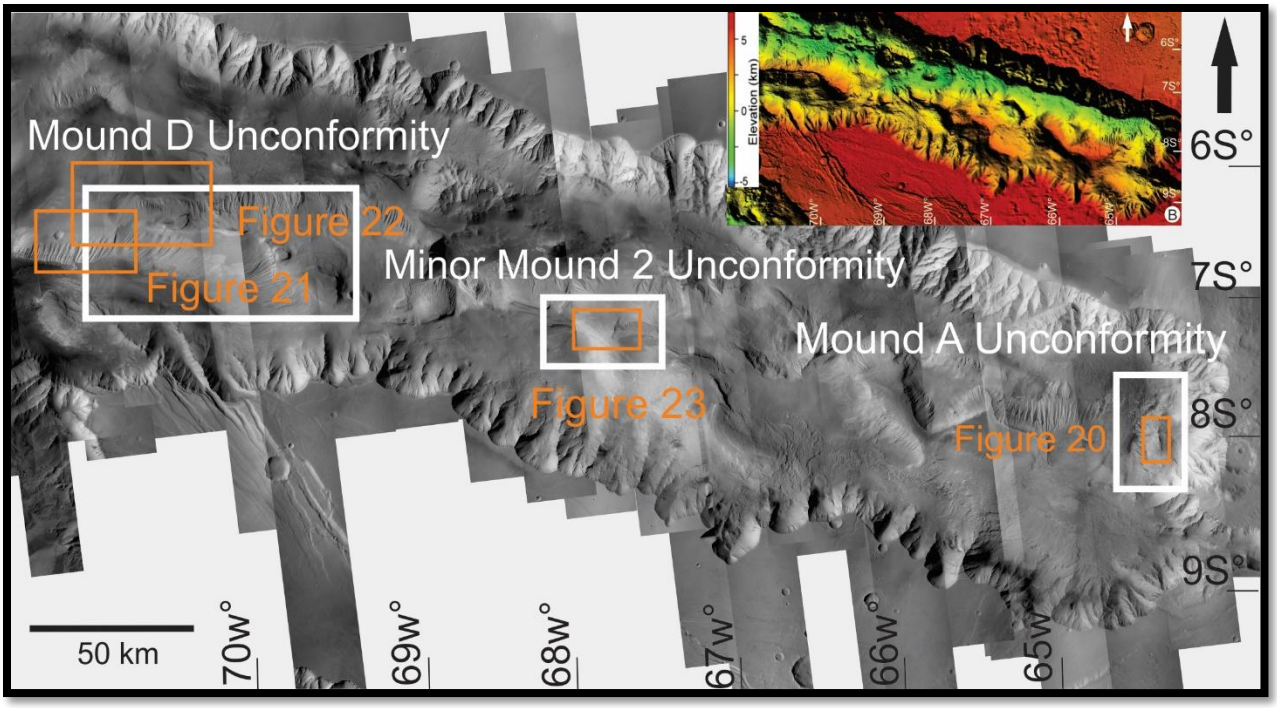

Figure 3-24: Location map indicating the outlined areas where unconformities have been observed in East Candor Chasma

Two unconformities were observed in Mound A, based on the attitudes discussed above (Fig. 3-25). The lower stratigraphic section of the mound contains two packages with opposing dips. Further up in stratigraphy, lying unconformably over the two packages, is a third thick layer package with a much shallower dip. This area is unique as the mound is isolated from the other central mounds by almost 35 km and contains three distinct packages with different attitudes in a comparatively smaller area.

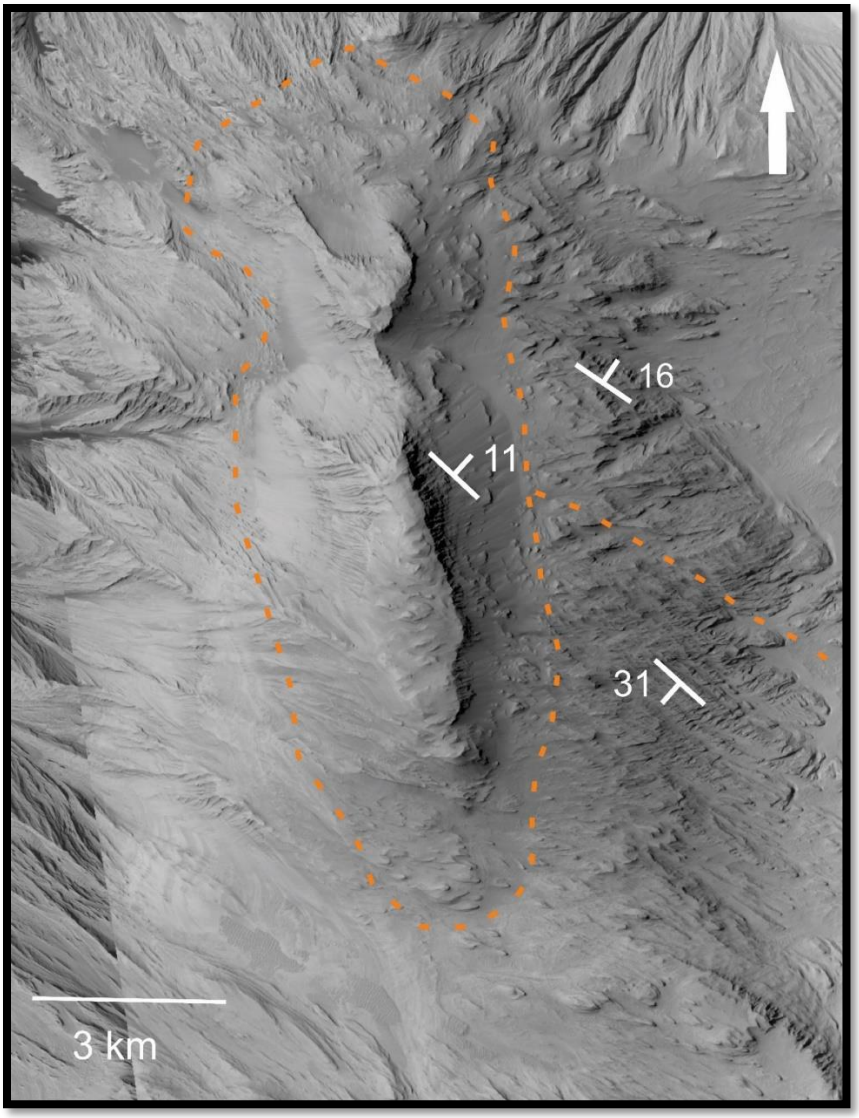

Figure 3-25: Mound A displaying multiple packages with two unconformities outlined by the orange dashed lines.

A large unconformity has been observed truncating much of Mound D (Fig. 3-26), where two distinct layered units are observed truncating one another. The older layered unit (Fig. 3-26B) is heavily eroded, with a dip of 12˚ to the southwest. The younger unit (Fig. 3-26C) truncates the older unit and contains thinner layering, with a dip of 7˚-9˚ to the west-southwest.

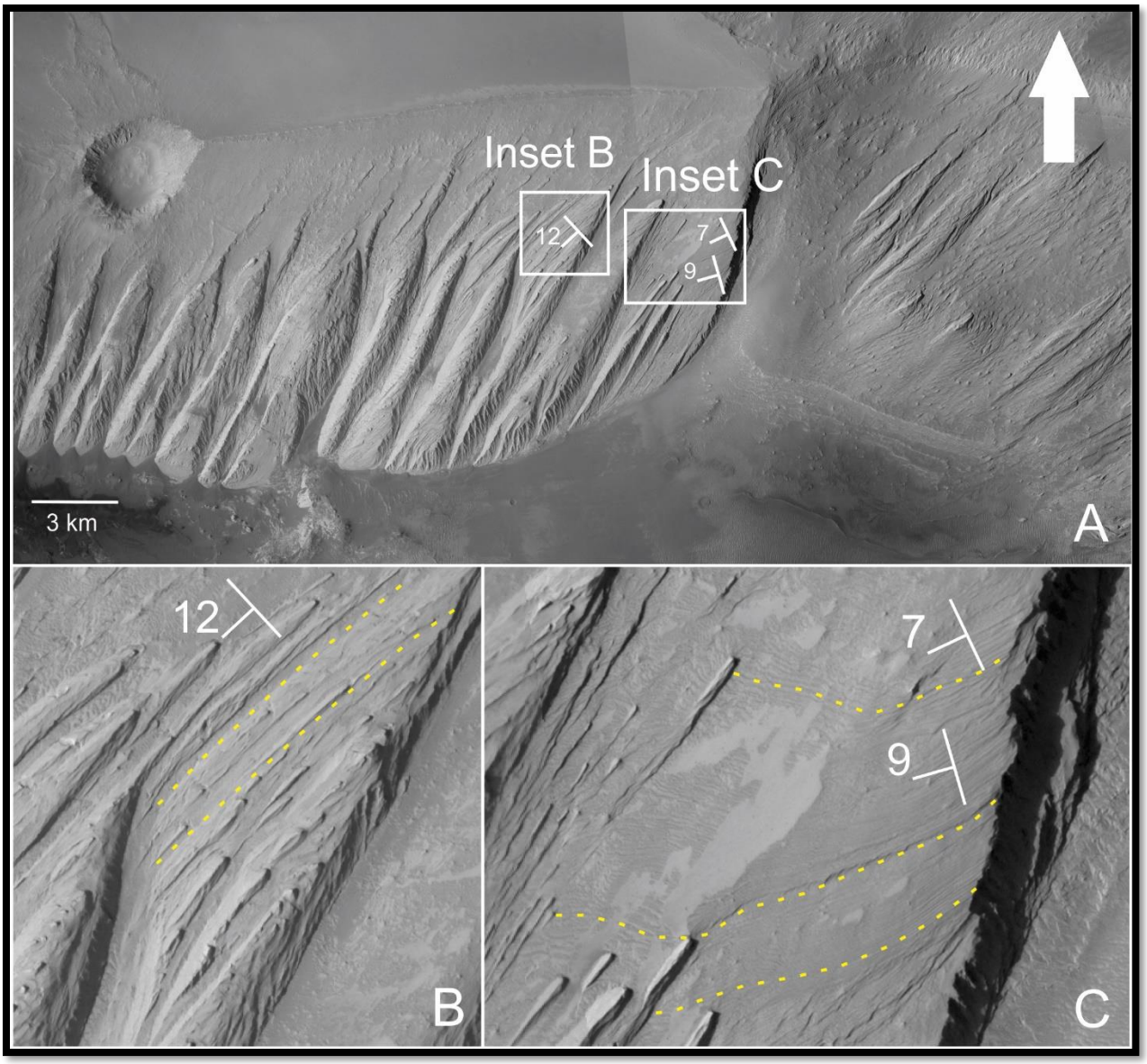

Figure 3-26 A: South face of Mound D displaying two separate thick layered units. B: magnification of primary layered unit with attitude and layering outlined in yellow dashed lines. C: Magnification of secondary layered unit that truncates primary with attitudes and layering outlined in yellow dashed lines. The more resistant outcrops rising above the surface are interpreted as outcrops of lower unit

The north face of mound D also displays an unconformity separating two thick layer units. The layering within the packages is difficult to measure due to the erosion at the surface. The younger unit appears

to lie unconformably over the older unit, tracing its eroded slope with a dip of 6˚ to the northeast (Fig. 3-27).

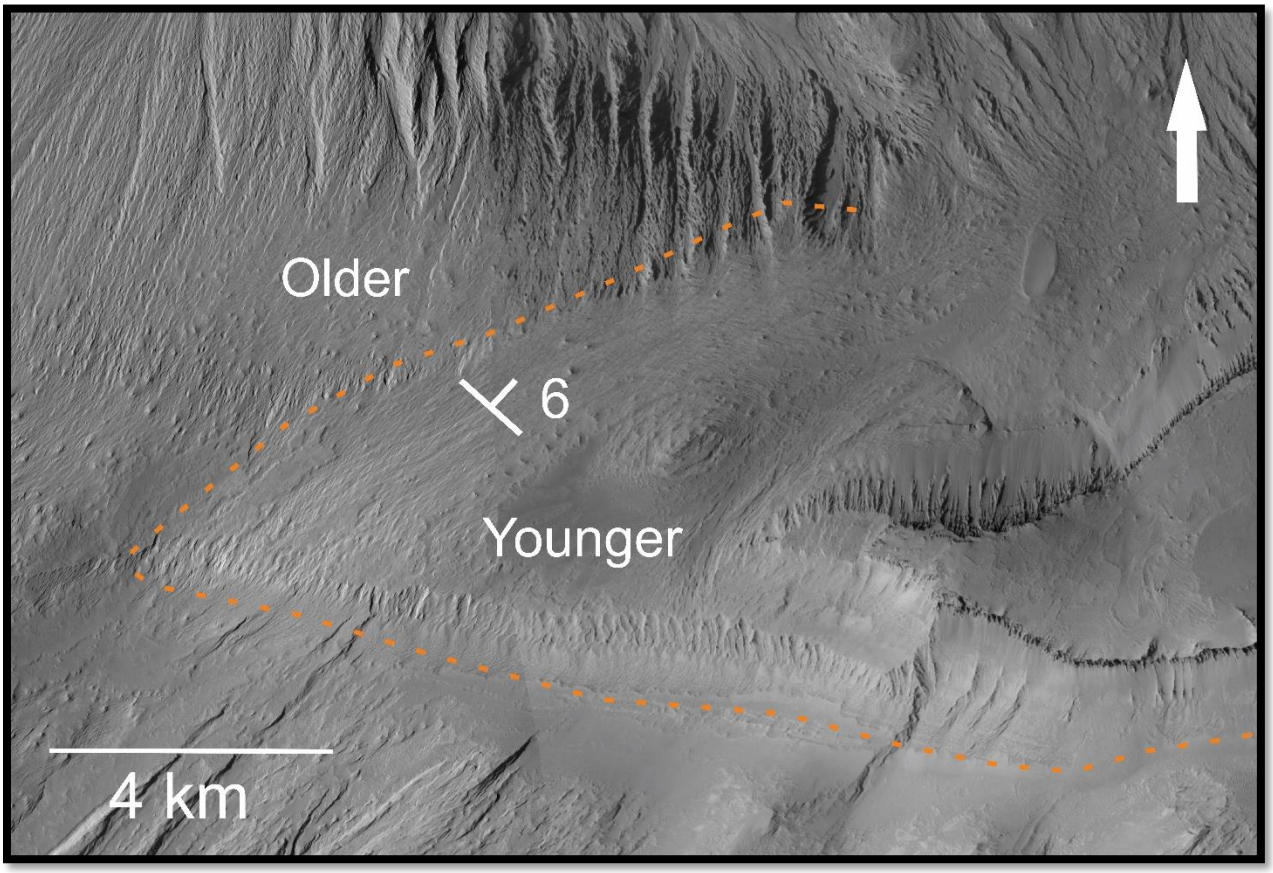

Figure 3-27: North face of Mound D displaying one thick layer unit laying unconformibly over the other.

Located along the northern section of Minor Mound 2 are two unconformities (Fig. 3-28 A) that are smaller and less distinct than the previous. The unconformities consist of a thick layered unit which truncates two other layers. Layering on either side of the unconformity is near horizontal (~3˚ to 6˚), while the unit which disrupts the near horizontal layering is almost perpendicular to it dipping at 21˚ (Fig. 3-28 C).

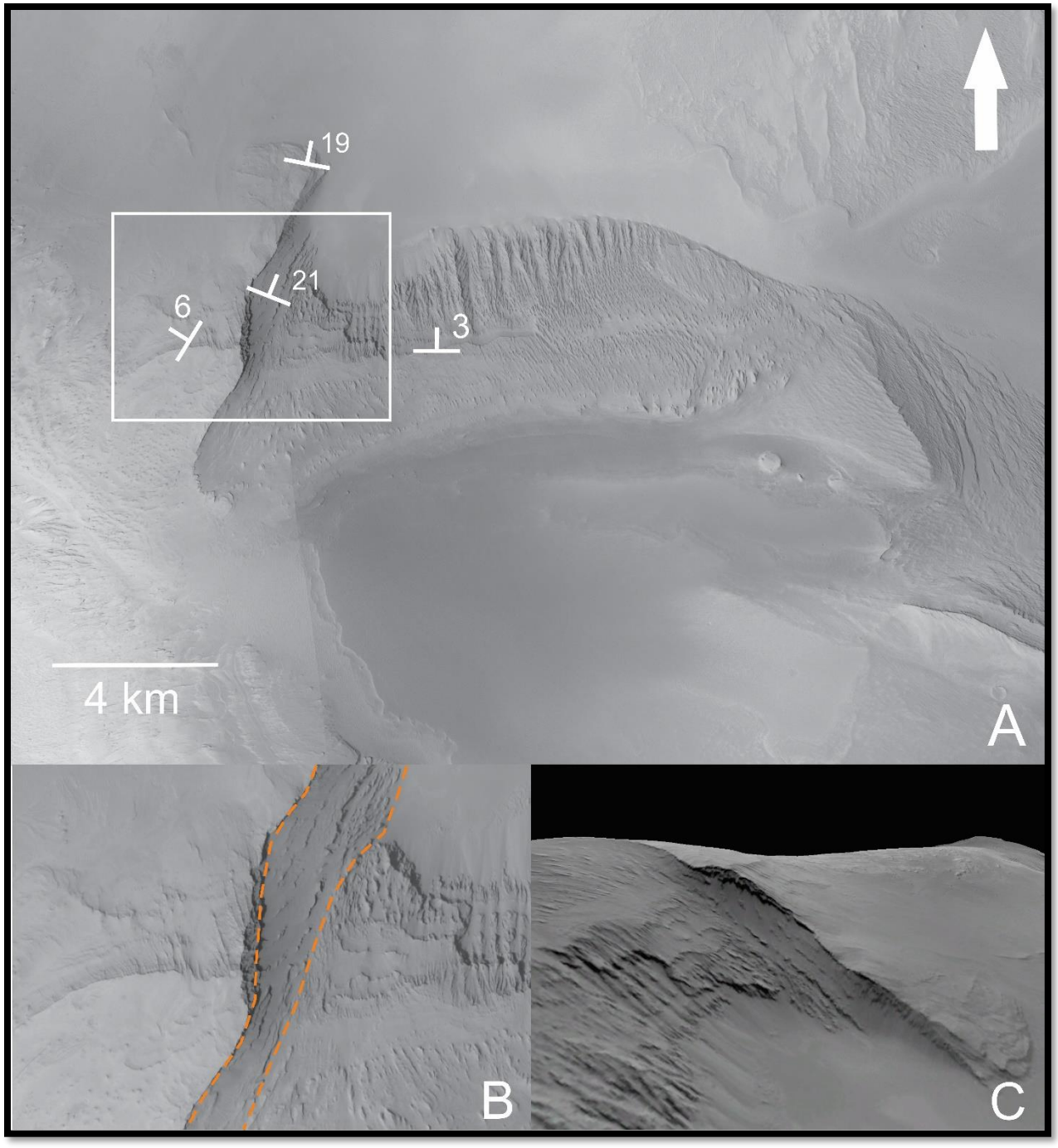

Figure 3-28: Minor Mound 2 displaying two unconformities. (A) Unconformities with dips of various layers, white box shows inset of image (B); Topographic slope is to the north of the image. (B) Inset of unconformity area shown in (A), orange dashed lines indicate unconformity boundaries. (C) 3D view of unconformity facing southwest VX=1.

Unconformities in East Candor Chasma are significant as they occur in thick layered units, at ~500 m-1000 m near the upper portions of the mounds and are widely spaced throughout the chasma.

3.6.1. Dips vs. Elevation

Depending on the deposition process, sediments filling a pre-existing basin will show evidence of draping onto underlying geology and chasma walls (Okubo, 2010). They often infill the lowest lying topographical areas first, with layers taking on the dip of the pre-existing geology or adhering to the angle of repose for the depositional environment (Mangold & Ansan, 2005). Central mounds in East Candor Chasma display a decrease in dip value with an increase in elevation. As mentioned in chapter 2, stratigraphy and elevation are not the same. Stratigraphy is the order in which sedimentary deposits are laid down. In geology elevation is considered a measurement of a topographical surface. In this thesis elevation is only used to correlate units that appear to be of the same origin.

Attitudes of thick layer units in mound A decrease with an increase in elevation (Fig. 3-29). No thin layering was observed in Mound A. Anomalous steep layering on Mound A are shown in orange. The dip of thick and thin layered unit in Mound B decrease with an increase in elevation (Fig. 3-29). Mound C is closer to the south wall and at a higher elevation compared to other mounds within East Candor Chasma. Attitude measurements were taken from the upper section of the mound and the lower northeast face of the mound. The separation of attitudes measurements is apparent in the diagram (Fig. 3-29). In the upper section of Mound C thick layering dips decrease with an increase in elevation. Dips of thin layering on the upper section of Mound C are ~ 3˚-5˚ between 2500 m and 3000 m. The lower section of Mound C does not display a decrease in dip value with increased elevation. Dips of thick layering clusters are ~7˚-10˚ between 1000 m and 1500 m. Mound C's proximity to the south wall may

have affected the layer attitudes of the lower section. Thin layering Mound D is observed along the tops of the mound with dip angles of the underlying geology. Attitudes of thick layering within Mound D display a wider distribution than the other mounds (Fig. 3-29). Erosional unconformities are likely the cause of for complexities observed within the mound.

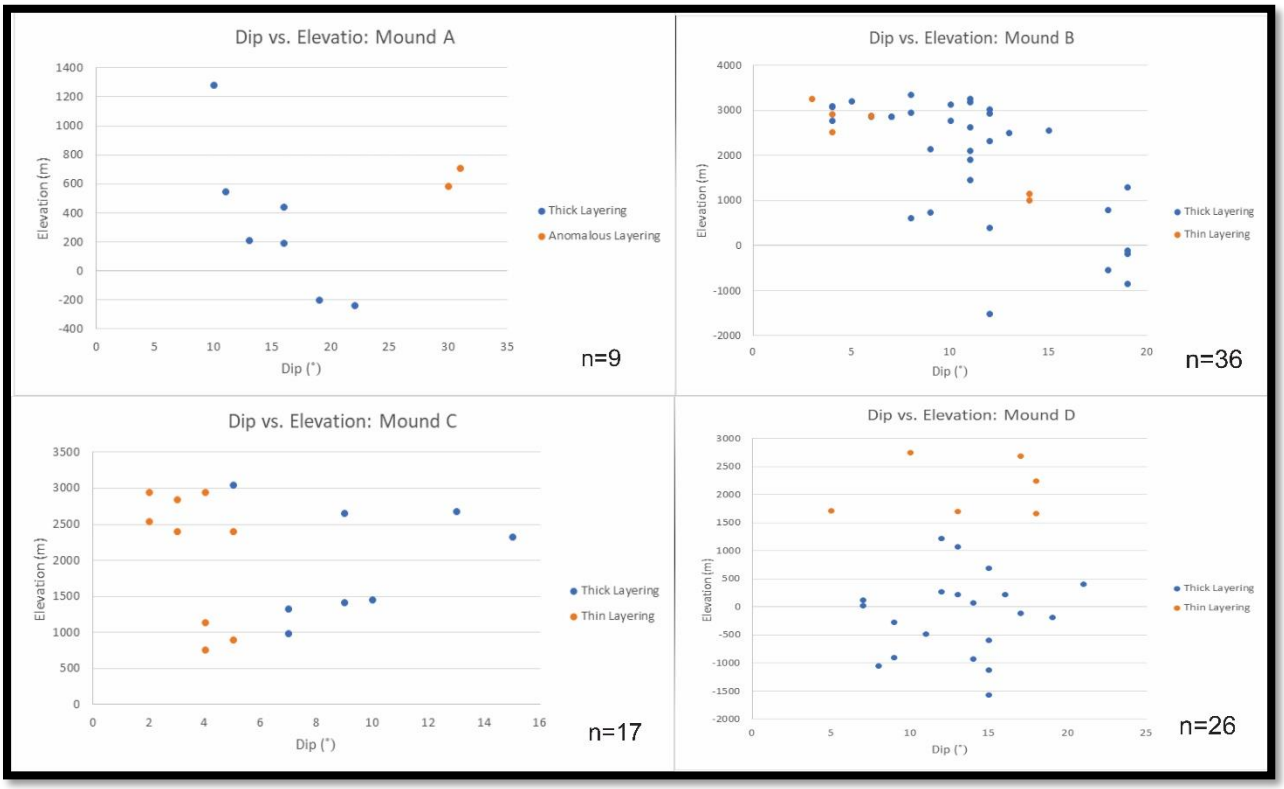

Figure 3-29: Plot of dip versus elevation in thick and thin layer units of the central major mounds within East Candor Chasma

3.7.1. Discussion

Throughout the central mounds in East Candor Chasma dips of layer units vary greatly, from near horizontal (3˚-4˚) to 21˚. Layer dip tends to decrease higher up in the stratigraphic sequence, as does layer thickness, as outlined in chapter 2 (Fig. 3-30). The stratigraphically lower units have dips of 14˚-19˚ and are primarily thick layered units. Near the tops of the mounds attitude dips away from the crest at

a low angle. These outwardly dipping units tend to be thin layer units. In the central mounds, most attitudes dip towards the north with strike roughly paralleling the length of the chasma (E-W). The exception to this is near horizontal layering found on the tops of the mounds. These results are consistent with some of the findings described by Fueten et al. (2014 & 2017), Okubo et al (2008 & 2010) & Kite et al. (2016) in their studies of Southwest Candor Chasma, Juventae Chasma and VM.

In their discussion of the ILD formations in Juventae Chasma Fueten et al. (2017) found the four mounds in the chasma were not deposited contemporaneously and a series of progressive collapses enlarged the chasma to its current shape. In Juventae's Mound B dips become more shallow as you move up in stratigraphic sequence. These features can be observed throughout East Candor Chasma.

Attitudes of the central mounds in East Candor primarily dip north, towards the topographic low along the north wall of the chasma. This, in conjunction with a decrease in dip angle further up in stratigraphic sequence, indicate basin infill. The angle of repose on Mars is ~20˚-25˚ in a dry environment (Schultz, 2002). If the sediment size is fine and deposited under water in a lake setting, the angle will be less (Mangold & Ansan, 2005). The angle of repose could be greater if the sediment were deposited in a delta environment (Mangold & Ansan, 2005). The stratigraphically lowest measurable layers in the central mounds are ~20°, indicating the sediments could be deposited as basin infill or along an uneven surface. These findings are consistent with those of Fueten et al. (2014, 2017) and Okubo (2008. 2010). Layer thinning further up in sequence is observed throughout the central mounds in East Candor. Attitudes on the top sections of the mounds tend to dip away from the crest, similar to Kite et al. (2016) findings.

Unconformities outline changes or breaks in the chasms' depositional history. The three major unconformities separate thick layered units and outcrop at an elevation of approximately 500 m-1000 m. This is important as these three locations could indicate a regional event which may indicate that there was a change in environment that affected the whole chasma.

By combining layer varieties described in the second chapter and attitude measurements presented in this chapter, possible connections identified between separate mound sections. This information can provide insight into the chasms' depositional history. The fourth chapter focuses on identifying ILD sections within East Candor that are possibly of the same origin and presents a model for the geological history of the chasm.

References

Andrews-Hanna, J. C., 2012a. The formation of Valles Marineris: 1. Tectonic architecture and the relative roles of extension and subsidence. *Journal of Geophysical Research,* Issue 117.

Broxton, M. J. & Edwards, L. J., 2008. *The Ames Stereo Pipeline" Automated 3D Surface Reconstruction from Orbital Imagery.* s.l., s.n., p. Abstract 2419.

Chapman , M. G. & Tanaka, K. L., 2001. Interior trough deposits on Mars: Subice volcanoes?. *Journal of Geophysical Research: Planets,* 106(E5), pp. 10087-10100.

Chapman, M. G., 2001. Layered, massive and thin sediments on Mars: possible late Noachian to Late Amazonian tephra?. *Geological Society,* Volume 202, pp. 273-293.

Chapman, M. G. & Smellie, J. L., 2007. *Mars interior layered deposits and terrestrial sub-ice volcanos compared: observations and interpretations of similar geomorphic characteristics.* Cambridge: Cambridge University Press.

Fueten, F. et al., 2006. Structural study of an interior layered deposit in southwestern Candor Chasmaa, Valles Marineris, Mars, using high resolution stereo camera data from Mars Express. *Geophysical Research Letters,* 33(7).

Fueten, F. et al., 2008. Stratigraphy and structure of interior layered deposits in west Candor Chasma, Mars, from High Resolution Stereo Camera (HRSC) stereo imagery and derived elevations. *Journal of Geophysical Research: Planets,* 113(E10), pp. 1-19.

Gourronc, M. et al., 2013. One million cubic kilometers of fossil ice in Valles Marineris: Relicts of a 3.5 Gy glacial landsystem along the Martian equator. *Geomorphology,* Volume 204, pp. 235-255.

Hynek, B. M. & Phillips, R. J., 2008. The stratigraphy of Meridiani Planum, Mars, and implications for the layered deposits' origin. *Earth and Planetary Science Letters,* 274(1-2), pp. 214-220.

Komatsu, G., Ori, G., Ciarcelluti, P. & Litasov, Y., 2004. Interior Layered Deposits of Valles Marineeris, Mars: Analogus subice volcanism related to Baikal rifting, southern Siberia. *Planetary and Space Science,* pp. 167-187.

Lewis, K. W., Aharonson, O., Grotzinger, J. P. & Suer, T. A., 2008. Quasi-periodic bedding in the sedimentary rock record of Mars. *Science,* 322(5907), pp. 1532-1535.

Lucchitta , B. K., 1990. Young volcanic deposits in the Valles Marineris, Mars?. *Icarus,* pp. 476-509.

Lucchitta , B. K., 2010. Lakes in Valles Marineris. In: N. A. Cabrol & A. G. Edmond, eds. *Lakes on Mars.* Oxford: Elsvier, pp. 111-152.

Lucchitta, B. K., 1982. Ice Sculpture in the Martian Outflow Channels. *Journal of Geophysical Research,* pp. 9951-9973.

Lucchitta, B. K., 1994. Topography of Valles Marineris: Implications for erosional and structural history. *Journal of Geophysical Research,* pp. 3783-3798.

Mege, D. & Masson, P., 1996. A plume tectonics model for the Tharsis province, Mars. *Planetary and Space Science,* 22(12), pp. 1499-1546.

Moratto, Z. M. et al., 2010. *Ames Stereo Pipeline, NASA's Open Source Automated Stereogrammetry Software,*. s.l., s.n., p. Abstract 2364.

Nedell, S. S. & Squyres, S. W., 1987. *Formation of the layered deposits in the Valles Marineris, Mars.* Woodlands, United States, pp. 88-90.

Peterson, C., 1981. A secondary origin for the central plateau of Hebes Chasmaa. *Lunar Planetary and Science Conference,* Volume 11th, pp. 1459-1471.

Sharp, R. B., 1973. Mars: Toughed terrain. *Journal of Geophysical Research,* Volume 78, pp. 4063-4072.

4.0 Chapter 4: Interpretation for the Depositional History of East Candor Chasma

4.1.1 Introduction

The purpose of this chapter is to integrate the data of the previous chapters and to discuss the geological history of the ILDs within East Candor chasma. Using layer variety, associated attitude and observed geologic structures, a comprehensive model will be presented to illustrate chasma formation.

4.1.2 East Candor Chasma

East Candor Chasma is 475 km long, 145 km wide and ranges in elevation from -5.5 km to 3.5 km at the highest point within the ILD. Previous mapping suggests that the geological history of the chasma is complex (Okubo, 2016). East Candor Chasma contains four separate mounds of ILD and four separate minor mounds which are examined here (Fig. 4-1). These mounds are contained by walls on three sides; the fourth side opens into the western portion of Candor Chasma. The chasma can be separated topographically into three sections: a series of ILD mounds in the central part of the chasma, a floor at the base of the south wall with a relief of 1500 m and a floor at the base of the North wall with a relief of 2300 m. Lucchitta et al. (1994) proposed a chasma-wide fault that lies along the base of the north wall. Evidence presented in this chapter supports the proposed chasma-wide fault.

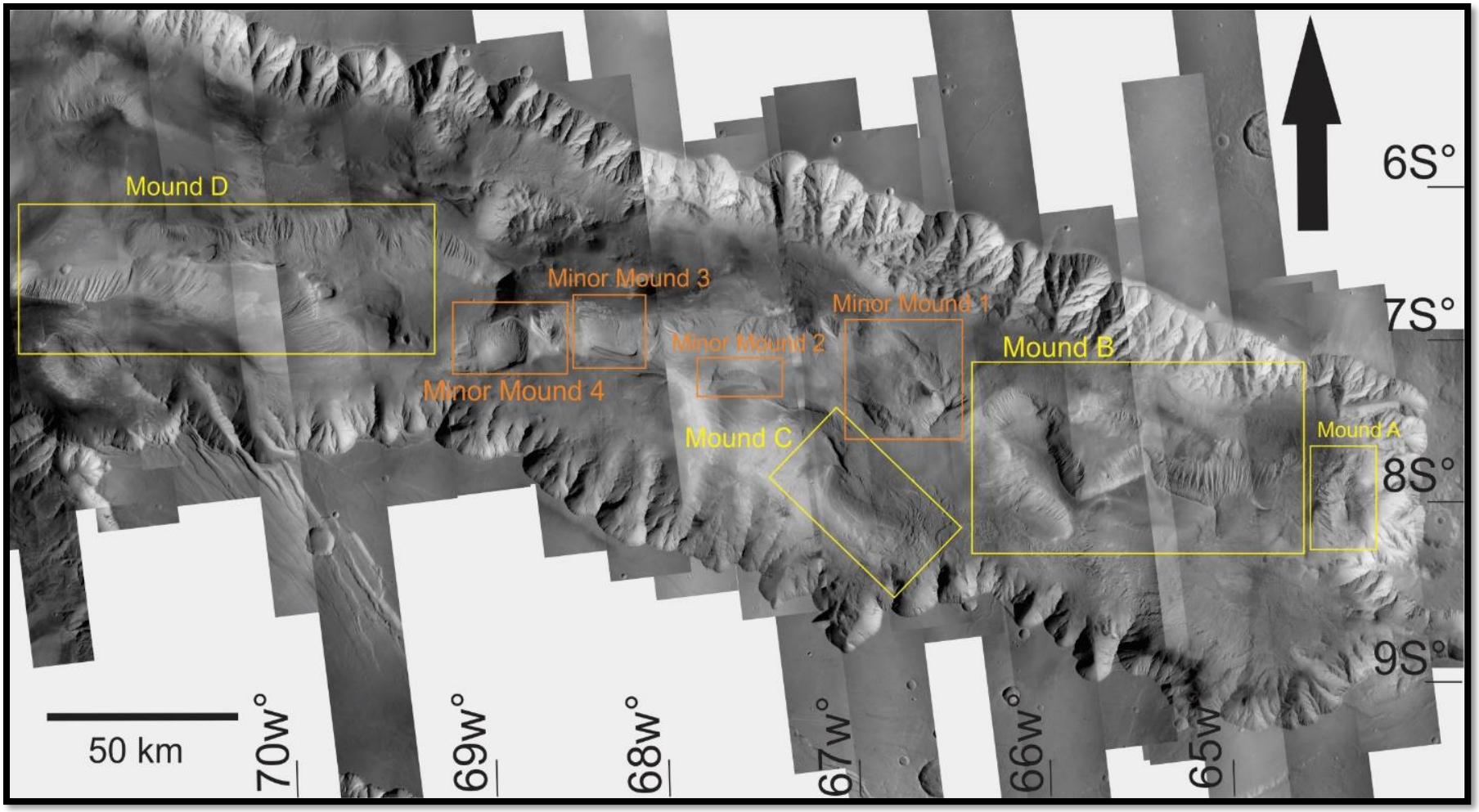

Figure 4-1: Identification of mounds and minor mounds of East Candor Chasma

4.2 ILDs within East Candor Chasma

East Candor Chasma contains six different ILD unit varieties previously discussed in Chapter 2: massive, thick layered, thin layered, thin mesa, deformed and steeply dipping. Each variety outcrops in the central mounds or along the chasma walls. Thick layered, thin layered and the deformed unit outcrop along the south wall. The floor along the north wall only contains one area of thick layer unit encompassing ~31 km^2 (Fig. 4-2). The remainder of the floor along the north wall is comprised of undefined sediments, dunes and debris from wall slides. Layer attitudes were measured for all layered units that were not deformed. Figure 4-3 is a composite map that shows locations of layer varieties as well as layer attitudes.

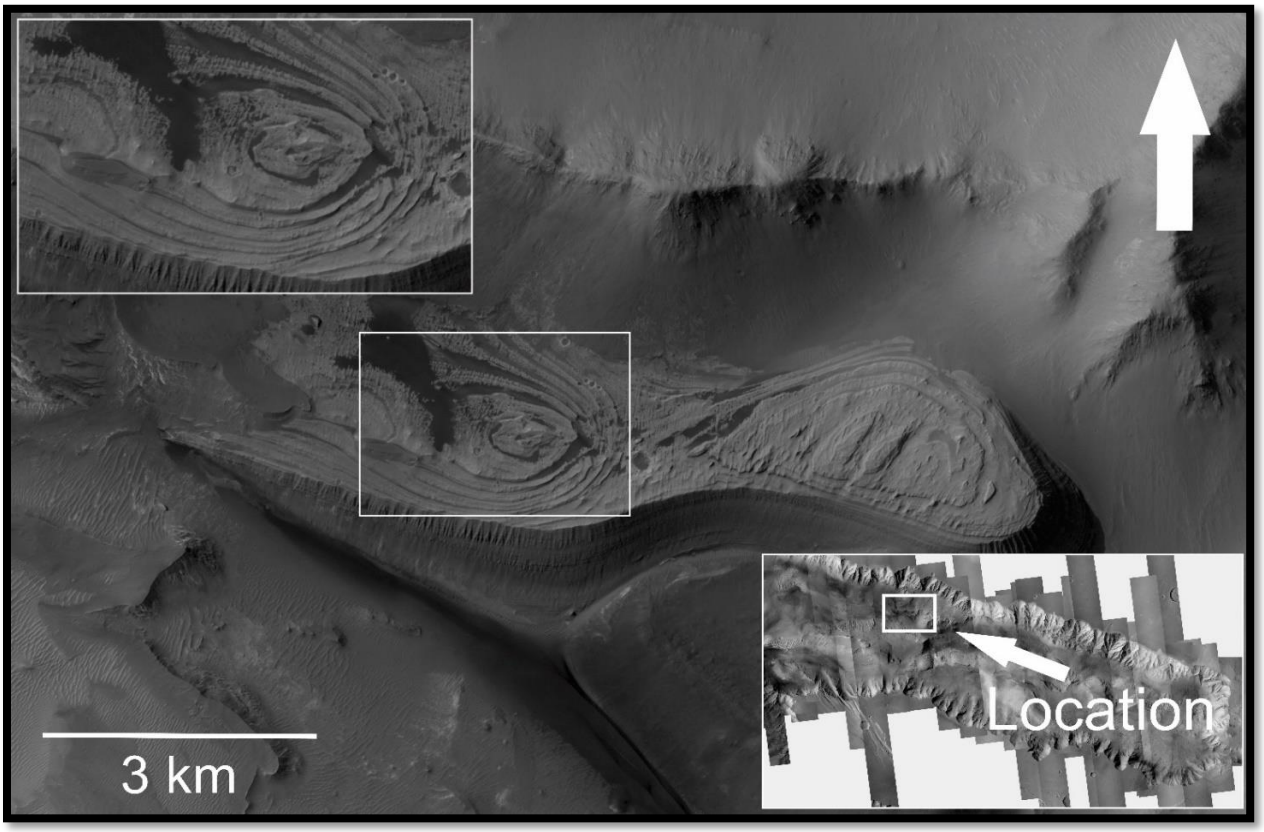

Figure 4-2: Thick layer unit observed along north wall in East Candor Chasma. Upper left inset displays layering observed in center of image. Lower right inset displays location layering is found in the chasma. Topographic high is to north of image.

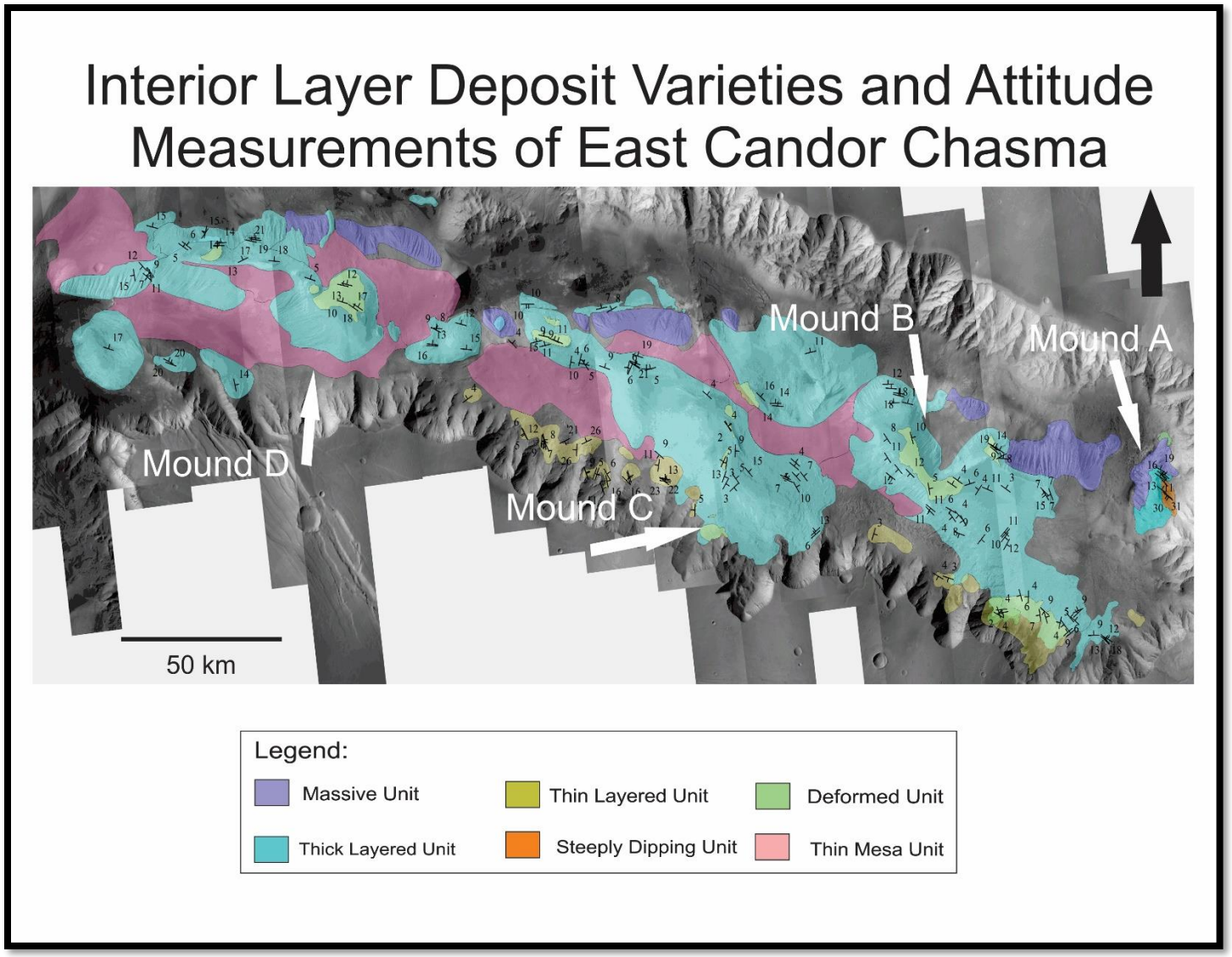

Figure 4-3: ILD varieties overlain by layer attitudes measured throughout the central mounds and south wall of East Candor Chasma.

The massive unit exclusively outcrops along the north face of the mounds. With a few exceptions that can be explained the massive unit appears to be the lowest ILD unit in the proposed sequence. The exposed outcrops occur at the lowest elevation of the central mounds displaying the ridge and gully erosional texture. The massive unit displays no visible layering in current imagery.

The thick layered unit contains the largest aerial extent of all units within East Candor. It is also the unit that displays the most complexity. This unit contains a bench layering sub-unit that primarily outcrops on the north face of the mounds and is exposed at lower elevations within the stratigraphy. Thick layering is present on every mound and sub-mound in the chasma. On Mound D a younger thick layered unit truncates an older, previously eroded thick layered unit. The thick layered unit is the lowest unit in the stratigraphy for which layer attitudes can be obtained. The lowest layered unit that can be measured for attitude is the benches sub-unit. This sub-unit tends to display northward dips between 9˚ and 21˚ along the north face of the mounds. Some of the thick layered units observed in the upper sections of mounds and along the southeast wall have attitudes as low as 3˚ in varying directions (Fig. 4-4). The bench sub-unit commonly outcrops on the north face of the central mounds and primarily dips northward. As indicated in figure 4 and documented previously this unit appears to be draping the massive unit. This indicates that the thick-layered unit was deposited on top of a north dipping surface of the massive unit.

The steeply dipping unit is anomalous in nature, being the only known unit in East Candor Chasma to dip ~30˚. It is observed on the southeast corner of Mound A and unconformably bounded by two thick units, one of which is located north of it. The other unit appears to overlie the steeply dipping unit. It is unclear

what causes the layering in this area to dip so steeply. However, it does provide further evidence that thick layer units are widely diverse.

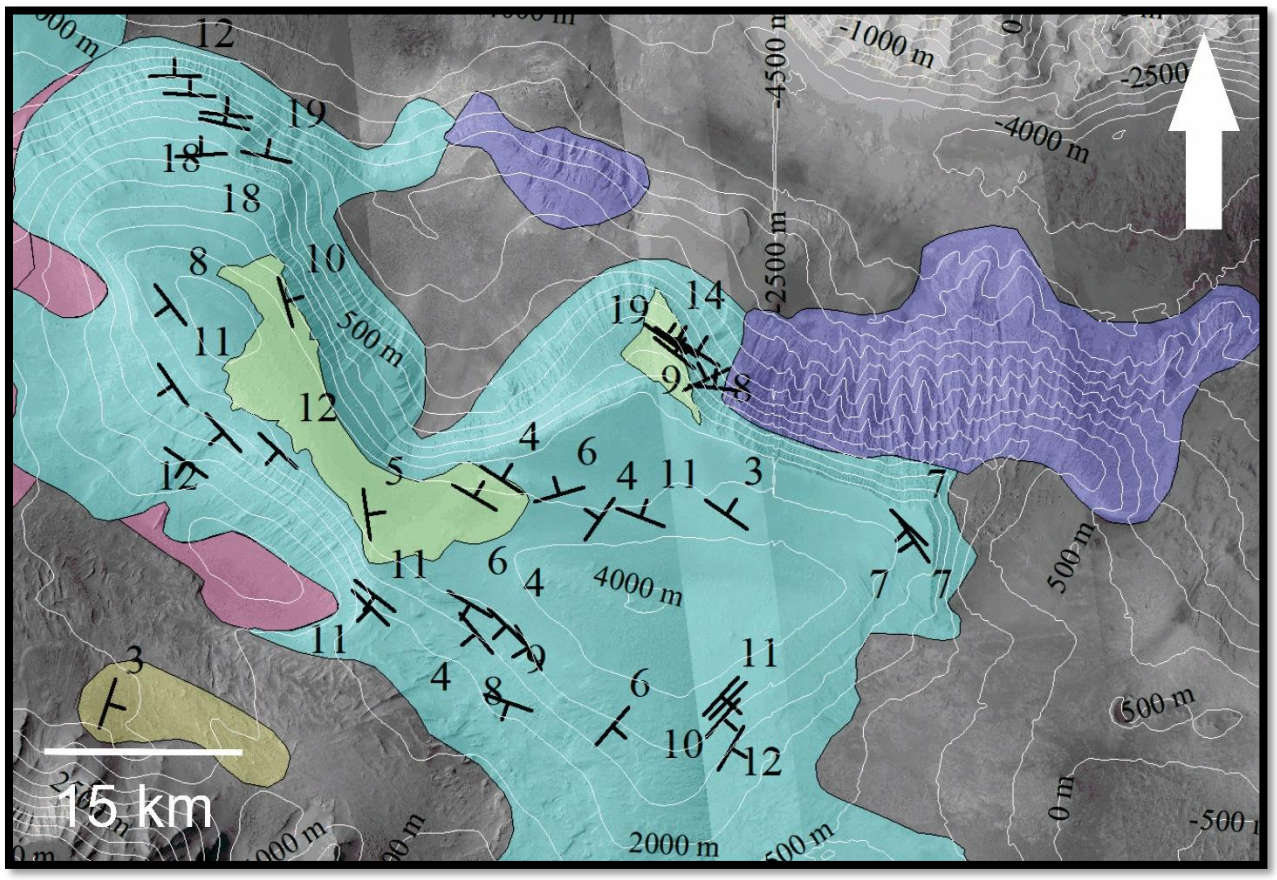

Figure 4-4: Mound B displaying layer varieties with associated dips. Topographic low is towards top of image; this is also where bench layer unit is found.

The thin layered unit is observed on the tops of mounds draped over the thick layered unit or along the south wall covering the spurs and gullies. This unit displays thin layering and appears to be easily eroded, as it is observed throughout the chasma but only covers small areas. It is best observed along the south wall. Thin layering located on the upper sections of mounds displays relatively low dip angles

of 3˚-5˚ (Fig. 4-5). The thin layer unit on the upper-most parts of the mounds tend to dip away from the crest. Along the south wall of the chasma thin, thick and bench layer units are observed. The thin layered unit drapes the spurs and fills in the gullies. Attitudes of this unit tends to vary greatly depending on its position relative to the slopes of the spurs. In some cases, attitudes had a dip of 26˚ along the southeast wall. This indicates that the thin layered unit was deposited as drape over the pre-existing geology.

Truncations are observed throughout the chasma. They are most commonly seen between different packages of thick layer units. Mound D displays truncation of two thick layer units spanning ~1 km from east to west.

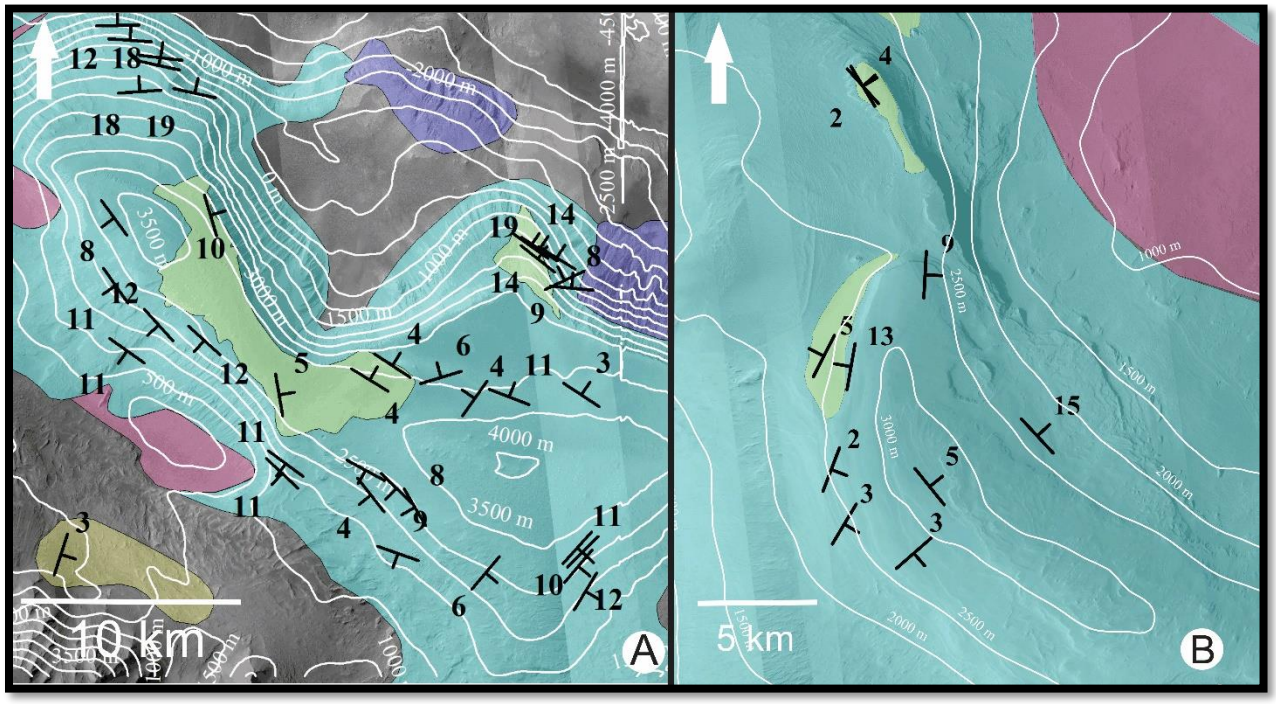

Figure 4-5: Attitudes of thin layering on the upper sections of Mound B (image A, left) and Mound C (image B, right)

The deformed layered unit is primarily observed along the chasma walls, with some areas of deformation likely being the result of post-depositional slumping. The post-depositional slumping is most likely analogous to the LSD documented by Okubo (2016), where chasma erosion produces a moat around the mounds in the center of the chasma. ILDs along the walls become unstable, normal faulting occurs along the head of the slide; while thrust faulting and folding occurring at the toe. The ILDs move from a high-standing position to fill the moat area causing deformation during movement.

The thin mesa unit is thought to be a late covering that drapes the pre-existing lithology throughout the chasma. This unit appears to be the uppermost in stratigraphy as it can be seen covering all units in East Candor Chasma. No visible layering is observed within this unit.

4.3 Stratigraphy of ILD Mounds in East Candor Chasma

Proposed stratigraphy of the central mounds from oldest to youngest is thought to be: massive unit, thick layered unit-with benches at the lower elevation, thin layered unit and thin mesa unit (Fig. 4-6). Evidence to support this stratigraphy is best observed on the north side of the central mounds. The proposed chasma-wide northern fault (Fig. 4-7) and the collapse associated with it could have exposed the lower units of the mounds along their north face. The difference in elevation between the base of the north wall and the south wall can be as much as 2500-3000 m, where the base of the north wall lies lower than the south. In this case the difference in elevation merely allows for the observation of the lower stratigraphic units that were likely covered at one point in the chasms' history. The massive unit can only be clearly observed outcropping on the north face of the mounds at the lowest topographic elevations. The sub-unit benches within the thick layered unit are almost always observed

stratigraphically just above the massive unit. The bench sub-unit progresses into the thick layered unit further up in the stratigraphic sequence. The thick layered unit is followed by the thin layered unit. The thin mesa unit is believed to be an ash cover that is observed throughout the chasma. It is observed draping the previously mentioned units and is thought to be the uppermost stratigraphic unit.

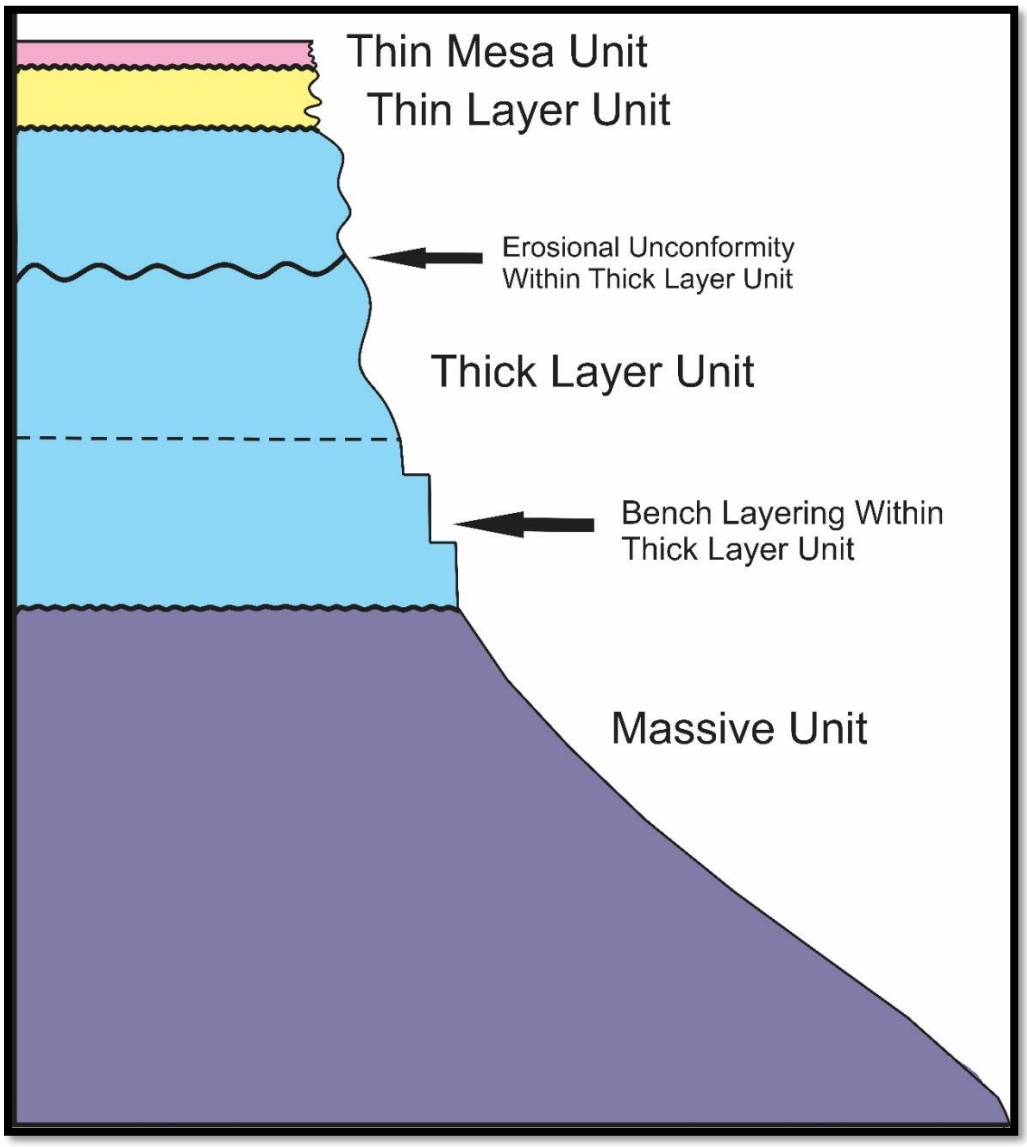

Figure 4-6: Proposed succession of central mounds found within East Candor Chasma. Please note that all unit contacts are most likely erosional unconformities. Units within this diagram we've chosen to indicate only the unconformity that appears to be consistent across mounds.

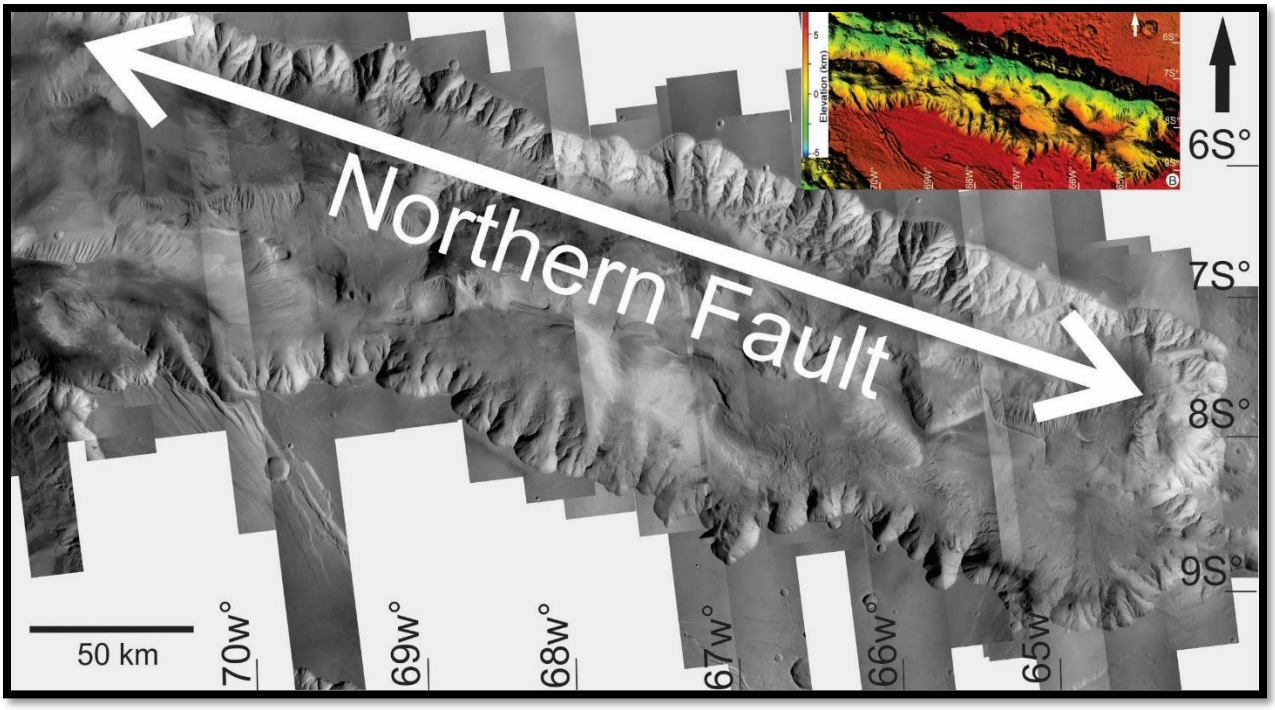

Figure 4-7: Location of proposed northern chasma-wide fault and associated collapse as indicated by the topographic low.

4.5 Proposed formation of East Candor Chasma ILDs

When layer variety and attitude are combined, overall trends are observed that can be used to interpret the geological history of East Candor Chasma. We suggest that a secondary collapse occurred along the north wall of the chasma after the massive unit was emplaced. Sedimentation and erosion continued after chasma collapse allowing for the emplacement of layer and thin mesa units. I present below two models for the proposed history of East Candor chasma.

The models are schematic and based on the following assumptions: (1) the deposition of the massive, thick layer and thin layer units are thought to have occurred in a lacustrine environment. Exposed layering within the measurable ILD contain long trace lengths indicative of deposition in a lacustrine environment. The west end of the chasma could have been closed in the past allowing for liquid to

remain in the chasma for a period of time. (2) Deposition took place over a long duration and included periods of erosion. Erosion may have taken place during periods of low water levels and aerial exposure. (3) The massive unit was emplaced after the initial collapse of the chasma. (4) In the absence of evidence for any additional units, it is assumed that the massive unit is the basal unit in the ILD stratigraphy and was deposited on the basement.

The two models differ in terms of the timing of the collapse of the northern part of the basin. The massive unit could have facilitated the collapse along the north wall. This assumption is supported by (Andrews-Hanna, 2012a; Andrews-Hanna, 2012b) where subsidence is enhanced by sedimentation. Andrews-Hanna proposed that moderate extension brought on by Tharsis-related volcanic activity allowed for dikes to intrude the area, later resulting in the subsidence of the trough floors. Any contemporaneous sediment loading, coupled with the viscous deformation of the lower crust, further enhanced the collapse of the existing basin by a factor of 4.4 (Andrews-Hanna, 2012b). Modeling provided by Andrews-Hanna (2012a, 2012b) allows the basin along the north wall to attain a depth great enough to bury any massive unit that may have once outcropped at the chasm's surface.

Fueten et al. (2017) argued for the collapse in Juventae without deposition. Where the initial collapse of the chasma is complex and multi-staged. Fueten (2017) presents two scenarios of basin collapse without previous sedimentation. In one scenario the chasma expands by a series of isolated or localized collapses. Implying that multiple centres of collapse existed below Juventae formed and grew during chasma evolution. In the second scenario the basin continuously collapses outward from one central area. It is widely accepted that the trough network of VM was formed with minor extension associated with vertical collapse (Mege & Masson, 1996). This can be explained by bounding faults that are basin-

parallel to normal faults (Schultz & Lin, 2001) or near vertical faulting (Andrews-Hanna, 2012a; Andrews-Hanna, 2012b).

In addition, the models have limitations. They include: the collapse along the north wall could have occurred before or after deposition of the massive unit. In both scenarios we assume the massive unit was emplaced before the collapse of the northern section of the chasma. The limitation of the massive unit emplacement prior to collapse of the north wall is that little to no ILD is observed along the collapsed section and north wall. This would mean that erosion would have to be high enough to remove any ILD that might have been emplaced after collapse.

Two models for the early history of the chasm are illustrated in figure 8. The different scenario descriptions are given below.

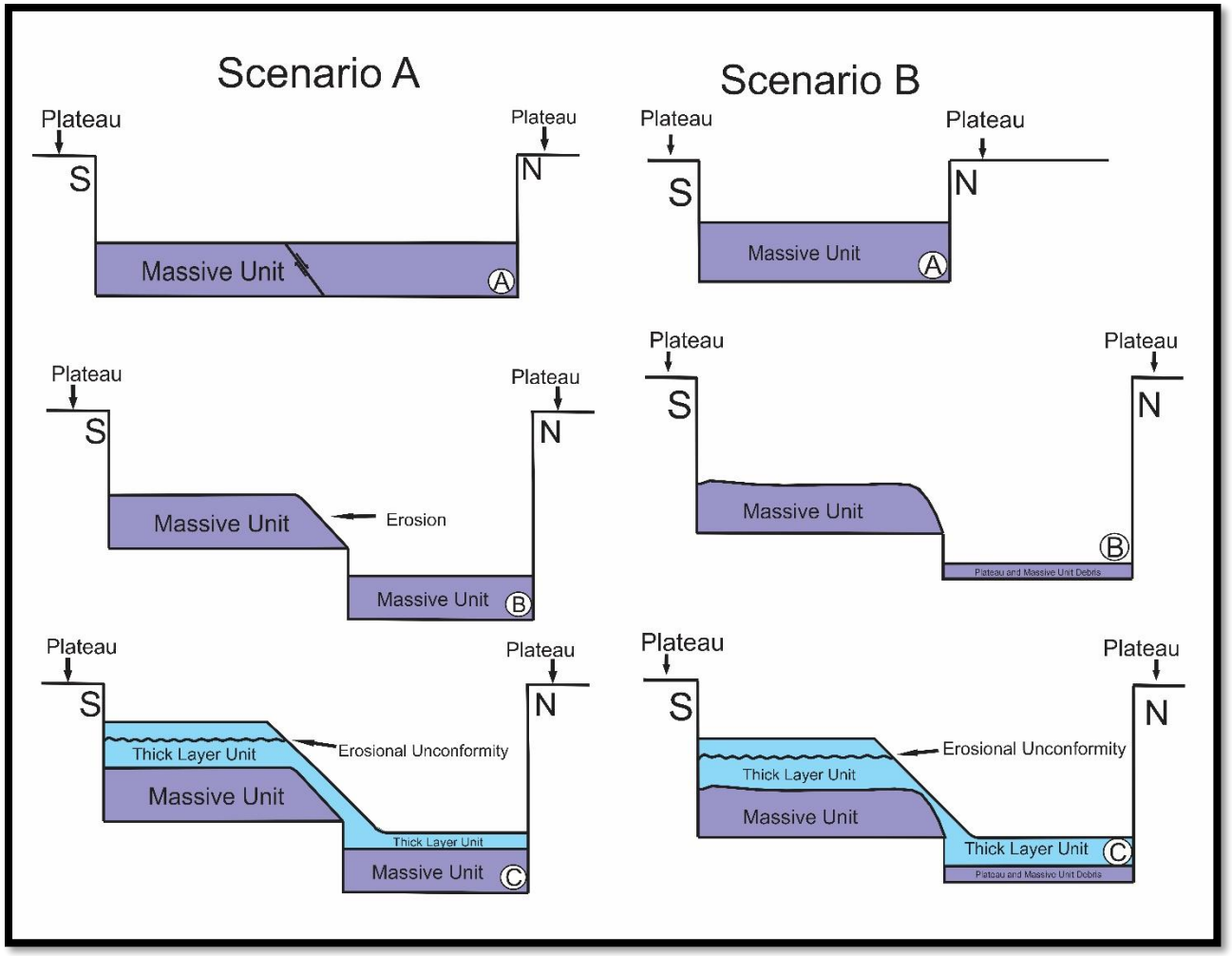

Figure: 4.8: Proposed scenarios of the early history formation of East Candor Chasm's secondary collapse. Scenario A depicts a secondary collapse where the chasma floor drops significantly. Scenario B depicts a secondary collapse where the chasma widens as the north wall collapses.

4.5.1. Scenario A: Early History of deposition in East Candor Chasma-deep basin collapse

In this proposed model the massive unit is deposited uniformly across the chasma floor and the initial width of the chasma is approximately the same as it is now (Fig. 4-8 Scenario A-A). Either during or after emplacement, a collapse occurs along the north wall the length of the chasma. The collapse must reach a minimal depth of ~3.0 km since the massive unit appears along the north face of the mounds and is not observed within the collapsed section or along the north wall. The collapse would have to be great

enough to remove the massive unit from outcropping at the surface of the chasma along the north wall. Since the massive unit observed outcropping the central mounds is ~3.0 km in thickness, the minimal collapse depth must be the same or greater. After the secondary collapse of the chasma erosion of the massive unit occurred (fig. 4-8 Scenario A-B). The thick layer unit was then emplaced along the length of the chasma, including deposition along the collapsed section (fig. 4-8 Scenario A-C). Evidence for this is presented in the lower sections of the central mounds, where steep dips in excess of 14˚-21˚ are observed within the thick layer unit and the bench sub-unit. The thick layer unit contains a series of unconformities, around 1000 meters, that likely occurred during periods of erosion (fig. 4-8 Scenario A-D). Further deposition of thick layer units follows the unconformities. This model accounts for an issue with stratigraphic sequence that was previously left unexplainable in chapter 2. Along the base of the central mounds, the thick layer unit appears to outcrop below the massive unit. The collapsed section allows for the thick layer unit to appear as though it has been emplaced lower than the massive unit, when it is emplaced north of the massive unit at a lower topographical elevation with the massive unit below it.

4.5.2. Scenario B: Early history of deposition in East Candor Chasma-north wall collapse

For this proposed model the massive unit is emplaced along a narrower chasma floor, corresponding to the approximate width of the main ILD mounds, than that of Scenario A (Fig. 4-8 Scenario B-A). After emplacement, the north wall collapses causing the chasma to widen (Fig. 4-8 Scenario B-B). As the chasma widens the floor of the chasma adjacent to the north wall drops; however, the depth in this scenario does not have to account for 3 km of massive unit observed in Model A as it was not present. The floor adjacent to the north wall would need to drop at least to the level of the floor adjacent to the south wall if not greater, as the floor currently is 2500-3000 m below the area adjacent to the south wall. This difference is the same thickness as the exposed thickness of the massive unit. The floor

adjacent may lie at a greater depth in order to accommodate any debris deposited during collapse. The thick layer unit and bench sub-unit is then deposited on top of the massive unit and along the newly collapsed section along the north wall (Fig. 4-8 Scenario B-C). Support for this is found where thick layer and bench deposits found on the north side of the central mounds dip steeply to the north and decrease as mound elevation increases. The thick layer unit underwent periods of erosion and deposition as a series of unconformities were observed around 1000 meters throughout the chasma (Fig. 4-8 Scenario B-C). Further erosion occurred throughout the chasma. Again, this model accounts for the issue with stratigraphic sequence that was previously left unexplainable in chapter 2. Along the base of the central mounds the thick layer unit appears to outcrop topographically below the massive unit. In this scenario the collapsed section allows for the thick layer unit to appear as though it has been emplaced lower than the massive unit, when it is only emplaced north of the massive unit at a lower topographical elevation without the massive unit below it. Figure 4-9 depicts the late history of the chasm.

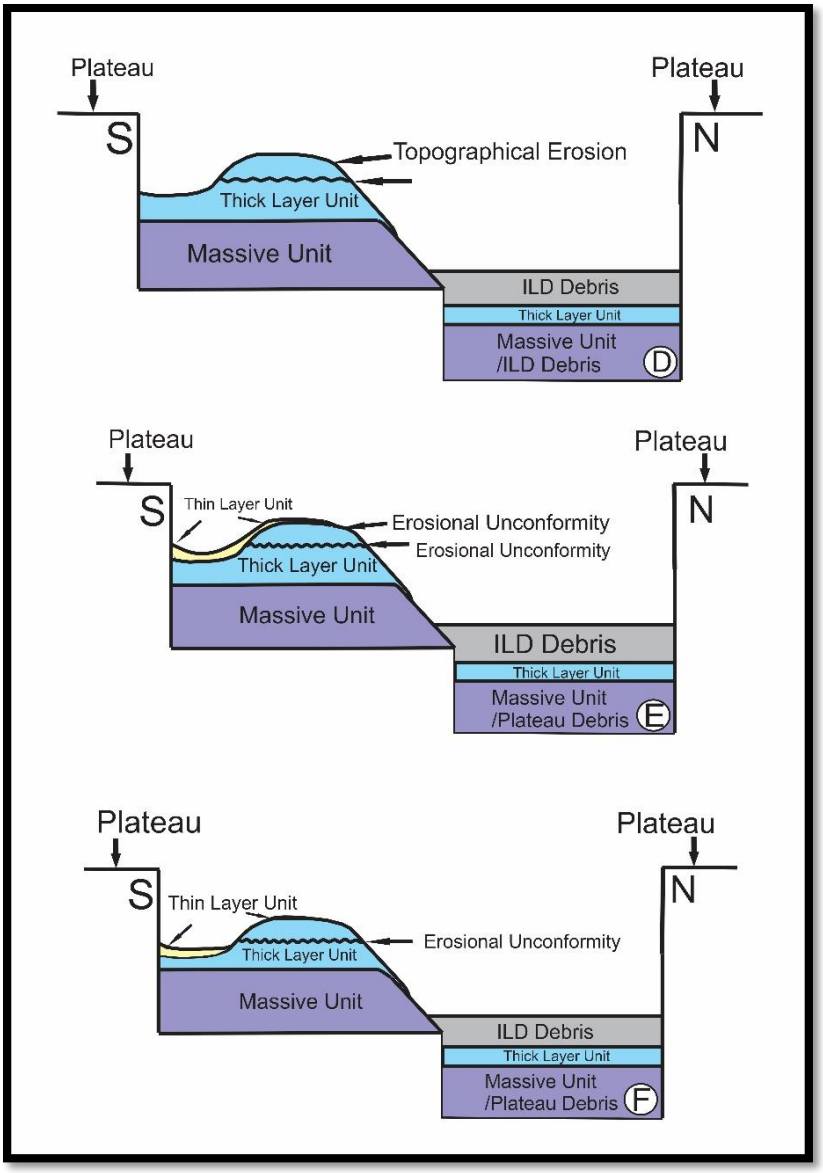

Figure 4.9: Proposed scenario of the late history formation of East Candor Chasm's secondary collapse. Note, the exact nature of the basement within the northern through depends the early history. Please see fig 4.8 for details. (E): Thin layer unit is deposited on top of the thick layer unit. (F): Further erosion takes place in the chasma

4.5.3. Late History of East Candor Collapse

During the late depositional stages of East Candor chasma, the models share the same history. The thick layer unit contains the largest, most diverse and structurally unique details of any ILD unit found within

East Candor Chasma. The deposition of this unit is thought to have taken place over a longer period of time than any other unit. The thick layer unit contains a series of unconformities, three of which occur at roughly the same elevation and all confined to thick layer units. This suggests that the thick layer unit was deposited over a long period of time with episodes of erosion occurring intermittently. This could be due to a regional change in environmental conditions, i.e., rising and falling liquid water levels (Fig. 4-9D). During this time the section of the chasma that collapsed could have had debris from ILD and wall erosion deposited along the trough adjacent to the north wall (Fig. 4-9D), as well as deformation of layer units along the chasma walls and landslides causing debris and slump of material. As time progresses a shift occurs in the Martian environment where fewer deposits are emplaced within the chasma, at which point the thin layer unit would have been emplaced (Fig. 4-9E) and subsequently eroded in vulnerable areas, i.e., the newly formed northern tough (Fig. 4-9F). The thin mesa unit is then deposited as the last known unit to be emplaced in East Candor Chasma occurring late in mound's depositional history.

4.6.1. Discussion

The chasma-wide collapse which parallels the north chasma wall is thought to be a late feature of chasma formation which occurred after sediments in the southern half of the chasma were deposited (Lucchitta, 1994). Lucchitta (1994) thought that the mutually exclusive rock types in the north and south, separated by a relatively straight scarp indicated a fault contact was present. Erosion of the massive unit following collapse accounts for the steep dips displayed in the overlying unit. The thick layer unit is then emplaced within the chasma after the collapse. Attitudes of the thick layer units, especially those found in the lower stratigraphy of the mounds, tend to dip north. Supporting the suggestion that the collapse occurred before the thick unit was emplaced. The strike corresponding to the lower stratigraphic dips

parallels the chasma walls, as well as the northern fault. The proposed stratigraphic succession is consistent through a large portion of the central mounds. Differences in succession at the same elevations between mounds can be explained by an uneven basement floor and erosional processes, as we know nothing of the original floor in East Candor Chasma.

The two models can be distinguished by the mechanisms of the secondary collapse-deep basin collapse or chasma widening. Deep basin collapse would account for the small amount of ILD material observed along the west end of the north wall. Chasma widening accounts for the mutually exclusive rock types observed within the mounds and those that make up the chasma wall. Either are likely candidates for the formation of East Candor following the chasms initial collapse. These models differ from previously proposed formations of East Candor by suggesting deposition occurred in a lacustrine environment. This is based on long trace lengths and shallow dips of individual layers within the central mounds.

4.7.1. Conclusion

The depositional history of East Candor Chasma displays a complex lithology involving a diverse variety of ILDs, a wide range of layer thickness, complex episodes of deposition with erosion and followed by further ILD deposition and tectonics. Findings from this study suggest that East Candor Chasma underwent at least one major secondary collapse which impacted the deposition of ILD material in the basin. Several deposition mechanisms have been proposed for ILDs throughout VM (Malin & Edgett, 2000; Fueten, et al., 2008; Okubo, 2010; Fueten, et al., 2017). It is possible that any one or a combination of mechanisms are possible for the ILDs found within East Candor Chasma. Long traces of layered deposits could indicate a lacustrine environment, while the truncation of thick layered

sediments observed in Mound D indicated periods of dominantly erosive forces. It is likely that East Candor and VM has been subjected to environmental changes throughout its history. A thinning up of layer sequences could suggest a decrease in sediment influx over time. Three unconformities have been identified throughout the central mounds, all of which are observed around the same elevation.

East Candor Chasma was an early basin feature in VM history (Lucchitta, 1994). Faulting along the northern chasma wall caused the exposure of sediments that would have otherwise been hidden in lower stratigraphic sections of the central mounds. These sediments are observed in sequence throughout the central mounds of East Candor. It is possible that as sediments were emplaced in the chasma environmental changes occurred throughout VM, and possibly Mars. These changes are indicated by large unconformities observed throughout the central mounds. Local variation exists within East Candor; however, the stratigraphic succession, attitudes of layering in the central mounds and unconformities are consistent throughout the chasma.

References

Al-Samir, M. et al., 2017. The paleolacustrine evolution of Juventae Chasma and Maja Valles and its implications for the formation of interior layered deposits on Mars. *Icarus,* pp. 125-143.

Andrews-Hanna, J. C., 2012a. The formation of Valles Marineris: 1. Tectonic architecture and the relative roles of extension and subsidence. *Journal of Geophysical Research,* Issue 117.

Andrews-Hanna, J. C., 2012b. The formation of Valles Marineris: 3. Trough formation through super-isostasy, stress, sedimentaton and subsidence. *Journal of Geophysical Research,* Issue 115.

Andrews-Hanna, J., Phillips, R. J. & Zuber, M. T., 2007. Meridiiani Planum and the global hydrology of Mars. *Nature,* pp. 163-166.

Carr, M. H. & Head III, J. W., 2010. Geologic History of Mars. *Earth and Planetary Sciences,* pp. 185-203.

Fueten, F. et al., 2014. Stratigraphy and mineralogy of Candor Mensa, West Candor Chasma, Mars: Insights into the geologic history of Valles Marineris. *Journal of Geophysical Research: Planets,* 119(2), pp. 331-354.

Fueten, F. et al., 2017. The Evolution of Juventae Chasma, Valles Marineris, Mars: Progressive Collapse and Sdeimentation. *Journal of Geophysical Research: Planets,* Volume 122.

Fueten, F. et al., 2006. Structural study of an interior layered deposit in southwestern Candor Chasma, Valles Marineris, Mars, using high resolution stereo camera data from Mars Express. *Geophysical Research Letters,* 33(7).

Fueten, F. et al., 2008. Stratigraphy and structure of interior layered deposits in west Candor Chasma, Mars, from High Resolution Stereo Camera (HRSC) stereo imagery and derived elevations. *Journal of Geophysical Research: Planets,* 113(E10), pp. 1-19.

Golombek, M. P. & Phillips, R. J., 2010. Mars Tectonics. In: T. R. Watters & R. A. Schultz, eds. *Planetary Tectonics.* New York: Cambridge University Press, pp. 183-232.

Gourronc, M. et al., 2013. One million cubic kilometers of fossil ice in Valles Marineris: Relicts of a 3.5 Gy glacial landsystem along the Martian equator. *Geomorphology,* Volume 204, pp. 235-255.

Kite, E. S. et al., 2016. Evolution of major sedimentary mounds on Mars: Buildup via anticompensational stacking modulated by climate change. *Journal of Geophysical Research: Planets,* Issue 121, pp. 2282-2318.

Komatsu, G., Ori, G., Ciarcelluti, P. & Litasov, Y., 2004. Interior Layered Deposits of Valles Marineeris, Mars: Analogus subice volcanism related to Baikal rifting, southern Siberia. *Planetary and Space Science,* pp. 167-187.

Lucchitta , B. K., 1990. Young volcanic deposits in the Valles Marineris, Mars?. *Icarus,* pp. 476-509.

Lucchitta , B. K., 2010. Lakes in Valles Marineris. In: N. A. Cabrol & A. G. Edmond, eds. *Lakes on Mars.* Oxford: Elsvier, pp. 111-152.

Lucchitta, B. K., 1982. Ice Sculpture in the Martian Outflow Channels. *Journal of Geophysical Research,* pp. 9951-9973.

Lucchitta, B. K., 1994. Topography of Valles Marineris: Implications for erosional and structural history. *Journal of Geophysical Research,* pp. 3783-3798.

Luccitta, B. K. et al., 1992. The canyon system on Mars. *Mars,* pp. 453-492.

Malin, M. C. & Edgett, K. S., 2000. Sedfimentary Rocks of Early Mars. *Science,* pp. 1927-1937.

Mege, D., 2001. Uniformitarian plume tectonics: The post-Archean Earth and Mars, in mantle plumes: Their identification through time. *Geological Society of America,* pp. 141-164.

Mege, D., 2006. Graben Morphology, Dike Emplacement, and Tension Fracturing in the Thrasis Igneous Province of Mars. *Journal of Geophysical Research,* pp. 4-6.

Mege, D. & Ernst, R. E., 2001. Contractional effects of mantle plumes on Earth, Mars and Venus in the mantle plumes: Their identification through time. *Geological Society of America,* pp. 103-140.

Mege, D. & Masson, P., 1996. A plume tectonics model for the Tharsis province, Mars. *Planetary and Space Science,* 22(12), pp. 1499-1546.

Mege, D. & Masson, P., 1996. Amounts of Crustal Streatching in Valles Marineris, Mars. *Planetary and Space Science,* Volume 44, pp. 419-422.

Mischna, M. A., Richardson, M. I., Wilson, R. J. & McCleese, D. J., 2003. On the orbital forcing of Martian water and CO2 cycles: A general circulation model study with simplified volatile schemes. *JGR: Planets,* pp. 1-25.

Okubo, C. H., 2010. Structural Geology of Amazonian-aged layered sedimentary deposits in southwest Candor Chasma, Mars. *Icarus,* pp. 210-225.

Okubo, C. H., 2016. Morphologic evidence of subsurface sediment mobilization and mud volcanism in Candor and Coprates Chasmata, Valles Marineris, Mars. *Icarus,* Volume 269, pp. 23-37.

Okubo, C. H., Lewis, K. W., McEwen, A. S. & Kirk, R. L., 2008. Relative age of interior layered deposits in southwest Candor Chasma based on high-resolution structural mapping. *Journal of Geophysical Research,* pp. 1-15.

Touma, J. & Wisdom, J., 1993. The chaotic obliquity of Mars. *Science,* pp. 1294-1296.

Appendices

A: List of CTX stereo pairs that were used to generate a map for calculating attitudes of ILD material within East Candor Chasm.

CTX Number	CTX Stereo Pairs
24	G20_025903_1730_XN_07S068W-P11_005333_1734_XI_06S068W
25	P01_001522_1734_XN_06S069W-P12_005755_1739_XN_06S069W
03	P03_002366_1723_XN_07S066W-P18_007904_1722_XN_07S065W
07	P07_003566_1711_XN_08S066W-P12_005623_1714_XI_08S066W
12	P10_005122_1724_XI_07S067W-P12_005900_1738_XI_06S068W
11	P13_005979_1721_XI_07S065W-P15_006757_1724_XI_07S065W
29	B02_010330_1717_XI_08S066W-D04_028725_1730_XI_07S066W
37	B06_011965_1725_XN_07S066W-B07_012242_1724_XN_07S066W
34	B07_012532_1707_XN_09S063W-P07_003856_1737_XN_06S064W
42	B09_013086_1749_XI_05S069W-D02_028013_1732_XN_06S068W
5	D04_028725_1730_XI_07S066W-D07_030004_1729_XI_07S066W
9	D06_029648_1723_XI_07S067W-D07_029925_1722_XI_07S067W
3	D09_030650_1715_XI_08S064W-P05_003078_1734_XI_06S065W
16	D14_032773_1721_XN_07S065W-D15_033195_1721_XN_07S065W
31	D15_032971_1734_XN_06S069W-P12_005755_1739_XN_06S069W
22	D16_033274_1720_XN_08S064W-D16_033419_1720_XN_08S064W
17	D17_033907_1719_XN_08S064W-D18_034263_1719_XN_08S064W
23	D19_034685_1727_XN_07S067W-D19_034751_1727_XN_07S067W

30	D20_034896_1724_XI_07S067W-P19_008260_1726_XN_07S067W
38	F01_036373_1735_XN_06S069W-F02_036518_1734_XN_06S069W
32	F06_038140_1742_XI_05S069W-P12_005755_1739_XN_06S069W
28	G04_019666_1745_XN_05S071W-P18_007891_1742_XN_05S071W
21	G05_020299_1735_XN_06S071W-P03_002353_1734_XN_06S071W
6	G06_020668_1727_XN_07S066W-G07_020813_1728_XN_07S066W
26	G10_022290_1736_XI_06S070W-P02_001931_1721_XN_07S069W
10	G11_022646_1736_XN_06S068W-P13_006256_1720_XN_08S068W
27	G18_025191_1739_XN_06S070W-P04_002709_1744_XN_05S070W

B: List of HiRISE stereo pairs used to a generate map for calculating attitudes of ILD material within East Candor Chasm.

HiRISE Number	HiRISE Stereo Pair
6	ESP_012809_1725_RED-ESP_013310_1725_RED-DEM
7	ESP_011886_1725_RED-PSP_005834_1725_RED-DEM
12	PSP_005979_1710_RED-PSP_006757_1710_RED-DEM
13	PSP_007192_1710_RED-PSP_008049_1710_RED-DEM
14	PSP_004344_1715_RED-PSP_005623_1715_RED-DEM
15	ESP_028514_1720_RED-ESP_028936_1720_RED-DEM
16	ESP_027248_1720_RED-ESP_027736_1720_RED-DEM
17	ESP_014286_1735_RED-ESP_020299_1735_RED-DEM
21	ESP_032918_1720_RED-ESP_032984_1720_RED-DEM
24	ESP_033907_1725_RED-ESP_034263_1725_RED-DEM

27	ESP_034896_1725_RED-ESP_036452_1725_RED-DEM
28	ESP_037586_1725_RED-ESP_037731_1725_RED-DEM
37	ESP_011965_1725_RED-ESP_012242_1725_RED-DEM
38	ESP_039604_1720_RED-ESP_039749_1720_RED-DEM

C: Attitude measurements obtained within the central mounds of East Candor Chasma; 20 meter/pixel CTX imagery.

X	Y	Elevation	Strike	Dip
-3924090	-435223	-1749.45	263.2	12
-3922992	-437089	-942.06	277.5	19
-3922118	-438131	-653.71	276.8	18
-3916670	-441879	-510.01	282.4	19
-3881812	-457402	-85	260.6	8
-3881698	-458044	184.2	229.1	9
-3922860	-440567	197.17	274.3	18
-3883997	-457921	1044.07	296.4	14
-3884250	-458067	1132.1	293.3	14
-3909651	-479039	1439.88	84.6	11
-3921574	-465432	1594.91	141	12
-3909714	-477993	1596.59	102.8	11
-3925793	-460826	2069.61	153.8	11
-3862855	-473047	2213.91	171	31
-3865579	-473122	2226.94	145.6	7
-3863046	-473013	2241.95	159.5	14
-3916158	-453304	2427.57	347.2	10
-3908543	-473230	2528.21	102.3	5
-3926233	-452996	2894.44	141.7	8
-3955608	-423401	-2171.56	287.4	17
-3968791	-441482	-1078.19	264.9	14
-3974630	-438939	-144.78	301	16
-4022858	-429360	874.08	224.9	44
-4017204	-429395	1206.86	179	1
-4024912	-429750	1449.38	203.1	6
-3994859	-439208	2168.36	360	2
-3985113	-445473	2319.23	335.5	22
-3986697	-444861	2425.76	291.5	10
-4035222	-408592	-4151.44	265.1	7

-4031482	-408955	-3846.4	238.6	8
-4064010	-407801	-2876.09	97.2	10
-4088637	-414580	-1884.49	286.5	14
-4089363	-415143	-1411.09	283.8	12
-4041183	-428444	-603.73	292.1	10
-4061038	-419232	-221.21	282.4	19
-4044570	-425908	-70.48	57.9	6
-4040089	-426040	24.46	112.1	22
-4054451	-423896	25.23	108	20
-4053451	-419489	311.93	287.1	11
-4055586	-419054	429.4	288.1	15
-4134477	-401318	1304.47	291.9	12
-4134029	-407629	2844.68	292	8
-4131083	-408299	2659.51	304.5	17
-4129413	-408090	2200.65	308.1	18
-4148432	-400656	1654.58	9.7	5
-4136547	-409914	3230.97	130.3	4
-4210624	-397908	-514.98	126.2	11
-4209779	-396624	-7.77	147.5	7
-4197094	-389654	701.66	282.6	6
-4173454	-391422	1475.68	263.2	16

D: Attitude measurements obtained along the south wall of East Candor Chasma; 20 meter/pixel CTX imagery.

X	Y	Elevation	Strike	Dip
-3840474	-522729	-400.77	298.3	18
-3841674	-522758	-293.76	314.6	13
-3841502	-522730	-291.43	310	12
-3845896	-521358	-230.71	267.1	9
-3880922	-513401	119.17	81.5	4
-3882406	-513427	160.22	340.4	2
-3882648	-514406	183.73	294.7	4
-3881335	-512395	187.66	84.4	4
-3862478	-525809	261.69	128.2	3
-3858606	-522312	585.31	216.2	17
-3874092	-507595	862.5	164.4	6
-3864572	-515649	931.4	342.9	7
-3856194	-520495	946.32	231.7	9
-3854799	-520460	956.17	233.2	26
-3852954	-516289	969.02	310.6	16
-3866960	-514720	975.04	172.3	7

-3871124	-508045	975.66	181.9	4
-3852149	-513811	1013.01	229.6	7
-3852225	-513691	1025.93	248.2	9
-3857866	-517484	1055.51	142.8	4
-3858524	-517267	1061.9	194.6	5
-3854753	-509934	1094.57	310.5	17
-3864921	-513032	1238.37	128.1	9
-3855104	-515549	1312.1	318	6
-3888587	-501978	1427.44	254.8	1
-3880447	-488560	2432.34	31.5	13
-3999626	-478295	-252.91	189.7	5
-3952720	-486442	246.04	237.6	6
-3960861	-462158	273.62	302.8	4
-3961446	-462832	353.95	306.3	5
-3952836	-485250	464.53	221.1	13
-3950890	-481939	488.63	130	5
-3958161	-466709	526.19	339.8	7
-3960679	-466765	617.51	320.8	4
-3964694	-466931	1009.67	291.8	7
-3963791	-467804	1059.12	296.8	9
-3960945	-470290	1077.52	333.2	10
-3986488	-442851	1690.67	352.1	15
-3978980	-465228	1923.18	318.4	15
-3987421	-469330	1965.07	33.6	3
-3988221	-461551	1998.18	208.8	5
-3986754	-444884	2003.87	323.8	10
-3983306	-459045	2166.25	4.9	9
-3987380	-461760	2210.99	189.5	13
-3984195	-445650	2249.11	330.3	13
-3984100	-470387	2309.09	59.1	3
-3983836	-467374	2577.14	320.5	5
-3985987	-450023	2595.84	127	4
-4033392	-465933	-1091.24	319	6
-4033437	-468075	-1004.47	355.7	6
-4058777	-454423	-986.36	6.1	8
-4058575	-454592	-984.52	0.6	9
-4057604	-455071	-970.24	347.4	7
-4057882	-453884	-966.01	352.4	12
-4056687	-455590	-910.57	151.2	8
-4056856	-455373	-894.75	175.2	8
-4035051	-470944	-818.51	324.4	11
-4037098	-465718	-739.59	26	12
-4013487	-462921	-670.99	184.8	11

-4045041	-457631	-647.35	176.4	26
-4037920	-465433	-640.8	13.8	5
-4013364	-459195	-583.85	129.4	9
-4049684	-454462	-282.63	57.6	21
-4025023	-466335	-71.75	353.3	13
-4025623	-467402	-57.14	314.8	16
-4025567	-466999	-49.2	328.8	16
-4024837	-466040	-27.95	1.5	13
-4041390	-465361	57.31	338.3	9
-4041420	-465289	72.26	325.9	6
-4041521	-454603	108.13	257.2	26
-4011398	-467421	250.73	278.5	13
-4010995	-466608	273.71	278.5	22
-4010840	-467283	276.32	260	13
-4010813	-466744	301.36	278.1	23
-4099150	-415862	-1334.22	270.9	8
-4099418	-416181	-1200.75	317.6	9
-4089536	-417495	-1185.13	277.4	12
-4067919	-445541	-786.7	261.4	4
-4069744	-446557	-761.63	192.1	6
-4065884	-445867	-728.08	258.7	14
-4087007	-440232	-702.06	246.2	4
-4067403	-446959	-696.5	259.4	8
-4086887	-440237	-696.3	250.2	4
-4066486	-446636	-693.35	254.3	11
-4064734	-451987	-570.14	145.7	5
-4065122	-452219	-551.13	159.4	5
-4064819	-451785	-550.55	147.9	6
-4103001	-419103	-514.36	18.9	11
-4100753	-420938	-297	279	13
-4100670	-420924	-178.15	279.5	16
-4087605	-422272	484.99	263.6	15
-4088212	-423105	716.15	299.9	6
-4231587	-430177	-1797.31	276	6
-4225851	-421969	-1403.83	284.7	17
-4202288	-426564	-158.47	282.8	20
-4201517	-426884	-77.62	281.4	20
-4176717	-435751	-6.04	326	14

E: Attitude measurements obtained within the central mounds of East Candor Chasma; 0.5 meter/pixel HiRISE imagery.

X	Y	Elevation	Strike	Dip
6850734	-466167	-860.5	321.7	22
6849157	-464379	-839.04	277.7	19
6849725	-466053	-452.98	296.9	13
6849915	-466594	-359.87	310.5	16
6849008	-466734	-63.11	293	11
6849979	-468578	56.56	313.1	16
6846824	-468763	1110.32	224.9	26
6847912	-470236	1996.87	308.1	10
-3817017	-474031	11.29	85.2	30
-3817188	-473618	15.86	51.8	18
-3816955	-474043	-17.86	86.7	31
-3817061	-474815	239.22	341.5	22

F: Layer thickness measurements obtained within the central mounds of East Candor Chasma

Layer thickness measurements were obtained by manually placing points where layer boundaries were observed. Layer thickness values were rounded to the nearest meter.

X	Y	ELEV	LATITUDE	LONGITUDE	LAYER	Thickness of layer	Average Thickness of Package	Thick vs thin
-3900617.51	-469569.993	3091	-7.921929811	-65.80577677	Mound B central top	0	1.428571	Thin
-3900590.12	-469584.287	3091	-7.922170959	-65.80531457	Mound B central top	3		Thin
-3900560.34	-469598.581	3094	-7.922412108	-65.80481217	Mound B central top	1		Thin
-3900525.79	-469612.875	3093	-7.922653256	-65.8042294	Mound B central top	0		Thin
-3900494.82	-469624.787	3093	-7.922854213	-65.80370691	Mound B central top	4		Thin
-3900462.66	-469641.463	3097	-7.923135553	-65.80316433	Mound B central top	0		Thin
-3900431.69	-469654.566	3097	-7.923356606	-65.80264184	Mound B central top	2		Thin
-3900401.91	-469671.243	3095	-7.923637946	-65.80213945	Mound B central top			Thin
X	**Y**	**ELEV**	**LATITUDE**	**LONGITUDE**	**LAYER**	**Thickness of layer**	**Average Thickness of Package**	**Thick vs thin**
-3900066	-468839.212	3007	-7.909601094	-65.79647246	Mound B central top	6	5.63636364	Thin
-3900058.86	-468874.947	3013	-7.910203965	-65.79635188	Mound B central top	6		Thin
-3900052.9	-468914.256	3019	-7.910867123	-65.7962514	Mound B central top	6		Thin
-3900044.56	-468963.094	3025	-7.911691047	-65.79611073	Mound B central top	5		Thin
-3900037.42	-469026.226	3030	-7.91275612	-65.79599016	Mound B central top	4		Thin
-3900024.31	-469079.828	3034	-7.913660427	-65.79576911	Mound B central top	18		Thin

-3900006.45	-469260.885	3052	-7.916714974	-65.79546767	Mound B central top	4		Thin
-3899999.3	-469310.914	3056	-7.917558994	-65.7953471	Mound B central top	5		Thin
-3899996.92	-469346.65	3061	-7.918161865	-65.7953069	Mound B central top	0		Thin
-3899996.92	-469375.238	3061	-7.918644162	-65.7953069	Mound B central top	4		Thin
-3899995.72	-469409.781	3065	-7.919226938	-65.79528681	Mound B central top	4		Thin
-3899994.53	-469453.855	3069	-7.919970479	-65.79526671	Mound B central top			Thin
X	**Y**	**ELEV**	**LATITUDE**	**LONGITUDE**	**LAYER**	**Thickness of layer**	**Average Thickness of Package**	**Thick vs thin**
-3914452.29	-455304.881	2519	-7.681268737	-66.03917775	Mound B West Limb	32	40.75	Thick
-3914505.76	-455347.659	2551	-7.681990427	-66.04007986	Mound B West Limb	32		Thick
-3914563.51	-455424.659	2583	-7.68328947	-66.04105414	Mound B West Limb	45		Thick
-3914623.4	-455495.243	2628	-7.684480259	-66.04206451	Mound B West Limb	64		Thick
-3914730.34	-455608.605	2692	-7.686392739	-66.04386873	Mound B West Limb	63		Thick
-3914796.65	-455692.022	2755	-7.687800035	-66.04498735	Mound B West Limb	31		Thick
-3914833.01	-455775.439	2786	-7.689207331	-66.04560079	Mound B West Limb	44		Thick
-3914901.45	-455852.439	2830	-7.690506374	-66.04675549	Mound B West Limb	30		Thick
-3914950.65	-455916.606	2860	-7.69158891	-66.04758544	Mound B West Limb	41		Thick
-3915019.09	-456000.023	2901	-7.692996206	-66.04874014	Mound B West Limb	45		Thick
-3915089.68	-456066.329	2946	-7.694114826	-66.04993093	Mound B West Limb	37		Thick
-3915153.84	-456141.19	2983	-7.695377784	-66.05101347	Mound B West Limb	25		Thick

-3915200.9	-456209.635	3008	-7.696532489	-66.05180733	Mound B West Limb			Thick
X	**Y**	**ELEV**	**LATITUDE**	**LONGITUDE**	**LAYER**	**Thickness of layer**	**Average Thickness of Package**	**Thick vs thin**
-3918399.64	-448042.52	2157	-7.558748319	-66.10577196	Mound B West limb	6	64	Thick
-3918652.38	-447725.44	2151	-7.553398985	-66.11003593	Mound B West limb	9		Thick
-3918767.27	-447555.412	2142	-7.550530502	-66.11197409	Mound B West limb	50		Thick
-3918983.25	-447128.043	2092	-7.543320532	-66.11561784	Mound B West limb	34		Thick
-3919075.16	-446935.038	2058	-7.540064416	-66.11716837	Mound B West limb	76		Thick
-3919341.69	-446420.357	1982	-7.53138144	-66.12166491	Mound B West limb	182		Thick
-3919603.62	-445721.862	1800	-7.519597402	-66.12608392	Mound B West limb	91		Thick
-3919773.65	-445395.591	1709	-7.514093016	-66.12895241	Mound B West limb			Thick
X	**Y**	**ELEV**	**LATITUDE**	**LONGITUDE**	**LAYER**	**Thickness of layer**	**Average Thickness of Package**	**Thick vs thin**
-3881152.06	-459335.394	427	-7.749265925	-65.47738274	Mound B Central Cliff	194	229.6	Thick
-3881411.6	-459544.705	621	-7.752797137	-65.48176144	Mound B Central Cliff	179		Thick
-3881637.66	-459728.899	800	-7.755904603	-65.48557515	Mound B Central Cliff	349		Thick
-3882073.03	-460122.405	1149	-7.762543281	-65.49292007	Mound B Central Cliff	208		Thick
-3882340.95	-460289.854	1357	-7.765368251	-65.49744002	Mound B Central Cliff	218		Thick

-3882633.98	-460440.558	1575	-7.767910723	-65.50238372	Mound B Central Cliff			Thick
X	**Y**	**ELEV**	**LATITUDE**	**LONGITUDE**	**LAYER**	**Thickness of layer**	**Average Thickness of Package**	**Thick vs thin**
-3886508.34	-456939.824	1435	-7.708851208	-65.56774644	Mound B Central Top	2	6.4	Thin
-3886604.62	-456897.961	1437	-7.708144966	-65.5693708	Mound B Central Top	5		Thin
-3886654.86	-456864.471	1432	-7.707579972	-65.57021829	Mound B Central Top	5		Thin
-3886707.18	-456820.516	1427	-7.706838417	-65.57110109	Mound B Central Top	5		Thin
-3886761.61	-456755.629	1422	-7.705743742	-65.57201921	Mound B Central Top	9		Thin
-3886864.17	-456680.277	1413	-7.704472505	-65.5737495	Mound B Central Top	5		Thin
-3886910.22	-456607.018	1408	-7.703236581	-65.57452637	Mound B Central Top	10		Thin
-3886985.57	-456517.014	1398	-7.70171816	-65.57579761	Mound B Central Top	5		Thin
-3887033.71	-456441.662	1393	-7.700446924	-65.57660979	Mound B Central Top	12		Thin
-3887098.6	-456370.496	1381	-7.699246312	-65.57770446	Mound B Central Top			Thin
X	**Y**	**ELEV**	**LATITUDE**	**LONGITUDE**	**LAYER**	**Thickness of layer**	**Average Thickness of Package**	**Thick vs thin**
-3883743.19	-458268.481	1320	-7.73126646	-65.52109671	Mound B Central Top	31	28.8571429	Thick
-3883783.62	-458292.37	1351	-7.73166949	-65.52177876	Mound B Central Top	32		Thick
-3883857.12	-458351.175	1383	-7.732661565	-65.52301885	Mound B Central Top	17		Thick

-3883901.23	-458373.227	1400	-7.733033594	-65.52376291	Mound B Central Top	31		Thick
-3883967.38	-458437.545	1431	-7.734118676	-65.52487899	Mound B Central Top	31		Thick
-3884011.49	-458476.136	1462	-7.734769725	-65.52562305	Mound B Central Top	29		Thick
-3884044.56	-458529.428	1491	-7.735668793	-65.52618109	Mound B Central Top	31		Thick
-3884108.88	-458579.044	1522	-7.736505856	-65.52726617	Mound B Central Top			Thick
X	**Y**	**ELEV**	**LATITUDE**	**LONGITUDE**	**LAYER**	**Thickness of layer**	**Average Thickness of Package**	**Thick vs thin**
-3924970.96	-439495.715	332	-7.414558552	-66.21663414	Mound B West Limb	4	4	
-3924874.88	-439495.715	328	-7.414558552	-66.21501319	Mound B West Limb			
X	**Y**	**ELEV**	**LATITUDE**	**LONGITUDE**	**LAYER**	**Thickness of layer**	**Average Thickness of Package**	**Thick vs thin**
-4087514.96	-422605.097	951	-7.129603602	-68.95884978	Landmark	1	7.1667	Thin
-4087454.77	-422641.65	950	-7.130220278	-68.95783435	Landmark	11		Thin
-4087427.7	-422665.15	939	-7.130616728	-68.95737757	Landmark	0		Thin
-4087397.05	-422682.519	939	-7.130909756	-68.95686046	Landmark	11		Thin
-4087367.42	-422707.551	928	-7.131332062	-68.95636059	Landmark	5		Thin
-4087337.28	-422741.268	933	-7.131900882	-68.9558521	Landmark	15		Thin

-4087301.52	-422776.517	918	-7.132495557	-68.9552488	Landmark			Thin
X	**Y**	**ELEV**	**LATITUDE**	**LONGITUDE**	**LAYER**	**Thickness of layer**	**Average Thickness of Package**	**Thick vs thin**
-3985372.2	-445754.999	2425	-7.520156448	-67.23563965	North of Minor Mound 1	8	6.889	Thin
-3985323.23	-445777.738	2417	-7.520540074	-67.23481338	North of Minor Mound 1	1		Thin
-3985249.76	-445793.481	2416	-7.520805662	-67.23357397	North of Minor Mound 1	8		Thin
-3985206.03	-445798.728	2408	-7.520894191	-67.23283623	North of Minor Mound 1	8		Thin
-3985169.3	-445819.718	2400	-7.521248307	-67.23221652	North of Minor Mound 1	0		Thin
-3985132.57	-445814.471	2400	-7.521159778	-67.23159682	North of Minor Mound 1	14		Thin
-3985080.09	-445833.712	2386	-7.521484385	-67.23071153	North of Minor Mound 1	8		Thin
-3985027.62	-445837.21	2378	-7.521543404	-67.22982624	North of Minor Mound 1	7		Thin
-3984983.89	-445845.956	2385	-7.521690953	-67.22908849	North of Minor Mound 1	8		Thin
-3984933.16	-445865.197	2377	-7.52201556	-67.22823271	North of Minor Mound 1			Thin

X	Y	ELEV	LATITUDE	LONGITUDE	LAYER	Thickness of layer	Average Thickness of Package	Thick vs thin
-3820218.49	-466366.857	399	-7.867890969	-64.44939653	Mound A north	175	200.75	Thick
-3819710.15	-466095.073	224	-7.863305798	-64.44082056	Mound A north	158		Thick
-3819463.53	-465959.18	66	-7.861013212	-64.43665994	Mound A north	219		Thick
-3819086.05	-465762.891	-153	-7.8577017	-64.43029165	Mound A north	251		Thick
-3818688.44	-465491.107	-404	-7.853116529	-64.42358371	Mound A north			Thick
X	Y	ELEV	LATITUDE	LONGITUDE	LAYER	Thickness of layer	Average Thickness of Package	Thick vs thin
-3989063.33	-461036.379	2285	-7.777962578	-67.29791119	Mound C west flank	53	62.5	Thick
-3988047.79	-469327.778	2338	-7.917843484	-67.28077833	Mound C west flank	39		Thick
-3987781.85	-469281.239	2377	-7.917058345	-67.27629183	Mound C west flank	56		Thick
-3987495.97	-469234.7	2433	-7.916273206	-67.27146883	Mound C west flank	52		Thick
-3987236.68	-469194.809	2485	-7.91560023	-67.26709448	Mound C west flank	152		Thick
-3986698.16	-469161.567	2637	-7.915039416	-67.25800931	Mound C west flank	73		Thick
-3986432.22	-469128.325	2710	-7.914478603	-67.2535228	Mound C west flank	81		Thick
-3985986.78	-469154.919	2791	-7.914927254	-67.2460079	Mound C west flank	94		Thick
-3985395.07	-469088.435	2885	-7.913805627	-67.23602542	Mound C west flank	45		Thick
-3985029.41	-469041.896	2930	-7.913020488	-67.22985647	Mound C west flank	48		Thick
-3984610.56	-468968.763	2978	-7.911786698	-67.22279022	Mound C west flank	26		Thick

-3984284.79	-468928.873	3004	-7.911113722	-67.21729425	Mound C west flank	31		Thick
-3983826.04	-468835.795	3035	-7.909543444	-67.20955502	Mound C west flank			Thick
X	**Y**	**ELEV**	**LATITUDE**	**LONGITUDE**	**LAYER**	**Thickness of layer**	**Average Thickness of Package**	**Thick vs thin**
-3985001.59	-473600.978	2113	-7.989934956	-67.22938725	Mound C west flank	22	27.1875	Thick
-3984906.08	-473584.72	2135	-7.989660672	-67.22777583	Mound C west flank	12		Thick
-3984828.85	-473578.623	2147	-7.989557816	-67.22647297	Mound C west flank	12		Thick
-3984692.69	-473558.3	2159	-7.98921496	-67.22417584	Mound C west flank	23		Thick
-3984593.11	-473540.01	2182	-7.98890639	-67.22249585	Mound C west flank	19		Thick
-3984458.98	-473540.01	2201	-7.98890639	-67.22023301	Mound C west flank	32		Thick
-3984284.2	-473481.074	2233	-7.98791211	-67.21728445	Mound C west flank	42		Thick
-3984107.4	-473432.3	2275	-7.987089257	-67.21430161	Mound C west flank	15		Thick
-3984011.88	-473424.171	2290	-7.986952114	-67.21269019	Mound C west flank	37		Thick
-3983833.04	-473377.429	2327	-7.986163547	-67.20967306	Mound C west flank	62		Thick
-3983535	-473319.928	2389	-7.985193476	-67.20464491	Mound C west flank	53		Thick
-3983322.61	-473264.863	2442	-7.984264502	-67.20106173	Mound C west flank	35		Thick
-3983172.16	-473240.281	2477	-7.983849782	-67.19852364	Mound C west flank	7		Thick
-3983108.25	-473196.033	2484	-7.983103285	-67.19744537	Mound C west flank	26		Thick
-3982986.32	-473161.617	2510	-7.982522677	-67.19538836	Mound C west flank	24		Thick
-3982911.59	-473138.018	2534	-7.982124546	-67.19412761	Mound C west flank	14		Thick

-3982802.44	-473102.619	2548	-7.981527348	-67.19228625	Mound C west flank			Thick
X	**Y**	**ELEV**	**LATITUDE**	**LONGITUDE**	**LAYER**	**Thickness of layer**	**Average Thickness of Package**	**Thick vs thin**
-3962609.61	-468879.203	1499	-7.910275757	-66.85162094	Mound C east flank	7	9.5	Thin
-3962555.2	-468811.188	1492	-7.909128303	-66.85070298	Mound C east flank	10		Thin
-3962497.39	-468739.772	1482	-7.907923478	-66.84972764	Mound C east flank	7		Thin
-3962432.77	-468685.36	1475	-7.907005515	-66.84863756	Mound C east flank	9		Thin
-3962378.36	-468620.746	1466	-7.905915434	-66.8477196	Mound C east flank	7		Thin
-3962286.54	-468573.136	1459	-7.905112217	-66.84617054	Mound C east flank	17		Thin
-3962177.72	-468471.113	1442	-7.903391037	-66.84433461	Mound C east flank			Thin
X	**Y**	**ELEV**	**LATITUDE**	**LONGITUDE**	**LAYER**	**Thickness of layer**	**Average Thickness of Package**	**Thick vs thin**
-4024963.86	-442996.226	1143	-7.473614291	-67.90357482	Minor Mound 2west flank	60	52.7	Thick
-4024797.34	-442949.098	1203	-7.472819208	-67.90076552	Minor Mound 2west flank	141		Thick
-4024256.93	-442801.429	1344	-7.470327947	-67.89164857	Minor Mound 2west flank	30		Thick
-4024074.7	-442722.882	1374	-7.469002808	-67.88857425	Minor Mound 2west flank	28		Thick
-4023927.04	-442682.038	1402	-7.468313736	-67.88608299	Minor Mound 2west flank	53		Thick

-4023597.14	-442581.497	1455	-7.466617558	-67.8805174	Minor Mound 2west flank	21		Thick
-4023436.9	-442506.092	1476	-7.465345425	-67.87781412	Minor Mound 2west flank	38		Thick
-4023254.67	-442449.538	1514	-7.464391325	-67.8747398	Minor Mound 2west flank	76		Thick
-4022877.65	-442396.126	1590	-7.463490231	-67.86837913	Minor Mound 2west flank	45		Thick
-4022626.29	-442392.984	1635	-7.463437225	-67.86413869	Minor Mound 2west flank	35		Thick
-4022456.63	-442389.842	1670	-7.46338422	-67.86127639	Minor Mound 2west flank			Thick
X	**Y**	**ELEV**	**LATITUDE**	**LONGITUDE**	**LAYER**	**Thickness of layer**	**Average Thickness of Package**	**Thick vs thin**
-3899997.99	-481544.176	2413	-8.12394151	-65.79532505	Mound B South flank	124	97.2	Thick
-3899760.03	-481057.185	2537	-8.11572568	-65.7913105	Mound B South flank	135		Thick
-3899488.86	-480448.446	2672	-8.105455893	-65.78673577	Mound B South flank	76		Thick
-3899289.64	-480138.543	2748	-8.100227638	-65.78337475	Mound B South flank	45		Thick
-3899184.5	-479895.048	2793	-8.096119723	-65.78160088	Mound B South flank	106		Thick
-3898918.86	-479446.795	2899	-8.088557425	-65.77711952	Mound B South flank			Thick

X	Y	ELEV	LATITUDE	LONGITUDE	LAYER	Thickness of layer	Average Thickness of Package	Thick vs thin
-3894114.2	-488263.427	2284	-8.23729934	-65.69606195	Mound C south flank	7	18.7777778	Thin
-3894050.59	-488244.58	2291	-8.236981388	-65.69498886	Mound C south flank	24		Thin
-3893975.21	-488218.666	2315	-8.236544204	-65.69371705	Mound C south flank	7		Thin
-3893890.4	-488192.752	2322	-8.23610702	-65.69228627	Mound C south flank	24		Thin
-3893815.01	-488180.973	2346	-8.2359083	-65.69101446	Mound C south flank	14		Thin
-3893683.09	-488171.55	2360	-8.235749324	-65.6887888	Mound C south flank	48		Thin
-3893478.13	-488107.943	2408	-8.234676237	-65.68533107	Mound C south flank	18		Thin
-3893416.88	-488065.539	2426	-8.233960845	-65.68429773	Mound C south flank	19		Thin
-3893372.12	-488025.49	2445	-8.233285198	-65.68354259	Mound C south flank	8		Thin
-3893289.67	-488006.643	2453	-8.232967246	-65.68215155	Mound C south flank			Thin
X	Y	ELEV	LATITUDE	LONGITUDE	LAYER	Thickness of layer	Average Thickness of Package	Thick vs thin
-3896477.08	-482040.548	2878	-8.132315614	-65.73592516	Mound C south flank	26	13.4545455	Thin
-3896359.29	-482031.125	2904	-8.132156638	-65.73393796	Mound C south flank	22		Thin
-3896241.5	-482021.702	2926	-8.131997663	-65.73195076	Mound C south flank	18		Thin
-3896142.56	-482040.548	2944	-8.132315614	-65.73028151	Mound C south flank	0		Thin
-3896142.56	-482040.548	2944	-8.132315614	-65.73028151	Mound C south flank	34		Thin
-3895991.78	-482049.971	2978	-8.13247459	-65.7277379	Mound C south flank	37		Thin

-3895873.99	-482026.413	3015	-8.132077151	-65.7257507	Mound C south flank	31		Thin
-3895713.8	-482016.99	3046	-8.131918175	-65.72304811	Mound C south flank	18		Thin
-3895605.43	-482021.702	3064	-8.131997663	-65.72121989	Mound C south flank	31		Thin
-3895426.39	-482045.26	3095	-8.132395102	-65.71819934	Mound C south flank	8		Thin
-3895335.82	-482054.16	3103	-8.132545246	-65.71667141	Mound C south flank	-77		Thin
-3895796.51	-482024.843	3026	-8.132050655	-65.72444357	Mound C south flank			Thin
X	**Y**	**ELEV**	**LATITUDE**	**LONGITUDE**	**LAYER**	**Thickness of layer**	**Average Thickness of Package**	**Thick vs thin**
-3816947	-472733.664	325	-7.975302847	-64.39420465	Mound A east flank	115	114.4	Thick
-3817150.84	-472854.457	440	-7.977340701	-64.39764353	Mound A east flank	62		Thick
-3817279.18	-472952.602	502	-7.978996457	-64.39980875	Mound A east flank	119		Thick
-3817455.34	-473078.428	621	-7.981119222	-64.40278062	Mound A east flank	123		Thick
-3817661.7	-473239.485	744	-7.98383636	-64.40626195	Mound A east flank	153		Thick
-3817807.65	-473380.411	897	-7.986213856	-64.40872436	Mound A east flank			Thick

X	Y	ELEV	LATITUDE	LONGITUDE	LAYER	Thickness of layer	Average Thickness of Package	Thick vs thin
-3825539.59	-475184.428	546	-8.016648726	-64.5391668	Mound A west flank	78	70	Thick
-3825390.03	-475203.521	624	-8.016970836	-64.53664361	Mound A west flank	77		Thick
-3825262.74	-475267.165	701	-8.018044536	-64.53449621	Mound A west flank	79		Thick
-3825129.09	-475298.986	780	-8.018581386	-64.53224144	Mound A west flank	78		Thick
-3824954.07	-475375.358	858	-8.019869826	-64.52928876	Mound A west flank	65		Thick
-3824826.79	-475435.819	923	-8.020889841	-64.52714136	Mound A west flank	42		Thick
-3824689.95	-475474.005	965	-8.021534061	-64.52483291	Mound A west flank	71		Thick
-3824543.57	-475563.106	1036	-8.023037241	-64.5223634	Mound A west flank			Thick
X	Y	ELEV	LATITUDE	LONGITUDE	LAYER	Thickness of layer	Average Thickness of Package	Thick vs thin
-3972143.95	-443214.222	569	-7.477292003	-67.01247107	Minor Mound 1 South	630	871.0833	Thick
-3970670.4	-442477.445	-61	-7.464862138	-66.98761134	Minor Mound 1 South	1161		Thick
-3968426.58	-441506.24	-1222	-7.448477316	-66.94975675	Minor Mound 1 South	889		Thick
-3966752.09	-440066.177	-2111	-7.424182579	-66.92150706	Minor Mound 1 South	706		Thick
-3955365.54	-426452.557	-1405	-7.194512573	-66.72940915	Minor Mound 1 North	334		Thick
-3954327.36	-425414.372	-1739	-7.176997763	-66.71189434	Minor Mound 1 North	1511		Thick

-3951715.15	-422199.347	-3250	-7.122758352	-66.66782481	Minor Mound 1 North			Thick
X	**Y**	**ELEV**	**LATITUDE**	**LONGITUDE**	**LAYER**	**Thickness of layer**	**Average Thickness of Package**	**Thick vs thin**
-4039796.38	-429009.9	-1168	-7.237656496	-68.15380835	Minor Mound 2	392	181.333333	Thick
-4039669.6	-428403.2	-776	-7.227421101	-68.15166961	Minor Mound 2	226		Thick
-4039615.27	-428050.046	-550	-7.221463184	-68.15075301	Minor Mound 2	65		Thick
-4039615.27	-427715.003	-485	-7.215810802	-68.15075301	Minor Mound 2	116		Thick
-4039515.66	-427171.689	-369	-7.206644777	-68.14907257	Minor Mound 2	65		Thick
-4039542.83	-426863.812	-304	-7.201450696	-68.14953087	Minor Mound 2	224		Thick
-4039452.28	-426510.658	-80	-7.195492779	-68.1480032	Minor Mound 2			Thick
X	**Y**	**ELEV**	**LATITUDE**	**LONGITUDE**	**LAYER**	**Thickness of layer**	**Average Thickness of Package**	**Thick vs thin**
-4056974.13	-423246.25	-44	-7.140420244	-68.44360752	Minor Mound 3	158	105.555556	Thick
-4056883.58	-422874.986	114	-7.134156794	-68.44207985	Minor Mound 3	235		Thick
-4056720.59	-422069.071	349	-7.120560523	-68.43933004	Minor Mound 3	108		Thick
-4056820.19	-421878.911	457	-7.117352414	-68.44101048	Minor Mound 3	97		Thick
-4056793.03	-421670.641	554	-7.113838771	-68.44055218	Minor Mound 3	69		Thick

-4056738.7	-421408.04	623	-7.109408525	-68.43963557	Minor Mound 3	56		Thick
-4056747.75	-421181.659	679	-7.105589348	-68.43978834	Minor Mound 3	0		Thick
-4056747.75	-421181.659	679	-7.105589348	-68.43978834	Minor Mound 3	65		Thick
-4056675.31	-420937.168	744	-7.101464637	-68.4385662	Minor Mound 3	162		Thick
-4056657.2	-420411.965	906	-7.092604145	-68.43826067	Minor Mound 3			Thick
X	**Y**	**ELEV**	**LATITUDE**	**LONGITUDE**	**LAYER**	**Thickness of layer**	**Average Thickness of Package**	**Thick vs thin**
-4170697.74	-385986.342	632	-6.511823057	-70.36219358	Mound D north face	114	291.4	Thick
-4170756.97	-385724.046	518	-6.507397966	-70.36319279	Mound D north face	160		Thick
-4170782.35	-385402.522	358	-6.50197366	-70.36362102	Mound D north face	339		Thick
-4170697.74	-384877.93	19	-6.493123477	-70.36219358	Mound D north face	481		Thick
-4170731.59	-383727.212	-462	-6.473710173	-70.36276455	Mound D north face	363		Thick
-4170689.28	-383033.397	-825	-6.462005092	-70.36205083	Mound D north face			Thick
X	**Y**	**ELEV**	**LATITUDE**	**LONGITUDE**	**LAYER**	**Thickness of layer**	**Average Thickness of Package**	**Thick vs thin**
-4087788.92	-422405.183	940	-7.126230939	-68.96347158	Minor Mound 4	1	2.875	Thin
-4087737.09	-422454.545	939	-7.127063696	-68.96259719	Minor Mound 4	5		Thin
-4087687.73	-422484.162	934	-7.127563349	-68.96176443	Minor Mound 4	5		Thin

-4087643.3	-422521.183	939	-7.128187916	-68.96101495	Minor Mound 4	0		Thin
-4087643.3	-422521.183	939	-7.128187916	-68.96101495	Minor Mound 4	7		Thin
-4087603.81	-422553.268	946	-7.128729208	-68.96034875	Minor Mound 4	0		Thin
-4087603.81	-422553.268	946	-7.128729208	-68.96034875	Minor Mound 4	0		Thin
-4087564.32	-422587.82	946	-7.129312137	-68.95968254	Minor Mound 4	5		Thin
-4087514.96	-422605.097	951	-7.129603602	-68.95884978	Minor Mound 4	0		Thin
-4087514.96	-422605.097	951	-7.129603602	-68.95884978	Minor Mound 4			Thin
X	**Y**	**ELEV**	**LATITUDE**	**LONGITUDE**	**LAYER**	**Thickness of layer**	**Average Thickness of Package**	**Thick vs thin**
-3987530.69	-443305.273	2307	-7.478828089	-67.27205464	North of Minor Mound 1	0	2.7778	Thin
-3987495.71	-443342.006	2307	-7.479447793	-67.27146445	North of Minor Mound 1	6		Thin
-3987443.23	-443376.989	2301	-7.480037987	-67.27057916	North of Minor Mound 1	1		Thin
-3987404.75	-443410.224	2300	-7.480598672	-67.26992994	North of Minor Mound 1	1		Thin
-3987355.77	-443448.706	2299	-7.481247885	-67.26910367	North of Minor Mound 1	1		Thin
-3987310.29	-443504.679	2298	-7.482192196	-67.26833642	North of Minor Mound 1	1		Thin
-3987261.32	-443551.907	2297	-7.482988959	-67.26751015	North of Minor Mound 1	8		Thin
-3987226.33	-443588.64	2289	-7.483608663	-67.26691995	North of Minor Mound 1	6		Thin

-3987191.35	-443621.874	2295	-7.484169347	-67.26632976	North of Minor Mound 1	1		Thin
-3987133.63	-443665.604	2294	-7.48490709	-67.26535594	North of Minor Mound 1			Thin
X	**Y**	**ELEV**	**LATITUDE**	**LONGITUDE**	**LAYER**	**Thickness of layer**	**Average Thickness of Package**	**Thick vs thin**
-3986923.73	-442746.41	2126	-7.469399734	-67.26181477	North of Minor Mond 1	9	4.625	Thin
-3986904.48	-442804.133	2135	-7.470373555	-67.26149016	North of Minor Mond 1	1		Thin
-3986862.5	-442856.608	2136	-7.471258846	-67.26078193	North of Minor Mond 1	9		Thin
-3986811.78	-442940.569	2145	-7.472675313	-67.25992615	North of Minor Mond 1	8		Thin
-3986785.54	-443003.539	2153	-7.473737662	-67.2594835	North of Minor Mond 1	1		Thin
-3986740.06	-443056.015	2152	-7.474622954	-67.25871625	North of Minor Mond 1	1		Thin
-3986694.58	-443139.975	2151	-7.47603942	-67.257949	North of Minor Mond 1	6		Thin
-3986633.36	-443209.942	2157	-7.477219809	-67.25691616	North of Minor Mond 1	2		Thin
-3986594.88	-443267.665	2155	-7.47819363	-67.25626694	North of Minor Mond 1			Thin

X	Y	ELEV	LATITUDE	LONGITUDE	LAYER	Thickness of layer	Average Thickness of Package	Thick vs thin
-4056805.42	-413215.903	-1398	-6.971202218	-68.4407612	Minor Mound 3 west flank	8	10.75	Thin
-4056773.31	-413205.199	-1406	-6.97102163	-68.44021944	Minor Mound 3 west flank	0		Thin
-4056744.76	-413194.494	-1406	-6.970841042	-68.43973787	Minor Mound 3 west flank	26		Thin
-4056719.78	-413181.411	-1432	-6.970620323	-68.4393165	Minor Mound 3 west flank	0		Thin
-4056686.48	-413169.517	-1432	-6.970419669	-68.43875467	Minor Mound 3 west flank	10		Thin
-4056636.53	-413150.488	-1442	-6.970098623	-68.43791192	Minor Mound 3 west flank	21		Thin
-4056579.44	-413140.973	-1463	-6.9699381	-68.43694878	Minor Mound 3 west flank	13		Thin
-4056530.68	-413126.7	-1476	-6.969697316	-68.4361261	Minor Mound 3 west flank	8		Thin
-4056489.05	-413113.617	-1484	-6.969476597	-68.43542382	Minor Mound 3 west flank			Thin
X	**Y**	**ELEV**	**LATITUDE**	**LONGITUDE**	**LAYER**	**Thickness of layer**	**Average Thickness of Package**	**Thick vs thin**
-4053863.64	-413389.683	-1872	-6.974134002	-68.39113156	Minor Mound 3	28	35.125	Thick
-4053856.03	-413480.979	-1844	-6.975674215	-68.3910032	Minor Mound 3	67		Thick
-4053886.46	-413659.766	-1777	-6.978690464	-68.39151661	Minor Mound 3	0		Thick
-4053886.46	-413659.766	-1777	-6.978690464	-68.39151661	Minor Mound 3	50		Thick
-4053886.46	-413811.926	-1727	-6.981257485	-68.39151661	Minor Mound 3	35		Thick

-4053886.46	-413907.025	-1692	-6.982861873	-68.39151661	Minor Mound 3	0		Thick
-4053886.46	-413907.025	-1692	-6.982861873	-68.39151661	Minor Mound 3	60		Thick
-4053939.72	-414047.773	-1632	-6.985236367	-68.39241507	Minor Mound 3	41		Thick
-4053970.15	-414218.952	-1591	-6.988124266	-68.39292847	Minor Mound 3			Thick
X	**Y**	**ELEV**	**LATITUDE**	**LONGITUDE**	**LAYER**	**Thickness of layer**	**Average Thickness of Package**	**Thick vs thin**
-3989013.47	-461049.676	2295	-7.778186904	-67.29706997	Mound C west flank	10	12.4210526	Thin
-3988971.91	-461039.703	2305	-7.77801866	-67.29636895	Mound C west flank	11		Thin
-3988918.73	-461049.676	2316	-7.778186904	-67.29547165	Mound C west flank	11		Thin
-3988875.51	-461053	2327	-7.778242985	-67.29474259	Mound C west flank	11		Thin
-3988819	-461066.297	2338	-7.77846731	-67.29378921	Mound C west flank	12		Thin
-3988764.15	-461069.621	2350	-7.778523392	-67.29286386	Mound C west flank	11		Thin
-3988700.99	-461086.242	2361	-7.778803799	-67.29179832	Mound C west flank	26		Thin
-3988627.86	-461091.229	2387	-7.778887921	-67.29056453	Mound C west flank	12		Thin
-3988559.71	-461099.539	2399	-7.779028124	-67.28941486	Mound C west flank	12		Thin
-3988501.54	-461124.471	2411	-7.779448734	-67.28843344	Mound C west flank	11		Thin
-3988459.99	-461131.119	2422	-7.779560897	-67.28773242	Mound C west flank	12		Thin
-3988421.76	-461139.43	2434	-7.7797011	-67.28708749	Mound C west flank	13		Thin
-3988376.88	-461147.74	2447	-7.779841303	-67.28633039	Mound C west flank	11		Thin
-3988312.06	-461161.037	2458	-7.780065629	-67.2852368	Mound C west flank	11		Thin

-3988265.52	-461174.334	2469	-7.780289954	-67.28445166	Mound C west flank	11		Thin
-3988187.4	-461180.982	2480	-7.780402117	-67.28313375	Mound C west flank	10		Thin
-3988130.89	-461182.644	2490	-7.780430158	-67.28218037	Mound C west flank	21		Thin
-3988052.77	-461199.265	2511	-7.780710564	-67.28086246	Mound C west flank	10		Thin
-3988002.91	-461214.224	2521	-7.78096293	-67.28002124	Mound C west flank	10		Thin
-3987959.69	-461219.21	2531	-7.781047052	-67.27929218	Mound C west flank			Thin
X	**Y**	**ELEV**	**LATITUDE**	**LONGITUDE**	**LAYER**	**Thickness of layer**	**Average Thickness of Package**	**Thick vs thin**
-3924798.01	-439505.324	326	-7.414720647	-66.21371644	Bank	2	8	Thin
-3924714.74	-439527.743	324	-7.415098868	-66.21231161	Bank	15		Thin
-3924647.49	-439553.364	339	-7.415531121	-66.21117695	Bank	1		Thin
-3924554.61	-439575.783	338	-7.415909342	-66.20961003	Bank	17		Thin
-3924455.32	-439614.216	355	-7.416557722	-66.20793505	Bank	2		Thin
-3924375.26	-439630.229	357	-7.41682788	-66.20658426	Bank	0		Thin
-3924375.26	-439630.229	357	-7.41682788	-66.20658426	Bank	19		Thin
-3924275.97	-439681.472	376	-7.417692386	-66.20490928	Bank			Thin